

1 2 9 0



UNIVERSIDADE D
COIMBRA

Giada Di Nunzio

**TRACING HEPATIC GLYCOGEN AND LIPID
METABOLISM WITH STABLE ISOTOPE
TRACERS: INSIGHTS FROM MURINE
STUDIES**

**Tese no âmbito do Doutoramento em Biologia Experimental e Biomedicina,
ramo de Biotecnologia e Saúde, orientada pelo Doutor John G. Jones e
coorientada pela Doutora Eugenia Carvalho e pelo Professor Doutor João
Ramalho Santos, apresentada ao Instituto de Investigação Interdisciplinar da
Universidade de Coimbra**

Abril de 2021

Institute for Interdisciplinary Research,
University of Coimbra

TRACING HEPATIC GLYCOGEN AND LIPID METABOLISM WITH STABLE ISOTOPE TRACERS: INSIGHTS FROM MURINE STUDIES

Giada Di Nunzio

Doctoral thesis submitted to the Institute of Interdisciplinary Research of the University of Coimbra to apply for the degree of Doctor of Philosophy in Experimental Biology and Biomedicine, specialization in Biotechnology and Health.

April 2021



**UNIVERSIDADE D
COIMBRA**

This work was conducted at the Center for Neurosciences and Cell Biology - CNC - (CNC Biotech and UC-NMR facility), University of Coimbra, Portugal; under the supervision of John G. Jones, PhD; and co-supervision of Eugenia Carvalho, PhD, and Professor João Ramalho Santos, PhD.

This project was funded by the European Union's Horizon 2020 research and innovation under the Marie Skłodowska-Curie grant agreement 721236-TREATMENT. The author also acknowledges financial support from the Portuguese Foundation for Science and Technology (research grant FCT-FEDER-02/SAICT/2017/028147). Structural funding for the Center for Neurosciences and Cell Biology and the UC-NMR facility was supported in part by FEDER – European Regional Development Fund through the COMPETE Programme, Centro 2020 Regional Operational Programme, and the Portuguese Foundation for Science and Technology through grants UIDB/04539/2020; POCI-01-0145-FEDER-007440; REEQ/481/QUI/2006, RECI/QEQ-QFI/0168/2012, CENTRO-07-CT62-FEDER-002012, and Rede Nacional de Ressonância Magnética Nuclear.



Published work

Sarsenbayeva A, Marques-Santos CM, Thombare K, **Di Nunzio G**, Almby KE, Lundqvist M, Eriksson JW, Pereira MJ. Effects of second-generation antipsychotics on human subcutaneous adipose tissue metabolism.

Psychoneuroendocrinology. 2019 Dec; 110: 104445

Belew GD, **Di Nunzio G**, Tavares L, Silva JG, Torres AN, Jones JG. Estimating pentose phosphate pathway activity from the analysis of hepatic glycogen ¹³C-isotopomers derived from [U-¹³C]fructose and [U-¹³C]glucose.

Magn Reson Med. 2020 Nov; 84 (5): 2765-2771.

Di Nunzio G, Belew GD, Torres AN, Silva JG, Silva LP, Barosa C, Tavares L, Jones JG. Determining the contribution of a high-fructose corn syrup formulation to hepatic glycogen synthesis during ad-libitum feeding in mice.

Sci Rep. 2020 Jul; 10 (1): 12852

Sarsenbayeva A, Dipta P, Lundqvist M, Almby KE, Tirosh B, **Di Nunzio G**, Eriksson JW, Pereira MJ. Human macrophages stimulate expression of inflammatory mediators in adipocytes; effects of second-generation antipsychotics and glucocorticoids on cellular cross-talk.

Psychoneuroendocrinology. 2020 Dec; 125: 105071

Acknowledgements

A particular expression of gratitude for Dr. John G. Jones, not only for having given me the opportunity of carrying out these studies under his supervision, but also for his extensive scientific knowledge and precious perspectives, and for being always approachable and ready to help.

Special thanks go to my colleagues, for being helpful and understanding, for all the important tips and advice, and of course, for all the car rides.

A sincere thank you to all my friends. The old and the new ones. My old friends, my safe port, because we take each other for granted in the most beautiful way. My new friends, for being the ultimate support while navigating the difficulties of this journey. For being patients when I needed to vent and for recharging me with new energy when I needed it the most. Also, for all our adventures. After all, this may be “the best time of our life and we don’t even know it”, in that case, I am grateful we’ve got to share this ride together.

No man is an island and when sometimes I tend to forget it, you remember it to me in more ways than one. I am forever grateful for that.

A final thank you to my family, for being my solid ground, unconditionally on my side. Thank you for being my biggest supporters. I know that, despite the distance, you feel what I feel, at all times.

I feel you too.

A Federica

What, if some day or night a demon were to steal after you in your loneliest loneliness and say to you: "This life as you now live it and have lived it, you will have to live once more and innumerable times more; and there will be nothing new in it, but every pain and every joy and every thought and sigh and everything unutterably small or great in your life will have to return to you, all in the same succession and sequence - even this spider and this moonlight between the trees, and even this moment and I myself. The eternal hourglass of existence is turned upside down again and again - and you with it, speck of dust!" - Would you not throw yourself down and gnash your teeth and curse the demon who spoke thus? Or have you once experienced a tremendous moment when you would have answered him: "You are a god and never have I heard anything more divine!"

Friedrich Nietzsche

Table of Contents

List of Figures	VII
List of Tables.....	IX
Abbreviations.....	XII
Abstract	XVII
Resumo	XIX
INTRODUCTION: HEPATIC CARBOHYDRATE AND LIPID METABOLISM	1
Carbohydrate and Lipid Metabolism in the Healthy Liver	3
Overview: role of the liver in whole-body fuel homeostasis	5
Hepatic carbohydrate metabolism	8
<i>Glucose metabolism.....</i>	8
Glucose uptake.....	9
Glycolysis and the Krebs cycle.....	11
Glycogenesis	12
The pentose phosphate pathway (PPP)	13
Glycogenolysis.....	14
Gluconeogenesis	14
<i>Fructose metabolism.....</i>	16
Hepatic fatty acid metabolism	19
Fatty acid trafficking and uptake	21
Fatty acid oxidation.....	21
De novo lipogenesis (DNL).....	23
TG formation and the TG/fatty acid cycle	24
Hepatic TG export, role of lipoprotein carriers.....	25
Regulation of hepatic metabolism	27
<i>Mechanisms of metabolic regulation.....</i>	27
<i>Hormonal and neuronal regulation of metabolic pathways in the liver</i>	28
<i>Regulation of hepatic glucose and lipid metabolism: an overall description.....</i>	29

Regulation of hepatic glucose metabolism	29
Regulation of hepatic lipid metabolism	31
<i>Insulin: signaling and metabolic effects on the liver</i>	33
Insulin control of hepatic glycogen synthesis	35
Insulin control of gluconeogenesis	37
Insulin control of lipid metabolism.....	38
<i>Glucagon: signaling and metabolic effects on the liver</i>	39
Glucagon control of glucose homeostasis.....	39
Glucagon control of lipid metabolism	41
Physiology of the Insulin-Resistant Liver: Hepatic Insulin Resistance and Related Diseases	43
The insulin-resistant liver: glucose metabolism.....	46
The insulin-resistant liver: lipid metabolism	48
Molecular basis of insulin resistance	50
<i>Lipid-induced insulin resistance</i>	50
<i>The unfolded protein response (UPR) and insulin resistance</i>	52
<i>Hepatic inflammation and insulin resistance</i>	53
Insulin resistance and related diseases	55
<i>Nonalcoholic fatty liver disease (NAFLD)</i>	56
<i>Type 2 diabetes mellitus (T2DM)</i>	58
<i>Drug-induced metabolic dysfunctions</i>	59
Glucocorticoids (GCs)	59
Antihyperglycemic agents.....	60
Second-generation antipsychotics (SGAs).....	61
Interventions in the management of metabolic diseases	64
Insulin Resistance and Metabolic Perturbations: Common Methods and Experimental Approaches	67
Rodents in metabolic research: experimental considerations	72
AIM OF THE WORK.....	79
THEORY AND METHODS.....	85

Stable Isotope Tracers for the Analysis of Hepatic Glycogen and Lipid	
Synthetic fluxes: Theoretical Aspects	87
A general protocol.....	89
NMR spectroscopy: basic principles.....	89
Tracing hepatic glycogen metabolism with stable isotopes	91
<i>²H₂O for quantification of direct and indirect pathway contributions to hepatic glycogen synthesis</i>	<i>91</i>
<i>¹³C-labeled glycogenic precursors and ¹³C-isotopomers quantification: analysis of ¹³C-MAG spectra</i>	<i>96</i>
Tracing hepatic lipid metabolism with stable isotopes.....	99
<i>¹H-NMR for lipidomic analysis.....</i>	<i>99</i>
<i>²H₂O for the quantification of lipid synthesis fluxes.....</i>	<i>102</i>
Materials and Methods	107
Animals	109
<i>Study 1.....</i>	<i>109</i>
<i>Study 2 and 3.....</i>	<i>109</i>
Reagents.....	110
Liver processing.....	110
<i>Hepatic glycogen extraction and monoacetone glucose (MAG) synthesis.....</i>	<i>111</i>
<i>Hepatic glycogen quantification</i>	<i>112</i>
<i>Liver TG extraction and purification.....</i>	<i>112</i>
TG extraction from adipose tissue	113
NMR spectra acquisition.....	113
<i>Body water ²H-enrichment.....</i>	<i>113</i>
<i>MAG.....</i>	<i>114</i>
² H - NMR spectra.....	114
¹³ C-NMR spectra.....	114
TG.....	114
¹ H-NMR spectra.....	114
² H-NMR spectra.....	115
Statistics.....	115

<i>Study 1</i>	115
<i>Study 2</i>	115
<i>Study 3</i>	116
STUDY 1	119
Determining the Contribution of a High-Fructose Corn Syrup Formulation to Hepatic Glycogen Synthesis During Ad-Libitum Feeding in Mice	121
Introduction	123
Animals and experimental set-up	125
Intervention	125
Tracers administration:	125
Sacrifice	125
Results	127
<i>Body weight and body water ²H-enrichment</i>	<i>127</i>
<i>Hepatic glycogen enrichment from ²H₂O</i>	<i>127</i>
<i>¹³C-isotopomer analysis of hepatic glycogen enrichment from exogenous [U-¹³C]glucose and [U-¹³C]fructose</i>	<i>130</i>
<i>Estimates of exogenous glucose, fructose and other substrate contributions to hepatic glycogen synthesis</i>	<i>134</i>
<i>¹³C-isotopomer analysis of liver aqueous fraction</i>	<i>136</i>
Discussion	138
Conclusions	141
STUDY 2	143
Effects of Second-Generation Antipsychotics on Hepatic Glucose and Lipid Metabolic Fluxes	145
Introduction	147
Animals and experimental set-up	149
Intervention	149
Tracer administration:	149
Sacrifice	149

Results	150
<i>In vivo analysis</i>	150
Food intake and body composition:	150
Glucose tolerance and insulin sensitivity.....	151
<i>Hepatic glycogen metabolism</i>	152
Body water, hepatic glycogen enrichment from ² H ₂ O, and fractional contributions of direct and indirect pathways to hepatic glycogenesis	152
Glycogen content and absolute contribution of glycogenic sources to hepatic glycogenesis	153
<i>Hepatic lipid metabolism</i>	155
Lipidomic analysis	155
Lipid synthetic rates.....	157
Contributions of different lipid sources to overall hepatic TG content	159
<i>Lipid metabolism in adipose tissue</i>	161
Lipidomic analysis	161
Contribution of newly synthesized TGs to total adipose TG mass.....	162
Discussion	164
Conclusions	169
STUDY 3	173
Hepatic Metabolic Fluxes in an Animal Model of Insulin Hypersensitivity: Protein-Tyrosine Phosphatase 1B (PTP-1B)-Deficient Mice	175
Introduction	177
Animals and experimental set-up	179
Intervention	179
Tracer administration:	179
Sacrifice	179
Results	180
<i>In vivo analysis</i>	180
Food intake and body composition	180
Glucose tolerance and insulin sensitivity.....	181
<i>Hepatic glycogen metabolism</i>	182
Body water, hepatic glycogen enrichment from ² H ₂ O, and fractional contributions of direct and indirect pathways to hepatic glycogenesis	182
Glycogen content and absolute contributions of glycogenic sources to hepatic glycogenesis.....	184

<i>Hepatic lipid metabolism</i>	186
Lipidomic analysis	186
Fractional synthetic fluxes and contributions of different lipid sources to overall hepatic TG content	187
Discussion	189
Conclusions	193
GENERAL DISCUSSION	195
Bibliography	201

List of Figures

Figure 1.1 - Gluconeogenesis contributions to glucose and glycogen synthesis and the recycling of glucose via the Cori cycle.	6
Figure 1.2 - Schematics of hepatic glucose metabolism.	10
Figure 1.3 - Hepatic metabolism of fructose and glucose.	18
Figure 1.4 - Schematics of hepatic lipid metabolism and lipid transfer between liver and adipocytes during feeding (top) and fasting (bottom).	20
Figure 1.5 - Hepatic insulin signaling.	34
Figure 1.6 - Hepatic glycogen deposition.	36
Figure 1.7 - Insulin/glucagon control of glycolysis and gluconeogenesis via fructose-2,6-bisphosphate.	40
Figure 1.8 - Metabolic consequences of intact (left) and impaired (right) insulin signaling in hepatocytes.	49
Figure 1.9 - Some of the most investigated molecular mechanisms of hepatic insulin resistance.	54
Figure 2.1 - Schematic representation of glycogen synthesis and positional enrichment of glycogen units from $^2\text{H}_2\text{O}$	92
Figure 2.2 - Representative ^2H -NMR spectrum of monoacetone glucose obtained from mouse hepatic glycogen.	94
Figure 2.3 - Example of ^{13}C -MAG spectrum derived from rodents administered with a [U- ^{13}C]glucose load.	97
Figure 2.4 - Representative ^1H -NMR spectrum of hepatic mouse TGs.	100

Figure 2.5 - Schematic representation of palmitate synthesis operated by the fatty acyl synthase complex FAS.	102
Figure 2.6 - Positional ² H-enrichment of TG.....	103
Figure 2.7 - ² H-NMR spectrum of hepatic mouse TGs.....	104
Figure 2.8 - Schematic representation of monoacetone glucose (MAG) synthesis from glycogen.	111
Figure 3.1 - Graphical representation of the timeline and experimental set-up employed in Study 1.	126
Figure 3.2 - Representative ² H-NMR spectra of monoacetone glucose derived from liver glycogen of a mouse fed standard chow supplemented with 30% HSCS-55 in the drinking water (a) and a mouse fed standard chow only (b).	128
Figure 3.3 - Schematic of glycogen synthesis from unlabeled endogenous sources, and exogenous [U- ¹³ C]glucose and [U- ¹³ C]fructose.....	131
Figure 3.4 - ¹³ C-NMR spectra of hepatic glycogen following derivatization to monoacetone glucose obtained from a mouse fed a HFCS-55 enriched with [U- ¹³ C]glucose (a) and [U- ¹³ C]fructose (b).	132
Figure 3.5 - Sources of hepatic glycogen synthesis in mice fed normal chow (NC, n=9) and mice fed normal chow plus a mixture of fructose and glucose in the drinking water (HS, n=12).	135
Figure 3.6 - ¹³ C-NMR spectra of liver aqueous fractions from mice provided with glucose/fructose mixtures enriched with [U- ¹³ C]glucose (a) and [U- ¹³ C]fructose (b)..	136
Figure 4.1 - Total glycogen content and absolute contributions of various glycogenic sources to overnight glycogen appearance in control mice and mice treated with either OLA or ARI over a period of seven months.	154

Figure 4.2 – Rates (% per overnight) of hepatic DNL (**4.2a**), glycerol synthesis (**4.2b**), elongation (**4.2c**) and desaturation (**4.2d**) in CTL mice and mice that underwent a 7-months treatment with either OLA or ARI. 158

Figure 4.3 - Proposed model of adipose tissue expansion in mice treated with olanzapine. 168

Figure 5.1 - Total glycogen content and absolute contributions of various glycolytic sources to overnight glycogen appearance in PTP-1B wild-type and deficient mice. 184

Figure 5.2 - Rates (% per overnight) of hepatic DNL (**5.2a**), glycerol synthesis (**5.2b**), elongation (**5.2c**) and desaturation (**5.2d**) in CTL and PTP-1B^{-/-} mice. 187

List of Tables

Table 1.1 - Lifetime of hepatic glycogen for different species. 6

Table 1.2 - Principal mechanisms of metabolic regulation. 27

Table 2.1 - Formulas employed in Study 1, 2, and 3 for the estimation of different glycolytic sources to hepatic glycogen deposition during nocturnal feeding in mice administered with ²H₂O. 95

Table 2.2 - Formulas employed in the calculation of exogenous [U-¹³C]glucose and [U-¹³C]fructose contributions to glycogen synthesis in Study 1. 98

Table 2.3 - Functional groups and chemical shift corresponding to each peak in the ¹H spectrum obtained from mice TG showed in Figure 2.4. 100

Table 2.4 - Mathematical equations utilized in Study 2 and 3 to quantify the relative amount of different lipid species in mouse liver and adipose tissue. 101

Table 2.5 - Mathematical equations utilized in Study 2 and 3 to measure lipid fractional synthetic rates (% per overnight) in mice liver and adipose tissue from ¹H-²H-NMR analysis. 105

Table 3.1 - Liver glycogen positional ² H-enrichments (H1-H6) and body water ² H-enrichments (BW) for mice fed normal chow (NC, n=9) and mice fed normal chow supplemented with 30% HFCS-55 in the drinking water (HS, n=12).	128
Table 3.2 - Fraction of newly synthesized glycogen expressed as H ₂ corr / BW and fractional contributions of different glycogenic sources to overnight glycogen appearance for mice fed normal chow (NC, n=9) and mice fed normal chow supplemented with a 30% HFCS-55 in the drinking water (HS, n=12).	129
Table 3.3 - Liver glycogen ¹³ C-isotopomer enrichments from six mice fed normal chow plus HFCS-55 in the drinking water enriched with [U- ¹³ C]glucose (HS1), and six mice fed normal chow plus HFCS-55 in the drinking water enriched with [U- ¹³ C]fructose (HS2)..	133
Table 4.1 - Body, liver and visceral depots weights in control mice and mice treated with OLA or ARI over a period of seven months.....	150
Table 4.2 - In vivo assessment of different metabolic features in OLA and ARI animals.	151
Table 4.3 - BW and liver glycogen positional ² H-enrichments (H1-H6) in control mice and mice that underwent a treatment of 7 months with either OLA or ARI..	152
Table 4.4 - Fraction of newly synthesized glycogen expressed as H ₂ corr / BW and fractional contributions of different glycogenic sources to overnight glycogen appearance in control mice and mice treated with either OLA or ARI over a period of 7 months.	152
Table 4.5 - Percentages of different lipid species in the livers of CTL mice and mice that underwent a 7-months treatment with either OLA or ARI.	155
Table 4.6 - Relative percentages of different contributions to total hepatic TG content after one overnight feeding in CTL, OLA and ARI mice.	160
Table 4.7 - Percentages and absolute values (mg) of different lipid species in epididymal adipose tissue of CTL mice and mice that underwent a 7-month treatment with either OLA or ARI.	161

Table 4.8 – Different overnight contributions of newly synthesized TGs to total adipose TG content.	163
Table 5.1 - Body, liver and visceral depots weights in wild-type and PTP-1B deficient animals of 11 months of age.	181
Table 5.2 - BW and liver glycogen positional ² H-enrichments (H1-H6) in wild-type and PTP-1B deficient mice.	182
Table 5.3 - Fraction of newly synthesized glycogen expressed as H ₂ _{corr} / BW and fractional contributions of different glycolytic sources to overnight glycogen appearance in wild-type and PTP-1B deficient animals.	183
Table 5.4 - Percentages of different lipid species in the livers of CTL and PTP-1B ^{-/-} mice.	186
Table 5.5 - Relative percentages of different contributions to hepatic lipid content in CTL and PTP- 1B ^{-/-} mice after one overnight feeding.	188

Abbreviations

¹³C - Carbon 13

¹H - Proton

²H - Deuterium

²H₂O - Deuterated water

11β-HSD1 - 11β-hydroxysteroid dehydrogenase type 1

ABCA1 - ATP-binding cassette transporter A1

ACC - Acetyl-CoA carboxylase

acetyl-CoA - Acetyl coenzyme A

ACP - Acyl carrier protein

ADP - Adenosine diphosphate

AKT - Protein kinase B

AMP - Adenosine monophosphate

Apo A-1 - Apolipoprotein A-1

Apo B-100 - Apolipoprotein B-100

ATP - Adenosine triphosphate

BCAAs - Branched-chain amino acids

BW - Body water

cAMP - Cyclic adenosine monophosphate

ChoRE - Carbohydrate response element

ChREBP - Carbohydrate response element-binding protein

CNS - Central nervous system

CO₂ - Carbon dioxide

CoA - Coenzyme A

CPT-1 - Carnitine palmitoyltransferase I

CREB protein - cAMP response element-binding protein

CRTC2 - CREB-regulated transcription coactivator 2

D - Doublet

DAG - 1,2-Diacylglycerol

DHA - Docosahexaenoic acid

DHAP - Dihydroxyacetone phosphate

DNL - *De novo* lipogenesis

DPP4 - Dipeptidyl peptidase-4

EPS - Extrapyrarnidal symptoms

ER - Endoplasmic reticulum

F-1-P - Fructose-1-phosphate

F-6-P - Fructose-6-phosphate

F-2,6-P2 - Fructose-2,6-bisphosphate

FA - Fatty acid

FADH₂ - Dihydroflavine-adenine dinucleotide

FAS - Fatty acid synthase complex

FBPase-1 - Fructose-1,6-bisphosphatase

FFAs - Free fatty acids

FGAs - First-generation antipsychotics

FOXO1 - Forkhead box protein O1

G-1-P - Glucose-1-phosphate

G-6-P - Glucose-6-phosphate

G6Pase - Glucose-6-phosphatase

G3P - Glycerol-3-phosphate

G6P-isomerase - Glucose-6-phosphate isomerase

GA3P - Glyceraldehyde-3-phosphate

GCs - Glucocorticoids

GLP-1 - Glucagon-like peptide-1

GLUT2 - Glucose transporter 2

GLUT5 - Glucose transporter 5

GSK-3 - Glycogen synthase kinase-3

GTP - Guanosine triphosphate

HDLs - High-density lipoproteins

HFD - High-fat diet

HFCS - High-fructose corn syrup

HGP - Hepatic glucose production

HOMA - Homeostasis model assessment

IKK - I κ B kinase

IL-1 β - Interleukin-1 β

IL-6 - Interleukin-6

IR - Insulin receptor

IRK - Insulin receptor kinase

IRS - Insulin receptor substrate

ITT - Insulin tolerance test

JNK - c-Jun NH₂-terminal kinase

KHK - Ketohexokinase

L-PK - Liver-type pyruvate kinase

LDL-R - LDL receptor

LDLs - Low-density lipoproteins

M - Multiplet

MAG - Monoacetone glucose

MAPK - Mitogen-activated protein kinase

mRNA - Messenger RNA

MUFAs - Monounsaturated fatty acids

NADH - Nicotinamide adenine dinucleotide (NAD) + hydrogen (H)

NADP⁺ - Nicotinamide adenine dinucleotide phosphate

NADPH - Nicotinamide adenine dinucleotide phosphate + hydrogen (H)

NAFLD - Nonalcoholic fatty liver disease

NASH - Nonalcoholic steatohepatitis

NMR - Nuclear magnetic resonance

Non- ω -3 FAs - Non-omega-3 fatty acids

OAA - Oxaloacetate

(O)GTT - (Oral) glucose tolerance test

PDK1 - Phosphoinositide-dependent kinase 1

PEP - Phosphoenolpyruvate

PEPCK - Phosphoenolpyruvate carboxykinase

PFK-1 - Phosphofructokinase-1

PFK-2/FBPase-2 - Phosphofructokinase-2/fructose-2,6-bisphosphatase

PGC1 α - Proliferator-activated receptor- γ coactivator 1- α

PH domain - Pleckstrin homology domain

PI3K - Phosphoinositide 3-kinase

PIP₂ - Phosphatidylinositol-4,5-bisphosphate

PIP₃ - Phosphatidylinositol-3,4,5-trisphosphate

PKA - Protein kinase A

PKC - Protein kinase C

PNLPA3 - Patatin-like phospholipase domain-containing protein 3

PP1 - Protein phosphatase 1

PPAR α - Peroxisome proliferator-activated receptor α

PPP - Pentose phosphate pathway

PTEN - Phosphatase and tensin homolog

PTP-1B - Protein-tyrosine phosphatase 1B

PTT - Pyruvate tolerance test

PUFAs - Polyunsaturated fatty acids

Q - Quartet

QUICKI - Quantitative insulin sensitivity check index

R_a - Rate of appearance

S - Singlet

SCFAs - Short-chain fatty acids

SFAs - Saturated fatty acids

SGAs - Second-generation antipsychotics

SGLT-2 - Sodium-glucose co-transporter-2

SHIP2 - SH2 Domain-Containing 5-Inositol Phosphatase-2

SREBP-1c - Sterol regulatory element-binding protein-1c

SU - Sulfonylureas

T2DM - Type 2 diabetes mellitus

TG - Triglyceride

TNF α - Tumor necrosis factor α

Triose-Ps - Triose phosphates

TZDs - Thiazolidinediones

UCP - Uncoupling protein

UDPG - Uridine diphosphate glucose

UPR - Unfolded protein response

UTP - Uridine triphosphate

UV - Ultraviolet

VAT - Visceral adipose tissues

VHFD - Very-high-fat diet

VLDL - Very-low-density lipoproteins

Xu-5-P - Xylulose-5-phosphate

ω -3 FAs - Omega-3 fatty acids

Abstract

Humans evolved in environments where calorie supply and availability were scarce and unpredictable, thereby developing mechanisms that allowed them to store nutrients during times of plenty for utilization in times of need. In a remarkably short time, humanity has managed to profoundly change the environment from which it originally evolved. Nowadays, food is easily available in most societies and is frequently consumed in excess. At the same time, caloric requirements have diminished as lifestyle has become more sedentary. As a consequence, obesity and associated diseases became endemic in the last fifty years and have currently taken a tremendous toll on many aspects of society.

Insulin resistance is considered a *sine qua non* for the development and progression of most common metabolic diseases. Although insulin resistance induces a multi-organ pathological response, disruption of insulin regulation has different manifestations on the various insulin-sensitive tissues of an organism.

The liver plays a central role in systemic glucose and lipid homeostasis and a well-coordinated hepatic metabolism is essential for the overall metabolic health. Hepatic insulin resistance is an important element in the pathogenesis and precipitation of metabolically altered states and many therapeutic approaches target the liver specifically. Insulin governs metabolic fluxes in the liver by stimulating anabolic pathways during states of nutrients abundance, mostly by prompting glycogen and lipid synthesis. Thus, impaired glycogen deposition and aberrant lipid production are major hallmarks of the insulin-resistant liver.

This thesis is constructed around three sets of animal model studies that applied stable isotope tracers coupled with Nuclear Magnetic Resonance (NMR) analysis of their enrichment of hepatic glycogen and/or lipids. The objectives were to enhance our understanding on the impact of diet, drugs and genetic manipulation - mediated in part by their effects on hepatic insulin actions - on hepatic glycogen and lipid metabolism.

In Study 1, we combined the use of deuterated water ($^2\text{H}_2\text{O}$) with ^{13}C uniformly labeled fructose and glucose to study the effect of high-fructose corn syrup, a very much investigated nutrient in the context of metabolic diseases, on hepatic glycogenesis in mice fed a high-sugar diet for a prolonged period of time. We observed that the fructose and the glucose components of the sugar administered to the animals under study contributed equally to hepatic glycogenesis. Moreover, overall glycogen synthesis and glycogen deposition via direct pathway were not compromised after chronic high-sugar feeding in mice.

In Study 2, $^2\text{H}_2\text{O}$ was employed for the first time to examine the effects of second-generation antipsychotics, widely used medications associated with detrimental metabolic side effects, on hepatic metabolic fluxes in mice. Despite some early systemic metabolic alterations, we found intact hepatic glycogen and lipid fluxes in animals treated with second-generation antipsychotics over a period of seven months.

In Study 3, $^2\text{H}_2\text{O}$ was utilized to characterize the hepatic metabolism of PTP-1B knockout mice, an animal model of insulin hypersensitivity. We observed reduced glycogen concentration and lipid synthetic fluxes in PTP-1B knockout mice, an outcome that contradicted our expectations from a mouse model of hypersensitivity to insulin.

Resumo

Os seres humanos evoluíram em ambientes onde o provimento e a disponibilidade calórica eram escassos e imprevisíveis, por isso desenvolveram mecanismos que lhes permitiram armazenar nutrientes durante tempos de abundância para serem utilizados em tempos de necessidade. Num espaço de tempo notavelmente curto, a humanidade conseguiu mudar profundamente o ambiente do qual originalmente evoluiu. Nos nossos dias, os alimentos estão facilmente disponíveis na maioria das sociedades e frequentemente são consumidos em excesso. Ao mesmo tempo, as exigências calóricas diminuíram à medida que o estilo de vida se tornou mais sedentário. Como consequência, a obesidade e as doenças associadas tornaram-se endêmicas nos últimos cinquenta anos e atualmente têm tido um tremendo impacto em muitos aspetos da sociedade.

A resistência à insulina é considerada *sine qua non* para o desenvolvimento e progressão das doenças metabólicas mais comuns. Embora a resistência à insulina induza uma resposta patológica multi-orgão, a rutura da regulação da insulina resulta em manifestações diferentes nos vários tecidos dependentes da insulina de um organismo.

O fígado desempenha um papel central na homeostase da glicose sistémica e lipídica, e um metabolismo hepático bem coordenado é essencial para a saúde metabólica geral. A resistência hepática à insulina é um elemento importante na patogénese e no rápido aparecimento de estados metabolicamente alterados e muitas abordagens terapêuticas visam especificamente o fígado. A insulina rege os fluxos metabólicos no fígado, estimulando as vias anabólicas durante estados de abundância de nutrientes, principalmente por promover a síntese de glicogénio e de lípidos. Assim, alterações no armazenamento de glicogénio e uma síntese lipídica aberrante são os principais sinais de um fígado resistente à insulina.

Esta tese é construída em torno de três conjuntos de estudos em modelos animais nos quais foram utilizados marcadores com isótopos estáveis, combinados com a análise do seu enriquecimento no glicogénio hepático e/ou lípidos por Ressonância Magnética Nuclear (RMN). Os objetivos foram o aprofundamento da nossa compreensão sobre o impacto da dieta, drogas e

manipulação genética - mediado em parte pelos seus efeitos sobre a ação da insulina no fígado - no metabolismo hepático do glicogénio e lipídico.

No Estudo 1, combinámos a utilização da água deuterada ($^2\text{H}_2\text{O}$) com frutose e glicose uniformemente marcadas com ^{13}C para estudar o efeito do xarope de milho com elevado teor de frutose, um nutriente muito investigado no contexto de doenças metabólicas, na glicogénese hepática em murganhos alimentados com uma dieta rica em açúcar durante um período prolongado de tempo. Observámos que a frutose e a glicose, componentes do açúcar administrado aos animais estudados, contribuíram de igual forma para a glicogénese hepática. Além disso, a síntese e o armazenamento do glicogénio pela via direta não ficaram comprometidos nos murganhos após uma alimentação crónica com elevado teor de açúcares.

No Estudo 2, empregámos a $^2\text{H}_2\text{O}$ para examinar os efeitos de medicamentos antipsicóticos de segunda geração nos fluxos metabólicos hepáticos em murganhos. Apesar de algumas alterações metabólicas sistémicas precoces, verificámos que os fluxos de glicogénio e de lípidos hepáticos se encontravam intactos naqueles animais tratados com antipsicóticos de segunda geração durante um período de sete meses.

No Estudo 3, foi utilizada a $^2\text{H}_2\text{O}$ para caracterizar o metabolismo hepático em murganhos knockout para PTP-1B, um modelo animal de hipersensibilidade à insulina. Observámos uma redução da concentração de glicogénio e dos fluxos de síntese lipídica nos murganhos knockout para PTP-1B, um resultado que contradisse as nossas expectativas para um modelo de murganho de hipersensibilidade à insulina.

**INTRODUCTION: HEPATIC
CARBOHYDRATE AND LIPID
METABOLISM**

***Carbohydrate and Lipid Metabolism in the
Healthy Liver***

Overview: role of the liver in whole-body fuel homeostasis

The liver is a key metabolic organ that coordinates nutrient availability with whole-body substrate demands for energy generation and biosynthesis of cellular components. For these processes to be performed with the maximum caloric efficiency while at the same time ensuring optimal energy substrate availability for all tissues of the body, the liver has a central role in fuel homeostasis. Circulating glucose is the primary fuel for the central nervous system (CNS) and the sole energy substrate for erythrocytes, hence there is a critical requirement for maintaining blood glucose levels above a baseline level. Excessive concentrations of circulating glucose, while not immediately life-threatening, are harmful to many tissues. Therefore, circulating glucose levels are continuously maintained within a relatively narrow concentration range. The liver plays a key role in buffering blood glucose levels in the face of a discontinuous availability of external carbohydrate during feeding and fasting states.

In the postprandial state, when glucose availability exceeds endogenous demands, the liver converts a substantial portion of this excess glucose to glycogen. A smaller part is also converted to lipid via the process of *de novo* lipogenesis. Once glucose absorption from the meal ceases, the liver upregulates its capacity for endogenous glucose production to maintain systemic demands. The previously stored glycogen is hydrolyzed to glucose via glycogenolysis, which is then released into the bloodstream. Since there is insufficient hepatic glycogen for maintaining systemic glucose demands beyond the short term (Table 1.1) glucose is also produced from non-carbohydrate precursors by the process of gluconeogenesis (Figure 1.1). Although recent studies have identified gluconeogenic capacity in other tissues, notably kidney and intestine, the liver is considered to be the main site for this process. Also, new roles of gluconeogenesis above and beyond the sustenance of endogenous glucose production in the fasted state have been identified. These include a significant contribution to hepatic glycogen synthesis during feeding via the so-called indirect

pathway as well as the extensive recycling of circulating glucose carbons via the Cori cycle as shown in Figure 1.1.

Table 1.1 - Lifetime of hepatic glycogen for different species.

Specie	Hepatic glycogen lifetime	Reference Paper
Mouse	12 hours	Geisler <i>et al.</i> , 2016 [1]
Rat	24 hours	Dohm <i>et al.</i> , 1983 [2]
Guinea pigs	24 hours	Fréminet <i>et al.</i> , 1980 [3]
Bat	24 hours	Freitas <i>et al.</i> , 2003 [4]
Human	48 hours	Nilsson <i>et al.</i> , 1973 [5]
Dog	72 hours	De Bruijne <i>et al.</i> , 1983 [6]
Seabass	21 days	Martins <i>et al.</i> , 2013 [7]
Turtle	30 days	Oliveira <i>et al.</i> , 2013 [8]

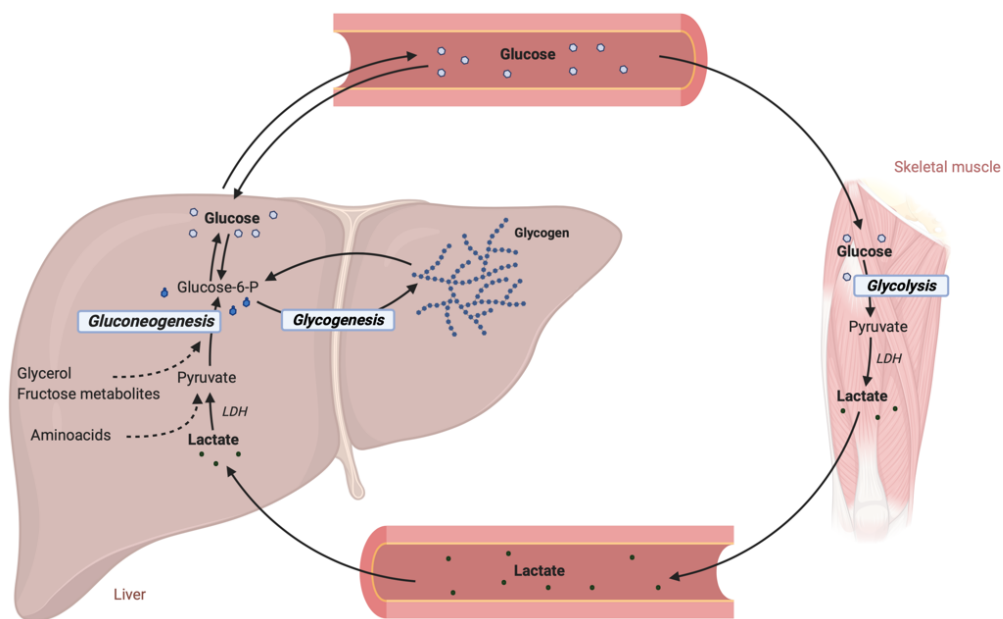


Figure 1.1 - Gluconeogenesis contributions to glucose and glycogen synthesis and the recycling of glucose via the Cori cycle. Lactate produced during anaerobic glycolysis in skeletal muscle is transported to the liver where it is reconverted to glucose via gluconeogenesis. The glucose produced during gluconeogenesis is mostly released into circulation during fasting but can also be used to replenish hepatic glycogen stores during feeding. Some metabolic intermediates have been omitted for clarity. [Figure created with BioRender.com].

For tissues other than the CNS which comprise most of the lean body mass and include the heart, skeletal muscle and kidneys, the bulk of their metabolic energy requirements are met by lipid oxidation. While storage of excess lipid during feeding and release of free fatty acids fuel during fasting is mediated by adipocytes either adjacent to or embedded in these peripheral tissues, the liver plays key roles in the transfer of lipids to adipocytes after feeding, and in regulating the levels of circulating free fatty acids during fasting (Figure 1.4). Regulation of glucose and lipid homeostasis is highly interconnected for at least three important reasons. First, the bulk of the body's tissues can use either lipid or glucose for energy according to the availability of each substrate. Since glucose is a mandatory fuel for the CNS and erythrocytes, its uptake and consumption by other tissues are inhibited by abundant lipid levels giving rise to the reciprocal control of glucose and lipid oxidation in heart and muscle, as originally postulated by Randle [9]. Second, an excess of dietary glucose above and beyond the capacity for storage as glycogen can be re-purposed as a long-term energy source by conversion into lipid, much of which is mediated by the liver. Third, under conditions of low glucose availability, where endogenous glucose production is unable to meet whole body demand such as during prolonged fasting, fatty acids are converted to ketone bodies by the liver. Ketone bodies can be oxidized for energy by the CNS thereby extending CNS survival.

Hereby we will go over the most important aspects of the human liver physiology, focusing on glucose and fatty acid metabolism. The objective of this chapter is to draw a clear picture of the intricate mechanisms and regulatory processes that go under the definition of functional hepatic metabolism and whose understanding is fundamental for the comprehension of what is, on the other hand, considered dysfunctional.

Hepatic carbohydrate metabolism

Dietary carbohydrates can be categorized as digestible and non-digestible. Digestible carbohydrates include simple and complex carbohydrates that are converted into monosaccharides by enzymes present in the saliva, stomach and intestine; while non-digestible carbohydrates such as fibers and resistant starches, cannot be broken down by digestive enzymes and reach the large intestine without being absorbed into the body. In the large intestine, non-digestible carbohydrates can become the substrate of the intestinal microbiota that metabolizes them into short-chain fatty acids (SCFAs) and some gases. SCFAs are either used as a source of energy by the bacteria, are excreted in the feces, or absorbed into the cells of the colon with a small fraction being transported to the liver.

Although digestible carbohydrates come from several sources and are of different types and lengths, they are all digested and broken down into three simple monosaccharides: glucose, fructose and galactose. Glucose is preferentially uptaken and metabolized by extra-splanchnic tissues such as muscle and brain that absorb approximately two-thirds of the ingested glucose [10], whereas fructose and galactose are predominantly metabolized by the liver. Galactose's primary metabolic pathway is the Leloir pathway that converts it into intermediates of glucose metabolism. On the other end, intact fructose cannot be directly converted into glucose and it is broken down into three-carbons precursors before being further metabolized. In the following paragraphs, we will review the metabolic fates of glucose and fructose, well-described in the literature especially from a liver-centric perspective.

Glucose metabolism

As shown in Figure 1.2 the liver has a very high degree of metabolic flexibility with regard to glucose, including the capacity for net glucose utilization for sustaining numerous biosynthetic pathways as well as net glucose production to maintain whole-body glucose homeostasis. The main

pathways involved in net hepatic glucose utilization are glycolysis, glycogenesis and the pentose phosphate pathway, while net hepatic glucose production involves glycogenolysis and gluconeogenesis.

Glucose uptake

Glucose uptake into hepatocytes occurs by concentration gradient through GLUT2. GLUT2 is a glucose transporter that, when compared to other glucose transporters prevalently expressed in other tissues, has high capacity but low affinity for its substrate. GLUT2 rate of transport is directly proportional to the change in glucose concentration; this ensures rapid equilibrium of glucose across the hepatocyte membrane and only the uptake of glucose in the concentration range required for glucose homeostasis. In the postprandial state, when circulating glucose levels are high, there is a net import of glucose inside the hepatocytes; but during fasting, when circulating glucose is scarce, the concentration of free glucose is higher inside the cell as a result of increased glycogenolysis and gluconeogenesis and thus, glucose leaves the hepatocyte through GLUT2 which is also responsible for transporting glucose out into circulation [11]. Upon entry, glucose is phosphorylated by glucokinase on the sixth carbon, generating glucose-6-phosphate (G-6-P) at the expense of one molecule of ATP. This step is fundamental to retain glucose inside the hepatocyte and to allow further uptake of exogenous glucose by diminishing the concentration of free glucose inside the cell. Glucokinase is a specific hexokinase isozyme predominantly expressed in the liver and pancreatic β -cells that, unlike other hexokinases, has low affinity for glucose and is not inhibited by physiological concentrations of its product (G-6-P) [12], [13].

G-6-P is the first intermediate of glucose metabolism and lies at the crossroads of several metabolic pathways, including glycolysis, glycogenesis and the pentose phosphate pathway.

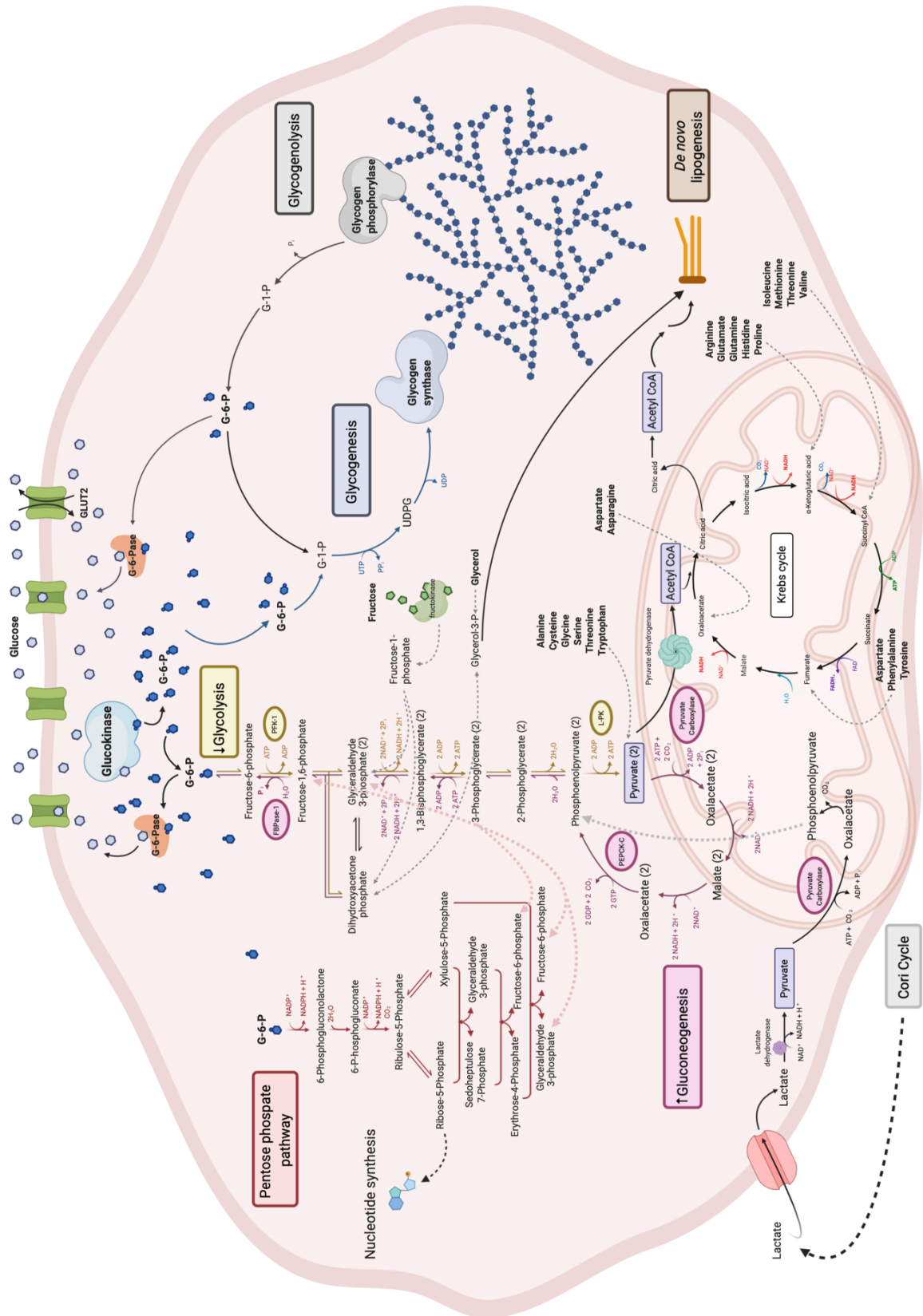


Figure 1.2 - Schematics of hepatic glucose metabolism [Figure created with BioRender.com].

Glycolysis and the Krebs cycle

Glycolysis is a cytosolic process that partially oxidizes a molecule of G-6-P into two molecules of pyruvate, with a net gain of two ATP and two NADH. Out of a total of ten reactions, three are irreversible and are catalyzed by enzymes that are tightly regulated by hormones which generally promote catabolic pathways [14]. The three rate-limiting reactions of glycolysis are: glucose phosphorylation on position 6 (considered in this context the first reaction of glycolysis) catalyzed by glucokinase, the conversion of fructose-6-phosphate (F-6-P) into fructose-1,6-bisphosphate catalyzed by phosphofructokinase-1 (PFK-1), which ultimately commits G-6-P to glycolysis; and finally, a reaction catalyzed by a liver-type pyruvate kinase (L-PK) which converts phosphoenolpyruvate (PEP) into pyruvate.

Under aerobic conditions, pyruvate is transported into the mitochondrion and decarboxylated to form acetyl-coenzyme A (acetyl-CoA) in an irreversible reaction catalyzed by pyruvate dehydrogenase. Acetyl-CoA further proceeds into the Krebs cycle to be fully oxidized to CO₂ in a series of reactions yielding a molecule of GTP as well as reducing equivalents NADH and FADH₂ which, together with the NADH produced during glycolysis, are oxidized in the mitochondrial respiratory chain for ATP production.

When cellular ATP and NADH levels are high, such as after feeding, acetyl-CoA is recruited for fatty acid synthesis in the cytosol via *de novo* lipogenesis. Transfer of acetyl-CoA from the mitochondrion to the cytosol occurs in the form of citrate via a citrate transporter in the mitochondrial inner membrane. In the cytosol, citrate is converted to acetyl-CoA and oxaloacetate by ATP citrate lyase [13].

Glycolysis is active in the liver in the fed state, but contrary to tissues such as the brain or exercising skeletal muscle, the liver does not derive a significant portion of its energy needs from this pathway. Instead, it can be considered to be part of the conduit for converting excess carbohydrate into lipid. Moreover, the generation of ATP and reducing equivalents from

conversion of glucose to acetyl-CoA does not meet the ATP and NADPH requirements for acetyl-CoA conversion into fatty acid. Therefore overall, the conversion of glucose to lipid has a negative energy balance.

Glycogenesis

G-6-P is also the precursor for glycogen synthesis. When G-6-P is abundant inside the cell, is first isomerized into glucose-1-phosphate (G-1-P) and then converted into the active form of glucose, UDPG, using one molecule of uridine triphosphate (UTP). Glycogen synthase elongates glycogen chains attaching UDPGs to a non-reducing end of the on-growing polymer via an α -1/4 linkage. The α -1-6 bonds that give glycogen its typical branched structure, are introduced by a branching enzyme which links a glucosyl chain of 6-8 units via α -1-6 linkage to a more interior position in the chain. This specific structure allows the glycogen polymer to be more accessible to the enzymes responsible for both its synthesis and degradation [13].

The G-6-P molecules recruited for glycogenesis have several metabolic origins. In the fed state, when glucose is abundant, and glycogenesis is fully operative, around 50-60% of glycogen units are derived from dietary glucose through the so-called direct pathway (glucose \rightarrow G-6-P \rightarrow G-1-P \rightarrow UDPG \rightarrow glycogen) [15]. Thus, by this first-pass clearance of absorbed glucose, the direct pathway is an integral component of postprandial glucose homeostasis. The remaining 40-50% of glycogen is derived via the indirect pathway, where gluconeogenic three carbons precursors generated either hepatically or extrahepatically are converted into G-6-P. Indirect pathway precursors include all gluconeogenic substrates that normally sustain endogenous glucose production such as lactate derived from extra-hepatic tissues (i.e., Cori cycle), amino acids and glycerol. Metabolism of dietary fructose also feeds the indirect pathway, (see page 11). Formally, the indirect pathway also includes hepatic glucose that was metabolized to pyruvate via glycolysis and then converted into G-6-P via gluconeogenesis.

It has been proposed that the indirect pathway is prevalent in the periportal cells of the liver, which

have high gluconeogenic capacity, while the direct pathway is more favored in the pericentral and perivenous regions which receive more oxygen and nutrients and thus might utilize the direct pathway as preferential route [16], [17]. Although this theory has not been corroborated by substantial evidence and the physiological role of the indirect pathway is still rather obscure, the indirect pathway is essential for functional glycogen deposition and an adequate understanding of the mechanisms that regulate direct and indirect pathways is fundamental to comprehend the basis of functional glycogen metabolism.

The pentose phosphate pathway (PPP)

Another oxidative fate of G-6-P is the pentose phosphate pathway (PPP) which converts G-6-P into pentose phosphates and also mediates exchanges between F-6-P and pentose pathway intermediates. Unlike glycolysis, this pathway does not have the catabolic function of generating ATP but instead provides metabolic precursors and co-factors for anabolic processes and for counteracting oxidative stress. The unique PPP products are ribose-5-phosphate and NADPH; the first serves as skeleton for nucleotide synthesis, whereas the second is a co-factor reductant that is necessary for the regeneration of reduced glutathione, and for many biosynthetic pathways, including *de novo* lipogenesis.

The partitioning of G-6-P among other pathways and the PPP is in part regulated by the cytosolic $\text{NADP}^+/\text{NADPH}$ ratio. The first part of the PPP cycle is coupled to the reduction of NADP^+ to NADPH; if the cytosolic $\text{NADP}^+/\text{NADPH}$ is low (i.e., high abundance of reducing equivalents), then G-6-P recruitment by the PPP is attenuated and diverted to alternative pathways instead, such as glycolysis and glycogenesis [13].

The first part of the PPP consists of a series of reactions known as oxidative phase that yields ribulose-5-phosphate and NADPH. Ribulose-5-phosphate is then isomerized into ribose-5-phosphate and used as precursor for the synthesis of nucleic acids. The remaining ribulose-5-phosphate carbons are recycled to G-6-P by the non-oxidative phase of the PPP [13].

The product of the first reaction of the non-oxidative phase, xylulose-5-phosphate (Xu-5-P), has been suggested to play an important role in potentiating the conversion of glucose to lipid. In the setting of high glucose inflow during feeding, elevated Xu-5-P concentrations, alongside those of G-6-P, have been shown to promote glycolytic flux and stimulate the transcription of genes expressing enzymes required during the process of *de novo* lipogenesis [18].

Glycogenolysis

When systemic glucose demand exceeds dietary supply, hepatic glycogenolysis and gluconeogenesis assume critical importance in maintaining glucose homeostasis.

Hepatic glycogen is degraded in the process of glycogenolysis. Unlike skeletal muscle, which is the other major glycogen producer of the body, the metabolic significance of glycogen synthesis in the liver is not of storing energy for its own consumption, but to provide glucose for other tissues during times of scarcity. Thus, while glycogen in the muscle functions as an energy resource available to muscle cells only, the liver does not utilize glycogen for its own energetic requirement but releases in circulation its glycogen reserves in order to maintain blood glucose concentrations within specific limits [13].

The two key enzymes of this process are glycogen phosphorylase and the glycogen debranching enzyme. Glycogen phosphorylase releases glycogen units as G-1-P from the linear chain components while the glycogen debranching enzyme releases glycogen units at the level of the branching points. G-1-P is then converted into G-6-P by phosphoglucomutase and G-6-P is dephosphorylated by glucose-6-phosphatase (G6Pase) prior release as free glucose.

Gluconeogenesis

During prolonged fasting, the majority of glucose is produced in the liver through gluconeogenesis, the process of converting pyruvate and other gluconeogenic precursors into G-6-P. The G-6-P produced by this pathway is used for both replenishing glycogen reserves (indirect

pathway) and maintaining physiological circulating glucose concentrations. The pyruvate fed into gluconeogenesis has several metabolic origins. It can be the product of hepatic glycolysis, or it can derive from the lactate produced in the muscle following glycolysis in the so-called Cori cycle. Amino acids are also effective gluconeogenic precursors, particularly during prolonged starvation. Apart from leucine and lysine, all amino acids can be transformed into Krebs cycle intermediates such as pyruvate and oxaloacetate and utilized for gluconeogenesis. Fructose metabolites are also utilized to make glucose through gluconeogenesis. Finally, glycerol deriving from adipose tissue lipolysis can too be used in this pathway and it is the only triglyceride component exploited in this process, as fatty acids carbons cannot be used for endogenous glucose production.

Gluconeogenesis and glycolysis can be considered inverse processes and share several enzymes. However, the three key irreversible reactions of glycolysis have to be performed in reverse by different enzymes during gluconeogenesis. Gluconeogenesis begins with the conversion of pyruvate into oxaloacetate by pyruvate carboxylase, a reaction that takes place in the mitochondrion. Oxaloacetate has to be utilized in the cytosol where the rest of the gluconeogenic enzymes are, it is therefore reduced to malate, exported out by a specific malate transporter, and then reconverted into oxaloacetate in the cytosol where phosphoenolpyruvate carboxykinase (PEPCK) phosphorylates it into PEP. This is the first highly regulated, irreversible and energetic expensive reaction of gluconeogenesis. This sequence of events is fundamental because reducing equivalents are also transferred along with the substrates in the cytosol, where they are scarce but essential for the next gluconeogenic steps. One molecule of NADH is indeed formed during the re-oxidation of malate to oxaloacetate and is later consumed in subsequent gluconeogenic reactions. When pyruvate derives from lactate, it bypasses the malate conversion step, and oxaloacetate is directly converted into PEP by a mitochondrial isozyme of PEPCK and transported out in the cytosol where it continues with the following gluconeogenic steps. The conversion into malate is in fact redundant in this case, as the oxidation of lactate into pyruvate operated by lactate dehydrogenase in the cytosol already generates a molecule of NADH.

PEP undergoes a series of reversible reactions to be finally converted into triose phosphates (triose-Ps), molecules that are condensed together to form fructose-1,6-bisphosphate. Glycerol and fructose metabolites can enter gluconeogenesis at this point by being directly converted into triose-Ps. Fructose-1,6-bisphosphate is then dephosphorylated of the phosphate group in position 1 in the second rate-limiting reaction of gluconeogenesis performed by fructose-1,6-bisphosphatase (FBPase-1) [13]. Finally, fructose-6-phosphate is converted into G-6-P which has to be dephosphorylated prior release into circulation through GLUT2. The enzyme responsible for this third irreversible reaction is G-6-Pase, that also dephosphorylates the G-6-P resulting from glycogen degradation. This is an enzyme expressed only in the liver and in other subsidiary gluconeogenic tissues such as kidney and intestine. The liver is the primary glucose producer in the body, but kidneys and intestine have increased contributions during prolonged fasting [19].

Fructose metabolism

A healthy diet contains an appreciable amount of fructose, found mostly in fruits and vegetables. Sucrose, which is a disaccharide composed of glucose and fructose, is the main circulating sugar in plants and is abundant in sweet fruits. While fructose is metabolized differently from glucose, each sugar promotes the metabolism of the other in a synergistic manner (Figure 1.3). Fructose enters intestinal cells mainly by facilitated diffusion through GLUT5, a transporter that has high affinity for fructose. GLUT2 also participates in this process, despite its lower affinity for fructose. Small doses of fructose can be almost entirely cleared by the small intestine and converted into glucose and organic acids prior release into circulation; however, high fructose doses saturate intestinal fructose clearance resulting in fructose spilling into circulation. [20]. Once released into the portal vein, fructose is for the major part extracted by the liver [21]. Only a minimal proportion of an oral fructose load reaches extra-splanchnic tissues, although several of them such as muscle, adipose tissue and kidney express GLUT5 and other enzymes involved in fructose metabolism.

GLUT2 is the transporter responsible for hepatic fructose uptake as the liver does not express GLUT5 abundantly [22]. Inside the hepatocyte, fructose is rapidly phosphorylated to fructose-1-phosphate (F-1-P) by ketohexokinase (KHK, also known as fructokinase) and F-1-P is then metabolized into the triose-Ph dihydroxyacetone phosphate (DHAP) and glyceraldehyde-3-phosphate (GA3P).

Fructose does not stimulate insulin secretion and fructolysis is not subjected to insulin control. KHK operates with phosphorylation rates 10 times higher than glucokinase's [23], whose activity is governed by insulin; whereas KHK is neither feed-back inhibited nor allosterically regulated. Moreover, fructolysis bypasses an important control checkpoint: the first, rate-limiting reaction of glycolysis performed by the enzyme PFK-1, whose activity is allosterically inhibited by high concentration of ATP and thus high energy statuses. This lack of regulation results in an unrestrained production of triose-Phs, substrates that can potentially fuel all major metabolic pathways in the liver such as glycolysis, gluconeogenesis, glycogen synthesis and *de novo* lipogenesis.

The role of dietary fructose consumption in human metabolism is controversial and has been associated with the surge of diabetes and metabolic diseases in western societies that consume high quantities of fructose through processed foods and sugar-sweetened beverages. It is well established that high fructose intake promotes hepatic steatosis, insulin resistance and high levels of circulating triglycerides [24]. Nonetheless, fructose is an important nutrient found in nature and moderate fructose consumption has no deleterious effect on the overall metabolism. On the contrary, small amounts of fructose, usually ingested along with glucose as part of the same meal, enhance glucose absorption and disposal through several mechanisms. Catalytic amounts of F-1-P positively regulate glucokinases; and by inhibiting glycogen phosphorylase, promote glycogen accumulation. The regulatory properties of F-1-P might have evolved as a "sugar sensing" mechanism, that informs the cell that sugar has been ingested and the metabolic machinery to process it needs to be potentiated [22].

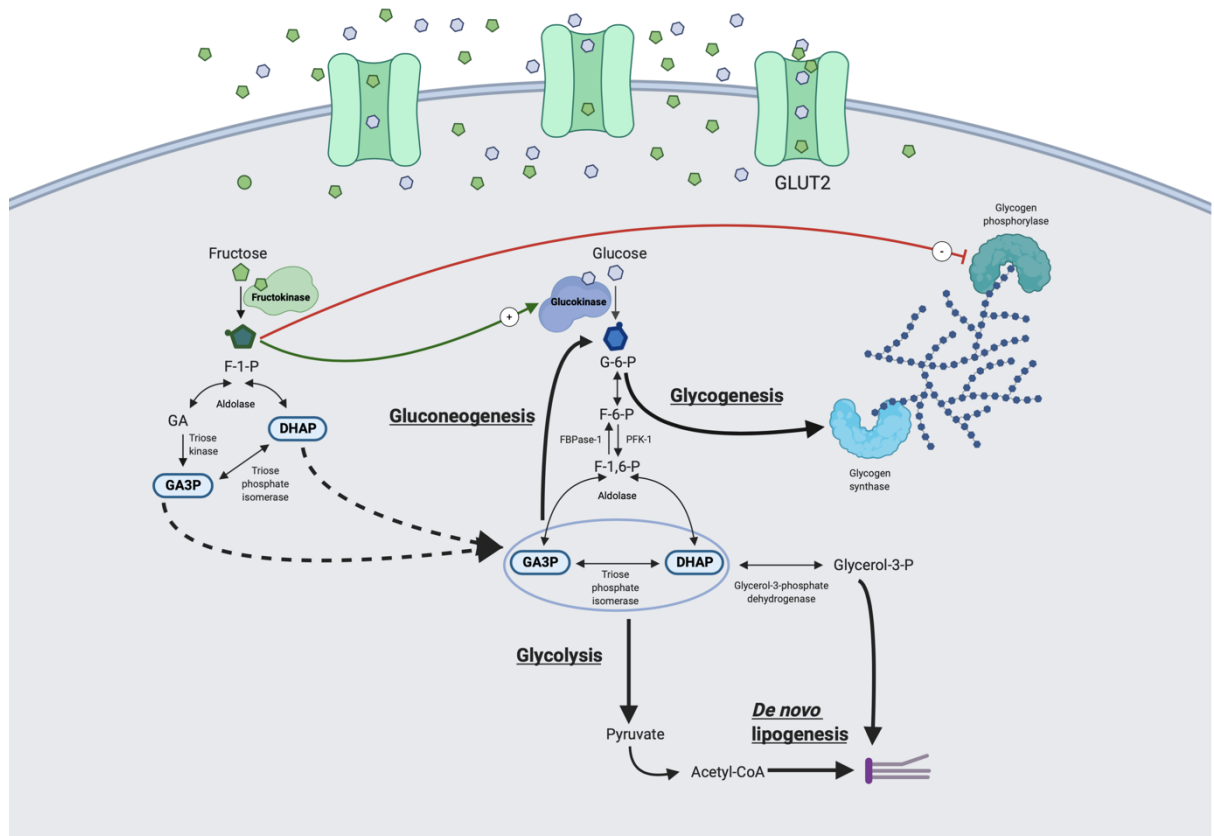


Figure 1.3 - Hepatic metabolism of fructose and glucose. While catalytic amounts of fructose promote glucose absorption and disposal via F-1-P by allosterically regulating enzymes such as glucokinase and glycogen phosphorylase, excessive fructose concentrations compete with glucose for glycogen and lipid synthesis in the liver. Fructose-derived GA3P and DAHP enter the glucose-derived glycolytic and gluconeogenic metabolite pool at the triose-P level. This results in the upregulation via substrate push of all glucose-related metabolic pathways in the liver, among which glycogenesis and *de novo* lipogenesis. [Figure created with BioRender.com].

Hepatic fatty acid metabolism

The liver plays a major role in storing, producing and providing glucose to other organs in need during times of “scarcity”, but its own energetic demands are for the most part fulfilled by the oxidation of fatty acids. Fatty acids are an excellent source of energy bearing more than double the energy of equivalent quantities of carbohydrates and proteins and, because of their chemical properties, can be stored efficiently and in large amounts in the form of triglycerides (TGs).

The liver fulfils its lipid demand in several ways. After a meal, a part of ingested lipids is uptaken by the liver to be stored in cytosolic particles or released inside very-low-density lipoproteins (VLDL), while dietary carbohydrates in excess are converted into lipids through the process of *de novo* lipogenesis, them too stored in the cytosol or packed into VLDLs and delivered to other organs, among which adipose tissue, the major storage site for fat in the body.

During fasting, a lipolytic program is initiated in the adipose tissue and free fatty acids (FFAs) are released into circulation. Circulating FFAs are directly absorbed from the plasma into the liver and can be either oxidized to produce energy and ketone bodies or re-esterified back into TGs.

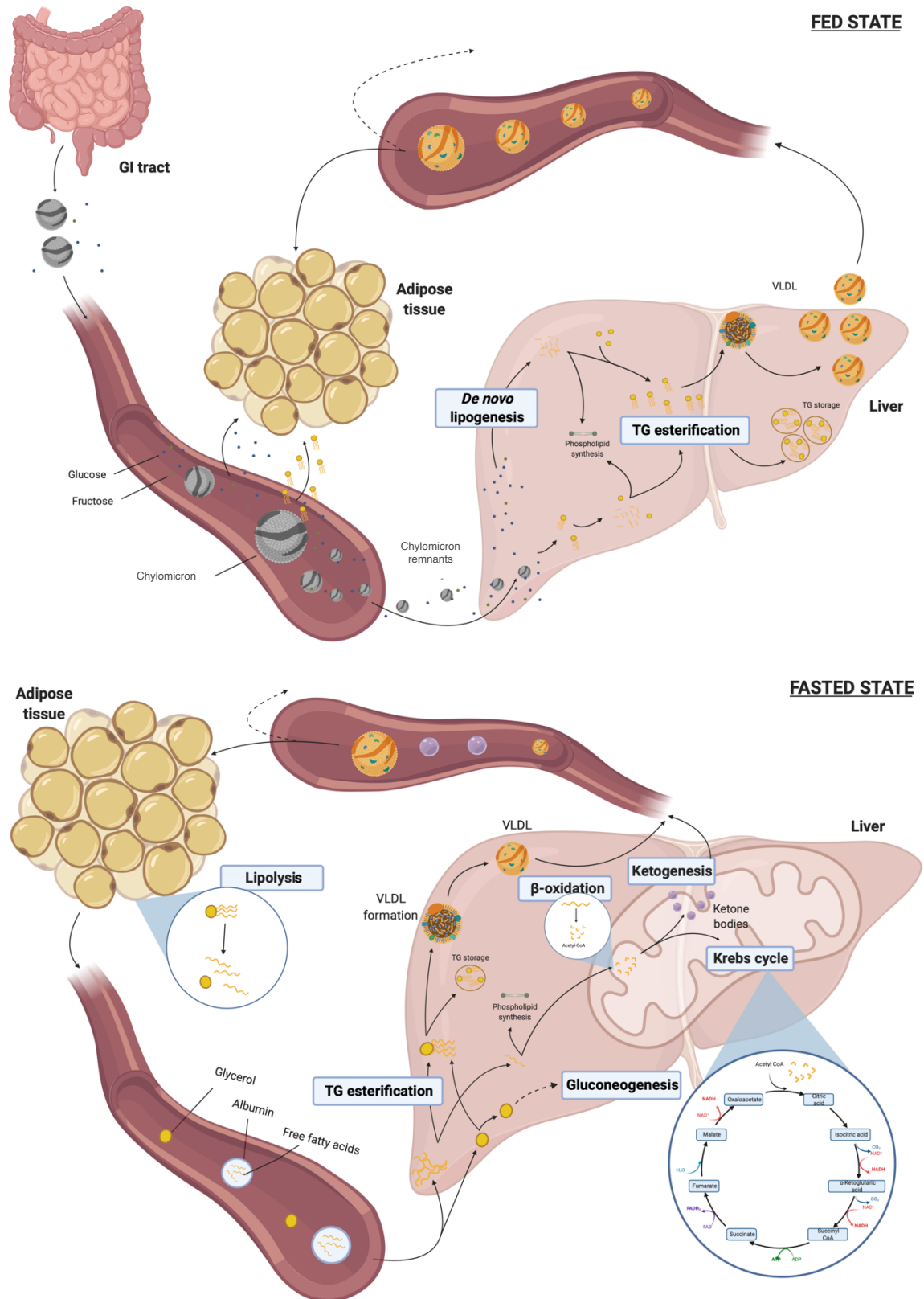


Figure 1.4 - Schematics of hepatic lipid metabolism and lipid transfer between liver and adipocytes during feeding (top) and fasting (bottom). [Figure created with BioRender.com].

Fatty acid trafficking and uptake

Fatty acids are insoluble in water, therefore their mobilization requires special mechanisms that counteract their insolubility. Inside the intestinal lumen, ingested TGs need to be emulsified by bile acids in order to be partially digested by pancreatic lipases and absorbed by enterocytes. In the cell, TGs are reassembled and packaged inside chylomicrons, large lipoprotein produced by intestinal cells. Chylomicrons are then released in the lymphatic system and eventually reach circulation. TGs in chylomicrons are taken up by muscle and adipose tissue first, whose endothelial surfaces express lipoprotein lipases; the remaining TGs are then delivered to the liver where chylomicron remnants are internalized by hepatocytes through receptor-mediated endocytosis [25]. On the other hand, FFAs deriving from lipolysis in the adipose tissue circulate in the bloodstream attached to albumin. Upon reaching their target organ, FFAs dissociate from albumin to be transported inside the cell by plasma membrane-associated proteins or by simple diffusion. Once inside, FFAs are immediately bound to cytoplasmatic proteins and/or esterified to coenzyme A (CoA). FFAs can be either re-esterified to TGs or used for the synthesis of complex lipids like phospholipids. However, especially during fasting conditions, a considerable fraction of FFAs is oxidized to generate ATP.

Fatty acid oxidation

The prevalent route for fatty acids catabolism is referred as β -oxidation and takes place for the most part in the mitochondria where the enzymes responsible for this pathway reside. Fatty acids need therefore to cross the double membrane structure of this organelle and reach the matrix. Carbon chains shorter than 10 carbons can diffuse across mitochondrial membranes without any facilitated transport, but longer chains undergo a sequence of three enzymatic reactions known as carnitine shuttle. First, a molecule of acetyl-CoA is attached to the fatty acid chain to yield a fatty acyl-CoA at the expense of one molecule of ATP. Fatty acyl-CoA is then converted into fatty acyl-carnitine by carnitine palmitoyltransferase I (CPT-1). This reaction commits the fatty acid chain to

the oxidative pathway and is rate-limiting, setting the pace to the whole process. CPT-1, allosterically inhibited by malonyl-CoA, the first intermediate of *de novo* lipogenesis, is in fact the key enzyme in this process. This concerted regulation guarantees that fatty acid oxidation is turned down if lipids are produced so that newly synthesized fatty acids do not risk undergoing degradation [26]. In the last reaction of the carnitine shuttle, fatty acyl-carnitine is able to enter the mitochondrial matrix and carnitine is substituted with a molecule of CoA to reconstitute fatty acyl-CoA.

In the mitochondrial matrix, the fatty acyl-CoA chain repetitively undergoes a sequence of four reactions leading to the depletion of two carbons from the chain at each cycle and yielding acetyl-CoA, NADH and FADH₂, until the whole chain is exhausted. The pool of acetyl-CoA obtained in this process can join the Krebs cycle for complete oxidation to CO₂, whereas NADH and FADH₂ are utilized in the electron transport chain.

Fatty acids that contain an odd number of carbons and/or unsaturated fatty acids, undertake slightly different processes that involve additional steps and auxiliary enzymes capable of resolving alternative structures in the chain. Very long fatty acids and branched chain fatty acids are preferentially transported in peroxisomes instead where the process of oxidation begins. These organelles not only possess the necessary enzymes to undertake β -oxidation but also a number of auxiliary enzymes capable of processing complicated structures. However, peroxisomes in the liver lack Krebs cycle enzymes; acetyl-CoA is therefore transported out and carried in the mitochondria where is oxidized [13].

CoA is present in the cell in a finite number and rapid β -oxidation leads to accumulation of acetyl-CoA and depletion of the CoA pool. In order to release CoA, acetyl-CoA can alternatively be converted into ketone bodies. Ketone bodies are emitted into circulation and taken up by several organs, including the brain, and then reconverted into acetyl-CoA to be utilized in the Krebs cycle. During prolonged fasting, gluconeogenesis is particularly active and Krebs cycle intermediates are redirected towards the production of endogenous glucose. This leads to accumulation of acetyl-

CoA that cannot be processed in the Krebs cycle. Under these circumstances, a high amount of ketone bodies is produced and released into circulation. Very high levels of ketone bodies in the blood can lower blood pH causing metabolic acidosis, a condition associated with several pathological states.

De novo lipogenesis (DNL)

The biosynthesis of fatty acids is strongly coupled with the catabolism of carbohydrates, meaning that, in fed conditions, ingested carbohydrates not only provide acetyl-CoA precursors, but also upregulate DNL.

DNL does not share any common metabolic pathway steps with its catabolic counterpart, β -oxidation, but is instead a fully independent pathway operating in the cytosol. Fatty acids are synthesized from the acetyl-CoA accumulating in the mitochondria as a result of high amount of carbohydrates entering glycolysis during the fed state. Once shuttled out of the mitochondria through the citrate shuttle, acetyl-CoA is carboxylated and converted into the three-carbon intermediate malonyl-CoA in a reaction carried out by acetyl-CoA carboxylase (ACC). Fatty acid chains are synthesized by repetitive condensation of malonyl-CoA monomers to a growing acyl chain, extending it two carbons at a time. The multienzyme fatty acid synthase complex (FAS), which possesses seven distinct enzymatic activities, is responsible for the whole process while the acyl carrier protein (ACP) functions as a tethering arm that carries the on-growing acyl chain from one active site of FAS to another. The overall process utilizes one ATP molecule and two NADPH per malonyl-CoA condensation. ATP is necessary for acetyl-CoA carboxylation into malonyl-CoA, whereas NADPH functions as a reducing agent and is generated for the most part through the PPP, whose regulation is coordinated with lipid biosynthesis.

Normally, the process ceases after the chain reaches 16 carbons in length (palmitate) and the nascent fatty acid is then released from FAS. Palmitate, the most abundant product of DNL, can undergo additional elongation and desaturation in the smooth ER. Desaturation usually occurs between

positions 9 and 10, generating the monounsaturated fatty acids palmitoleate, 16:1(Δ^9), and oleate, 18:1(Δ^9). Mammals cannot introduce additional double bonds after the 10th carbon, and therefore have to rely on dietary sources to obtain fatty acids like linoleate, 18:2 ($\Delta^{9,12}$), or α -linolenate, 18:3 ($\Delta^{9,12,15}$), which are important biosynthetic precursors [13].

TG formation and the TG/fatty acid cycle

Fatty acids can be stored either in the form of TGs or used as substrates for phospholipid synthesis, which among other things, are essential components of cellular membranes. A TG is constituted of three fatty acid chains condensed to a glycerol backbone and is synthesized from one precursor molecule of L-glycerol-3-phosphate (G3P) and three fatty acyl-CoAs. In the liver, G3P can be obtained through three different routes. During the fed state, G3P can derive from the glycolytic intermediate DHAP, then converted into G3P by glycerol-3-phosphate dehydrogenase. Alternatively, it can be produced from free glycerol via glycerol kinase. During fasting, when glycolysis is suppressed, G3P is produced *de novo* in a process known as glyceroneogenesis, where DHAP is the final product of a shorter version of gluconeogenesis that is then converted into G3P.

Even though DNL is suppressed during fasting, a source of glycerol is still necessary to maintain the TG/fatty acid cycle going at a constant rate. In fact, at any circumstance, fed or fasted state, 75% of the fatty acids released by lipolysis are re-esterified back to TG in the adipose tissue or in the liver, and when glycerol cannot be obtained from glucose, is synthesized *de novo* through glyceroneogenesis [27]. Although the physiological role of the TG/fatty acid cycle is not clear, it is speculated that it serves the purpose of rapidly increasing systemic fatty acid availability in the event of a sudden need, such as a “fight or flight” situation [13].

Hepatic TG export, role of lipoprotein carriers

Hepatic TGs destined to export, together with cholesterol esters, are packed into VLDLs, lipoproteins that function as body's transport mechanism for lipids. Nascent VLDLs are assembled in the liver from apolipoproteins such as apolipoprotein B-100 (Apo B-100), the main structural component of VLDLs, and phospholipids. TGs and cholesterol esters constitute the hydrophobic core of VLDLs. Once VLDLs reach peripheral tissues, the TGs carried inside the lipoproteins are gradually hydrolyzed by lipoprotein lipases. Fatty acids are released and uptaken mainly by adipose tissue, muscle and heart, which express high levels of lipoprotein lipases. As VLDLs lose their TG content and become progressively denser and smaller (VLDL remnants), they are in part removed from circulation by the liver. The remaining particles, that further decrease in size as they remain in circulation, finally transition to low-density lipoproteins (LDLs), lipoproteins that at this point contain high proportions of cholesterol esters.

Approximately 70 % of LDL return to the liver, where they are internalized via endocytosis mediated by recognition of Apo B-100 with the LDL receptor (LDL-R). The remaining LDLs are cleared by peripheral tissues via the same mechanism. The levels of plasma LDL are determined by the level of LDL-R in the liver, which in turn is regulated by the cholesterol content of the hepatocyte. If cholesterol levels in the cell are high, then LDL-R transcription and expression are reduced, leading to diminished hepatic LDL uptake and thus, higher LDL plasma concentrations.

High levels of circulating LDL are associated with increased risk of coronary heart diseases. LDL, especially those small in size, can be easily trapped in the arterial wall by binding to intra-arterial proteoglycans. Subsequent LDL oxidation, favored by the local pro-oxidative environment, initiates the inflammatory process that will contribute to the formation of atherosclerotic plaques [28].

On the other hand, high levels of circulating high-density lipoproteins (HDLs), are inversely associated with cardiovascular risk. HDLs are produced and released by the liver and intestine

which can synthesize apolipoprotein A-1 (Apo A-1), the main structural component of HDLs. Newly synthesized Apo A-1 begins its maturation as lipoprotein by acquiring cholesterol and phospholipids that efflux from hepatocytes and enterocytes. Cholesterol efflux is mediated by the interaction of the ATP-binding cassette transporter A1 (ABCA1), a transporter expressed ubiquitously in the body, with Apo A-1. While circulating and acquiring cholesterol from peripheral tissues, HDLs grow in size and become mature spherical-shaped lipoprotein particles. The main function of HDLs is to efflux cholesterol from peripheral tissues and to deliver it to tissues able to catabolize cholesterol, such as liver and steroidogenic tissues. The majority of cells do not have a system for cholesterol disposal so, in order to decrease their cholesterol content, a mechanism of export is required. The cholesterol delivered to the liver is directly excreted into the bile or utilized for the production of bile acids, whereas the one delivered to steroidogenic tissues such as adrenals, ovaries and testes, is utilized for the synthesis of steroid hormones. HDLs can also efflux cholesterol from atherosclerotic plaques, thereby reducing the size of the plaque and potentially reversing atherosclerotic heart diseases. At the end of their life cycle, that lasts approximately 4-5 days, HDL are permanently catabolized either by the kidneys, which dispose of HDLs of smaller sizes, or by the liver via internalization [29].

Regulation of Hepatic Metabolism

Mechanisms of metabolic regulation

Table 1.2 - Principal mechanisms of metabolic regulation.

Mechanism	Type of control	Time of effect	Examples
Alterations in substrate, cofactor or metabolite concentrations	Thermodynamic	Very Rapid (seconds)	<ul style="list-style-type: none"> • Glucose → Glucose-6-P • Fructose → Fructose-1-P • Glucose-6-P → → Pentose P
Alterations in enzyme activity	Kinetic	Rapid (seconds)	<ul style="list-style-type: none"> • Glucokinase de-repression • Allosteric modification of Phosphofructokinase activity • Pyruvate dehydrogenase phosphorylation/dephosphorylation
Alterations in substrate or metabolite transporter activity	Kinetic	Rapid (seconds)	<ul style="list-style-type: none"> • Carnitine palmitoyltransferase-1 repression by malonyl-CoA
Alteration in enzyme expression	Kinetic	Slow (hours)	<ul style="list-style-type: none"> • <i>De novo</i> lipogenesis pathway enzymes

Metabolic processes are regulated through alterations in thermodynamic and/or kinetic control of individual pathway steps. As shown in Table 1.2, these alterations can be manifested by several different mechanisms. Substrate levels can directly alter metabolic fluxes by changing their thermodynamics: (i.e., the equilibrium constant and free energy change of a particular metabolic pathway step) and these effects are essentially instantaneous.

Alterations in enzyme activity can occur by different mechanisms including allosteric modulation of enzyme activity, for example positive and negative modification of PFK-1 activity by AMP and ATP, respectively. Glucokinase activity has an additional level of control combining

repression/derepression via the glucokinase regulatory protein with intracellular translocation.

Alterations in metabolic pathway enzyme(s) expression that substantially increase their cellular abundance over previously residual levels represent another form of kinetic control. This is typically mediated by transcription factors which themselves may be activated allosterically. These effects take longer (up to several hours) because of the time required by mRNA transcription and translation. Importantly, processes such as the reciprocal regulation of catabolic and biosynthetic pathways of glucose and lipid metabolism are dependent on the coordinated control of a large and diverse number of such mechanisms. This is mediated by intracellular signaling cascades that are in turn regulated by neural and hormonal mechanisms, among which insulin and glucagon regulatory control play a predominant role.

Hormonal and neuronal regulation of metabolic pathways in the liver

Since hormones circulate through the blood, they can integrate metabolic activities of liver with that of different tissues thereby facilitating efficient inter-organ nutrient transfer and whole-body substrate utilization. As the CNS communicates with the liver in a bidirectional manner, peripheral hormones can also trigger metabolic effects in the liver acting via central mechanisms. Both sympathetic and parasympathetic nervous systems innervate the liver and regulate its metabolism. In addition, the CNS and the peripheral neuronal network regulate the metabolism of liver and other peripheral tissues also by alternative mechanisms, such as nutrient-sensing systems, whose ultimate effects integrate with those of hormonal control.

Insulin and glucagon are among the most important hormones in the regulation of hepatic metabolism. High levels of insulin are secreted after a meal in order to promote glucose uptake, glycogen synthesis and *de novo* lipogenesis. Glucagon circulates during fasting periods and promotes gluconeogenic pathways.

Other important hormones that participate in the regulation of hepatic metabolism are epinephrine and cortisol. These hormones are capable of inverting metabolic fluxes to calibrate and redirect the

energy expenditure in the most convenient way in a given situation. Epinephrine is the hormone of the “fight or flight” response, that prepares the body for an outburst of energy in a sudden emergency, whereas cortisol is secreted in the presence of a long-term stressor.

Some tissues can secrete hormones to signal about their energy requirements, ultimately affecting hepatic metabolism. The adipose tissue releases circulating adipokines, two important ones being leptin and adiponectin. Leptin signals through the hypothalamus suppressing appetite and indicating that the fat storage is adequate, adiponectin antagonizes leptin and promotes catabolic pathways in the liver. The gut is also involved in regulating some hepatic metabolic functions; directly, releasing hormones and metabolites in the portal vein, and indirectly, signaling through the CNS.

Regulation of hepatic glucose and lipid metabolism: an overall description

Regulation of hepatic glucose metabolism

Several key enzymes involved in glucose metabolism, such as GLUT2 and glucokinase, are expressed in the liver as isoenzymes. The physiological reason for this lies behind the unique role that hepatic glucose metabolism plays in systemic glucose homeostasis. The liver removes and stores excess circulating glucose; however, glucose is hardly used by the liver to fulfil its own energetic demands which are for the major part satisfied by lipid oxidation. Unlike other tissues, where glucose metabolism is determined by energy demands and regulated by negative feedback inhibitory mechanisms, hepatic glucose metabolism is determined by glucose concentration in the portal vein and is regulated by feed-forward activation mechanisms. Thus, the kinetic properties of these liver-specific isoenzymes perfectly serve the purpose of guaranteeing the extraction and metabolism of glucose only in the amount that circulates in excess and that is convenient to store either as glycogen or, after conversion to fatty acid chains, in the form of triglycerides.

Hepatic glycogenesis is regulated at several levels and is fully active during fed states and high glucose availability. Insulin/glucagon ratios regulate this process in a concerted way balancing the shift between glycogen synthesis and degradation. Moreover, hyperglycemia *per se* enhances glycogen accumulation by inhibiting glycogen degradation [30] and increased glycogen accumulation diminishes appetite and food intake most likely acting through the vagus nerve [31]. The sympathetic fibers that innervate the liver regulate glycogenesis stimulating glycogen degradation, whereas parasympathetic afferents can detect glucose increase in the portal vein and trigger the activation of glycogen synthase [17].

Glycogen synthase, glycogen phosphorylase and glucokinase are the major regulators of glycogen fluxes. In general, stimuli that enhance (insulin and hyperglycemia) or inhibit (glucagon and epinephrine) hepatic glycogen synthesis, exert their culminating effects on these three enzymes. This fine regulation permits the almost complete pausing of glycogen degradation during fed states and its reactivation during fasting periods.

Similar to glycogen synthesis and degradation, glucose production and glucose utilization (glycolysis) are regulated accordingly in a reciprocal manner in order to avoid futile cycling of newly synthesized glucose. On the other hand, since producing glucose *de novo* is an energetically expensive process, gluconeogenesis rates are positively correlated with fatty acid oxidation rates. Acetyl-CoA, which is the product of β -oxidation, is in fact an allosteric activator of pyruvate carboxylase [32]. When β -oxidation is inactive, gluconeogenesis is attenuated, as fatty acids oxidation provides the abundant ATP supply necessary for the sustainment of high glucose production rates.

Although hepatic gluconeogenesis is mostly regulated by substrate availability rather than hormonal control, insulin and glucagon regulate both glycolysis and gluconeogenesis simultaneously via enzymatic regulation and transcriptional mechanisms. Glucagon promotes gluconeogenesis and insulin sustains glycolysis. Cortisol and epinephrine also enhance glucose production, acting on some gluconeogenic regulatory enzymes whereas high ADP concentrations, which indicate low

energy levels in the cell, inhibit the same enzymes. On the other hand, high ATP concentrations and alanine are inhibitors of critical glycolytic enzymes, thus redirecting pyruvate towards glucose production [33].

Regulation of hepatic lipid metabolism

The liver normally processes large quantities of lipids, but only small amounts are stored within hepatocytes (around 5% steady-state TG content). This is possible because fatty acid input, determined by the rates of lipid uptake from plasma and of *de novo* synthesis; balances, under physiological circumstances, fatty acid output, determined by the rate of lipid oxidation and export via VLDL. Thus, in order to maintain cellular lipid homeostasis, hepatic lipid input and output are at least in part, inter-dependent and cross regulated. Generally, in response to elevated lipid influx, the liver upregulates metabolic pathways (oxidation and VLDL export) that minimize intracellular lipid accumulation.

Lipid oxidation rates are dependent on fatty acid supply (via lipolysis) and the partitioning between oxidation and re-esterification. Fatty acid entry into mitochondria for oxidation is mediated by CPT-1, whose activity is inhibited by interaction with malonyl-CoA, the first product of DNL. Hence, during DNL, fatty acid oxidation is downregulated.

Several key enzymes involved in fatty acid oxidation in the liver are under the regulation of the peroxisome proliferator-activated receptor α (PPAR α). PPAR α is a ligand-activated transcription factor that promotes the expressions of several genes involved in fatty acid oxidation, ketogenesis and fatty acid uptake. PPAR α expression in the liver is higher in the fasted state and glucagon stimulates fatty acid oxidation in a PPAR α dependent manner [34]. Omega-3 fatty acids are natural ligands of PPAR α : one of the beneficial properties of these highly polyunsaturated fatty acids is indeed to be potent PPAR α agonists, and thus promoters of fatty acid oxidation. [35].

DNL is strongly regulated transcriptionally, but also allosterically, mostly at the level of ACC. ACC undergoes polymerization when exposed to certain stimuli, increasing its enzymatic activity.

Citrate, glutamate and insulin promote ACC polymerization, whereas glucagon and epinephrine induce ACC phosphorylation with subsequent depolymerization and decline in its enzymatic capacity. ACC is also feedback-inhibited by its own product, malonyl-CoA [36].

FAS is too regulated at several levels: insulin and substrates such as citrate promote FAS activity, whereas glucagon and increased intracellular fatty acid concentrations inhibit it [37].

At the transcriptional level, DNL is regulated by two major transcription factors, the sterol regulatory element-binding protein-1c (SREBP-1c) and the carbohydrate response element-binding protein (ChREBP), whose activities are upregulated by insulin and excess of carbohydrate respectively. SREBP-1c was first identified as transcription factor that controls the genes involved in cholesterol synthesis and thus essential for regulating cell membrane synthesis and composition [38]. SREBP-1c is regulated by cholesterol via end-product feedback suppression mechanisms. Later, SREBP-1c was discovered to be also regulated by insulin levels and became prominent as mediator of the insulin-stimulated lipogenic program. Insulin release and -induced signaling events trigger the activation of SREBP-1c by proteolytic release from the Golgi membrane and its translocation into the nucleus, where it promotes the transcription of lipogenic genes such as FAS and ACC [39], [40].

Similarly, rise in glucose and fructose concentrations and increase in glycolysis rates promote by a not so well-defined mechanism the activation of ChREBP that, translocating into the nucleus, induces the transcription of several genes containing the carbohydrate response element (ChoRE), including FAS, ACC, but also glycolytic enzymes such as pyruvate kinase, that provides pyruvate and thus acetyl-CoA via pyruvate dehydrogenase [41]. High glucose (and fructose) concentrations promote ChREBP activation independently of insulin. SREBP-1c and ChREBP dual action ensures that lipogenesis occurs at its maximum capacity in the presence of both insulin and high concentrations of ingested carbohydrates.

Insulin: signaling and metabolic effects on the liver

Insulin secretion by the pancreatic β -cells is stimulated by increasing levels of glucose in the portal vein blood that generally occur after a meal. This hormone signals a status of nutrient abundance and its major effect in the liver is to promote the anabolic synthesis of the three main classes of macromolecules: glycogen, lipids and proteins. At the same time, insulin strongly inhibits hepatic glucose production, repressing both glycogenolysis and gluconeogenesis.

Insulin binds its cognate receptor, the insulin receptor (IR), on the hepatocyte cell membrane. IR is a heterotetrametric receptor tyrosine kinase that, upon binding to insulin, undergoes conformational changes that stimulate trans-autophosphorylation of the receptor itself, a fundamental event for the recruitment of IR effectors [42]. The signaling cascade initiated by insulin can have several ramifications leading to different outcomes. Not only insulin triggers metabolic signals, but it can also initiate mitogenic responses through the mitogen-activated protein kinase (MAPK) pathway [43]. The characteristic metabolic response induced by insulin is, on the other hand, initiated downstream of phosphoinositide 3-kinase (PI3K), recruited by the phosphorylated insulin receptor substrate (IRS), a protein that functions as a scaffold for IR. PI3K catalyzes the conversion of phosphatidylinositol-4,5-bisphosphate (PIP₂) into phosphatidylinositol-3,4,5-trisphosphate (PIP₃). PIP₃, which resides on the plasma membrane, is able to bind proteins that possess a PH binding domain, among which also two important effectors of the insulin cascade, the phosphoinositide-dependent kinase 1 (PDK1) and AKT. Therefore, the increase of PIP₃ appearance on the plasma membrane due to PI3K activity, brings PDK1 and AKT into proximity and PDK1 can at this point phosphorylate AKT on its activation loop. Activated AKT has a number of substrates and mediates almost the entire anabolic program induced by insulin in the liver [44].

Insulin signaling is attenuated or terminated by a variety of mechanisms. First of all, insulin is itself a negative regulator of its own signaling; upon binding to insulin, IR undergoes internalization followed by either lysosomal degradation or recycling back to the cell membrane [45]. High

circulating insulin concentrations are therefore correlated with decreased IR levels on the cell surface, a phenomenon promptly reversed when insulin concentrations drop during the fasted state. However, insulin signaling continues from the internalized IR and is only effectively terminated by IR dephosphorylation operated by phosphatases such as protein-tyrosine phosphatase 1B (PTP-1B) that negatively regulates insulin signaling dephosphorylating tyrosine residues on IR and IRS proteins [46]. Other mechanisms that counteract insulin actions include dephosphorylation of PIP₃ by lipid phosphatases such as PTEN and SHIP2 [47] and inhibitory phosphorylation of IRS proteins on serine residues operated by multiple kinases, some of which activated by insulin itself in a negative feedback loop [48].

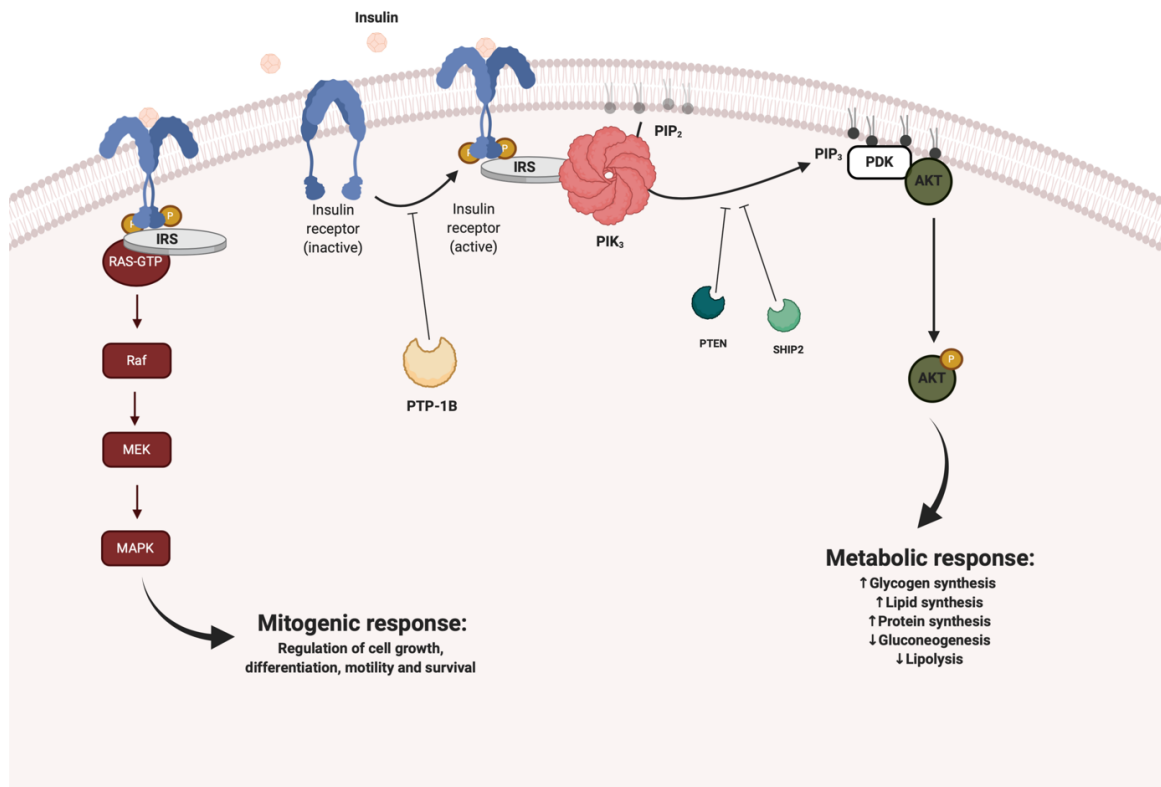


Figure 1.5 - Hepatic insulin signaling. Some effectors have been omitted for clarity. [Figure created with BioRender.com].

Insulin control of hepatic glycogen synthesis

Glycogen synthesis is one of the major events induced by food ingestion and insulin regulates this process in several ways. It is important to remind, however, that hyperglycemia is too a potent regulator of almost every aspect of hepatic glucose metabolism, including glycogenesis, and the sole increase in glucose concentration is in fact sufficient to allosterically stimulate glycogen accumulation in the liver. Nevertheless, insulin signaling is fundamental for optimal glycogen synthesis in hepatocytes [44].

Net glycogen deposition results from the sum of two glycolytic fluxes: glycogenesis and glycogenolysis and, as a rule, glycogenesis is sustained by insulin action, whereas hyperglycemia has an inhibitory effect on glycogenolysis [30]. Consistent with this paradigm, glycogen synthase and glycogen phosphorylase, the two key regulatory enzymes of these processes, are subjected to strong allosteric regulation by G-6-P and glucose respectively.

G-6-P, whose synthesis from glucose is upregulated by insulin action via glucokinase, is the main substrate of glycogenesis. Insulin controls glucokinase activity both at a transcriptional and post-transcriptional level: not only insulin promotes glucokinase expression but facilitates its translocation from the nucleus [15]. G-6-P accumulation in the cytoplasm signals nutrient abundance which needs to be promptly stored and thus high levels of G-6-P allosterically stimulate glycogen synthase and enhance glycogen deposition through substrate push [49]. The concomitant increase of free glucose levels in the cell is indicative of high circulating glucose, a condition that requires the hepatocyte to halt the release of endogenous glucose into circulation. Thus, cytoplasmatic free glucose allosterically inhibits glucose phosphorylase, which again results in net glycogen deposition [50].

Aside from this simplified model, other mechanisms are possibly involved. For example, insulin induces the inhibition of glycogen synthase kinase-3 (GSK-3) and activation of protein phosphorylase 1 (PP1), events that converge into glycogen synthase stimulation and glycogen

phosphorylase repression [51], [52]. Moreover, hyperglycemia further enhances glucokinase activation by stimulating glucokinase dissociation from its regulatory protein and translocation into the cytoplasm [15].

To conclude, insulin and hyperglycemia modulate glycogenic fluxes through different mechanisms, both required for maximal glycogen deposition in the liver.

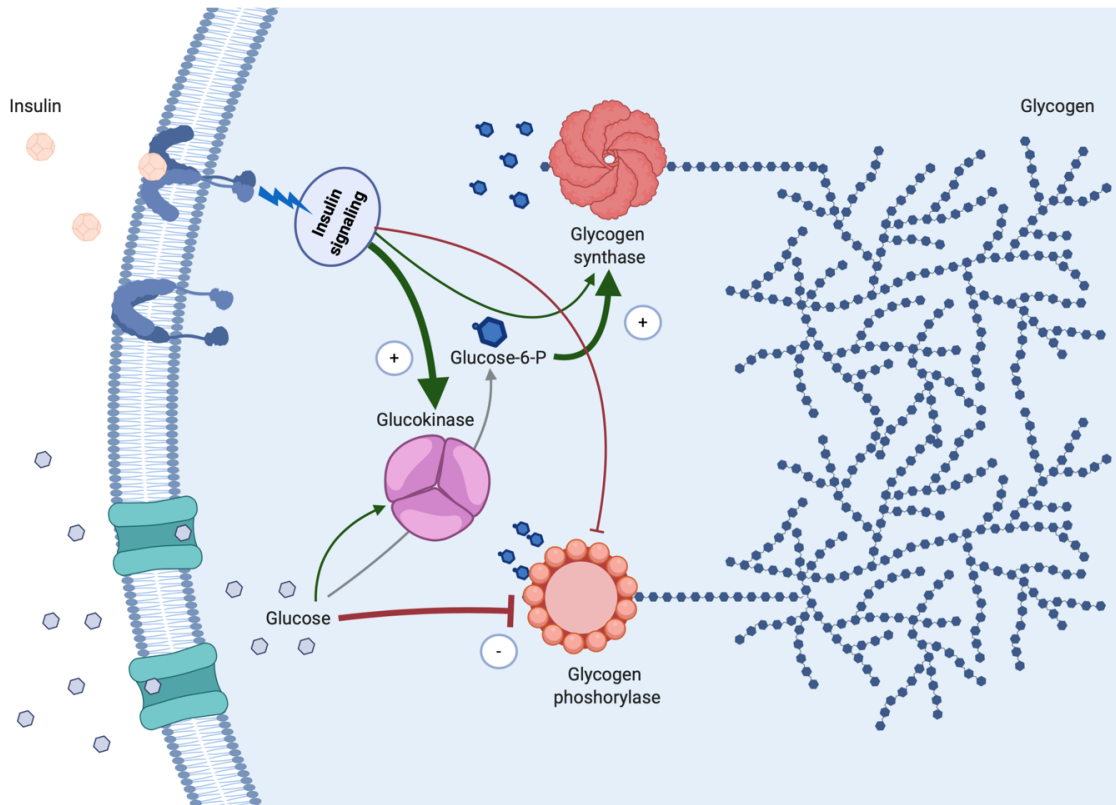


Figure 1.6 - Hepatic glycogen deposition. In the liver, glycogen deposition is stimulated by both insulin signaling and hyperglycemia. As a general rule, insulin promotes glycogen synthesis whereas hyperglycemia has an inhibitory effect on glycogen degradation, with glucose and G-6-P being the main regulators of glycogen phosphorylase and glycogen synthase respectively. Other mechanisms, such as the inhibitory effect of insulin on glycogen phosphorylase and hyperglycemia induction of glucokinase de-repression, are also involved. [Figure created with BioRender.com].

Insulin control of gluconeogenesis

Another important mechanism by which insulin regulates glucose homeostasis in the fed state is the suppression of hepatic glucose production (HGP). HGP is classically defined as the glucose output deriving from the joint contributions of hepatic glycogenolysis and gluconeogenesis. As explained above, glycogenolysis is acutely suppressed in the fed state by the combined regulatory actions of insulin and hyperglycemia. On the other hand, insulin direct suppression of gluconeogenesis occurs mostly at a transcriptional level via the transcriptional complexes FOXO1/PGC1 α and CREB/CRTC2 [44].

FOXO1 is a well-known AKT substrate and a transcription factor that, in association with PGC1 α , controls the gluconeogenic transcriptional program that includes G6Pase and PEPCK genes. Upon insulin stimulation, activated AKT phosphorylates FOXO1 on multiple sites causing its exclusion from the nucleus and disabling its transcriptional activity [53].

CREB is also responsible for the transcription of several gluconeogenic genes, and by promoting phosphorylation of its coactivator CRTC2, insulin induces CREB translocation and degradation [54]. The FOXO1/PGC1 α and CREB/CRTC2 modules are independent from one another and while the former is of critical importance after several hours of fasting, the latter is transcribed for the major part during short fasts [55].

However, insulin suppression of endogenous glucose production is an immediate consequence of food intake that occurs before any change in gluconeogenic protein levels is detected. Insulin suppresses hepatic gluconeogenesis within minutes, in a fashion that cannot be solely explained by transcriptional mechanisms [56]. The acute suppression of hepatic gluconeogenesis is in fact mostly an indirect consequence of a series of insulin-mediated events that occur in other tissues and organs. Insulin-dependent acute suppression of lipolysis in the adipose tissue plays a central role in this context. First, lipolysis cessation deprives gluconeogenesis of one of its main gluconeogenic substrates, glycerol; and secondly, decreased FFA flux to the liver, and consequent reduction in β -

oxidation rates, leads to diminished mitochondrial acetyl-CoA, allosteric activator of the gluconeogenic enzyme pyruvate carboxylase [56].

Other indirect mechanisms, such as insulin-mediated suppression of glucagon secretion and neural regulation of HGP, also influenced by insulin, participate in this scenario where, postprandially, hepatic gluconeogenesis is acutely suppressed mainly by extra-hepatic mechanisms, whereas direct acute insulin action on the hepatocytes mainly involves changes in glycogenic fluxes rates.

Insulin control of lipid metabolism

Insulin promotes lipids storage and inhibits their degradation. Thus, it up-regulates DNL while inhibiting lipolysis and free fatty acid availability for oxidation.

Insulin controls DNL by both transcriptional mechanisms and phosphorylation of key lipogenic enzymes. On a transcriptional level, insulin acts on the master transcriptional regulator SREBP-1c, not only by promoting its transcription but also facilitating its activation and import inside the nucleus [44]. However, this insulin-mediated transcriptional program is considerably slow [57]. A much faster mechanism involves insulin-activation of several lipogenic enzymes such as ACC and ATP citrate lyase and, although the exact signaling cascade leading to such events is not entirely understood, the activation most likely occurs by phosphorylation /dephosphorylation mechanisms. [58].

Finally, insulin stimulates DNL also by substrate push: glucokinase up-regulation, prompted by insulin through a much faster transcriptional mechanism, increases lipogenic substrate availability and thus lipogenic rates [57].

Glucagon: signaling and metabolic effects on the liver

Insulin anabolic action is counteracted by glucagon, which is secreted into the bloodstream when circulating glucose is low in order to stimulate hepatic glucose output and restore euglycemia. This is achieved through increase in glycogen breakdown and gluconeogenesis, concomitant with inhibition of glycolysis and glycogenesis. Apart from its major role in glucose homeostasis, glucagon is also known to affect lipid and protein metabolism, promoting the catabolism of both nutrient types.

The liver is the main target organ of glucagon, where the glucagon receptor, a seven-transmembrane G protein-coupled receptor, is highly expressed. Upon glucagon binding, the receptor undergoes conformational changes which induce the activation of associated G-coupled proteins. This leads to an increase in intracellular cAMP levels and activation of adenylate cyclase, which in turn stimulates protein kinase A (PKA) and cAMP response element-binding (CREB) protein. PKA is considered the main effector of this signaling cascade and promotes a number of intracellular events associated with the majority of glucagon physiological outcomes [59].

Glucagon control of glucose homeostasis

Glucagon rapidly increases HGP by modulating the rates of glycogenolysis, gluconeogenesis, glycogenesis and glycolysis.

Glycogen synthesis and breakdown are subjected to direct glucagon regulation via PKA. By inducing the phosphorylation of both glycogen phosphorylase and glycogen synthase, and thus, enhancing the activity of the first whilst inhibiting the second, PKA promotes net hepatic glycogenolytic flux [60]. Additionally, glucagon exerts strong control over glycolysis and gluconeogenesis fluxes by decreasing the concentrations of the regulatory metabolite fructose-2,6-bisphosphate (F-2,6-P₂). F-2,6-P₂ is not an intermediate of neither glycolysis nor gluconeogenesis and is synthesized and degraded by the bifunctional enzyme phosphofructokinase-2/fructose-2,6-

Glucagon control of lipid metabolism

Besides having a central role in glucose homeostasis, glucagon is also an important regulator of lipid metabolism. Glucagon promotes a switch towards lipid utilization over glucose for energy production and, also in this context, counteracts insulin action by repressing DNL and sustaining lipid catabolism through fatty acid oxidation.

The first rate-limiting reaction of β -oxidation is catalyzed by CPT-1, an enzyme under the transcriptional program of CREB, hence glucagon promotes CPT-1 transcription and accumulation. CPT-1 is inhibited by malonyl-CoA, synthesized by ACC during the first reaction of DNL. Malonyl-CoA is the regulatory element that inhibits fatty acid oxidation during DNL, therefore PKA, by phosphorylating and thus inhibiting ACC, promotes both repression of DNL and disinhibition of β -oxidation. Finally, glucagon exerts an additional transcriptional control at the level of PPAR α , which results in the enhanced transcription of several genes involved in β -oxidation, including CPT-1 and acetyl-CoA oxidase [59].

***Physiology of the Insulin-Resistant Liver:
Hepatic Insulin Resistance and Related
Diseases***

Insulin resistance is defined as a reduction in the ability of insulin to elicit a biological response in its target tissues. As a compensatory mechanism, greater concentrations of insulin are secreted by the β -cells to induce the same biological response that would have been achieved by normal concentrations of the hormone, resulting in hyperinsulinemia.

The main insulin-responsive tissues are liver, skeletal muscle and adipose tissue and insulin resistance has distinctive manifestations in each of them. On a temporal scale, skeletal muscle is the first tissue to become insulin-resistant in humans. The insulin-resistant muscle is unable to uptake glucose efficiently hence a major component of systemic glucose disposal is compromised. This results in increased disposal of glucose by other pathways, including hepatic DNL. Excessive DNL contributes to ectopic lipid accumulation in the liver and hepatic insulin resistance.

Hepatic insulin resistance is characterized by the inability of regulating endogenous glucose production during fasting and impaired glycogen deposition during feeding. At the same time, hepatic DNL remains responsive to insulin signaling, thereby potentiating hepatic steatosis under hyperinsulinemic conditions. This has been termed “selective hepatic insulin resistance” [64] and various explanations have been proposed to rationalize this paradox.

This chapter will focus on the insulin-resistant liver, on how the previously described metabolic fluxes become compromised in response to perturbed insulin signaling, and the on role played by such disturbances in the pathophysiology of some common metabolic diseases.

The insulin-resistant liver: glucose metabolism

Hepatic insulin resistance is associated with dysregulated glucose metabolism. Although all glucose-related metabolic processes in the liver have an additional level of regulation which is independent of insulin and relies on substrate push and availability, impaired insulin signaling is sufficient to significantly disrupt hepatic glucose metabolism with consequences on whole-body fuel homeostasis [65].

In insulin-resistant individuals, insulin fails to suppress hepatic glucose production resulting in increased glucose output that aggravates fasting hyperglycemia [66], with the gluconeogenic pathway being upregulated both acutely and chronically. Postprandial acute regulation of gluconeogenesis appears to be largely dependent on lipolysis in the adipocytes, a process also strictly controlled by insulin. Hence, insulin failure to suppress lipolysis indirectly results in unrestrained hepatic gluconeogenesis due to an oversupply of free fatty acids and glycerol. Acute suppression of hepatic gluconeogenesis might therefore be a consequence of adipocyte insulin resistance.

On the other hand, the direct effects of insulin on hepatic glucose production are attributed to the transcriptional regulation of gluconeogenic genes, mostly under the transcriptional control of FOXOs proteins, and to the direct acute regulation of glycogenolysis [44], [56].

FOXO1 inhibition in particular, mediates the insulin-induced chronic suppression of gluconeogenesis and unrestrained FOXO1 activity in the liver is sufficient to chronically upregulate gluconeogenesis in mice [67]. However, it is not clear whether the transcriptional regulation of gluconeogenic genes has an influential role in the pathophysiology of metabolic diseases such as T2DM in humans, given that diabetic patients display unaltered levels of gluconeogenic enzymes [68].

Glycogen synthetic fluxes in the liver are, on the other hand, a better manifestation of direct physiological function of postprandial insulin on the hepatocyte, although the exact mechanisms by

which insulin directly governs glycogen metabolism is difficult to fully comprehend, as glycogen deposition is also potently regulated by glucose and G-6-P, and glucose transport across the hepatocyte membrane does not respond to insulin.

T2DM patients display lower hepatic glycogen content and glycogen synthetic rates. Glycogenolysis is overall reduced but incompletely inhibited in response to insulin [69], [70], [71]. As a rule, the insulin-resistant liver fails to mobilize hepatic glycogen adequately in response to the normal feeding/ fasting cycle and glycogen amounts appear to be reduced and static [44]. Insulin strongly upregulates glucokinase, both at the transcriptional and post-transcriptional level. The loss of this function, together with the inability of stimulating glycogen synthase, leads to reduced postprandial glycogen deposition, in particular via the direct pathway.

In conclusion, although elevated rates of hepatic gluconeogenesis are a hallmark of many metabolic diseases, hepatic insulin resistance *per se* does not directly stimulate gluconeogenesis [72], [73]. In contrast, hepatic insulin resistance is expected to impair glycogen metabolism, since the regulation of glycogenic and glycogenolytic pathway fluxes in the liver is directly dependent on functional intracellular insulin signaling.

The insulin-resistant liver: lipid metabolism

Patients with insulin resistance states associated with conditions such as obesity and NAFLD, show elevated hepatic DNL rates accompanied by enhanced VLDL secretion [74], [75]. This is counterintuitive considering that these processes are dependent on hepatic insulin signaling. Mice that have no hepatic insulin signaling at all following ablation of the hepatic insulin receptor, do exhibit lower DNL rates and decreased plasma TGs alongside the dysregulation of carbohydrate metabolism [76].

This paradox is referred to as “selective hepatic insulin resistance”, and many studies over the years have attempted to rationalize whether defects in insulin signaling are selective for glucose metabolism, leaving lipid metabolism fully responsive to insulin.

Given the level of complexity of the insulin signaling pathway (Figure 1.5), one hypothesis is that an early bifurcation in the pathway could leave the “lipid-handling” arm intact whereas the “glucose handling arm” loses function. However, this hypothesis has not been fully supported by experimental data [77], [78], [44].

An alternative explanation proposes that the signaling processes involved in regulating lipid metabolism are inherently more sensitive to insulin compared to those controlling glucose metabolism. In this setting, the hyperinsulinemia required to maintain glucose homeostasis overstimulates hepatic lipid biosynthesis and export. This hyper-activation may not be limited to hepatic lipid metabolism but can also include processes in other tissues such as sodium reabsorption in the kidney and androgen production in the ovaries [79], [80].

Finally, it has been proposed that there is no such thing as selective insulin resistance but that overnutrition *per se* can impose a potent lipogenic program and induce hepatic steatosis independently of insulin actions. Adipose insulin resistance contributes to hepatic steatosis by inducing uncontrolled release of fatty acids which are re-esterified into triglyceride in the liver [76]. In fact, the hepatic lipogenic machinery does not necessarily need insulin to function: the DNL

transcriptional program can be activated by the sole presence of carbohydrates (i.e., ChREB transcription factor) which are ingested in large quantities and fed into the lipogenic apparatus pushing the process also on this level [81]. Fructose in particular, is a potent lipogenic substrate and at the same time, a lipogenic transcriptional regulator that participates in this process stimulating and sustaining high DNL fluxes [82].

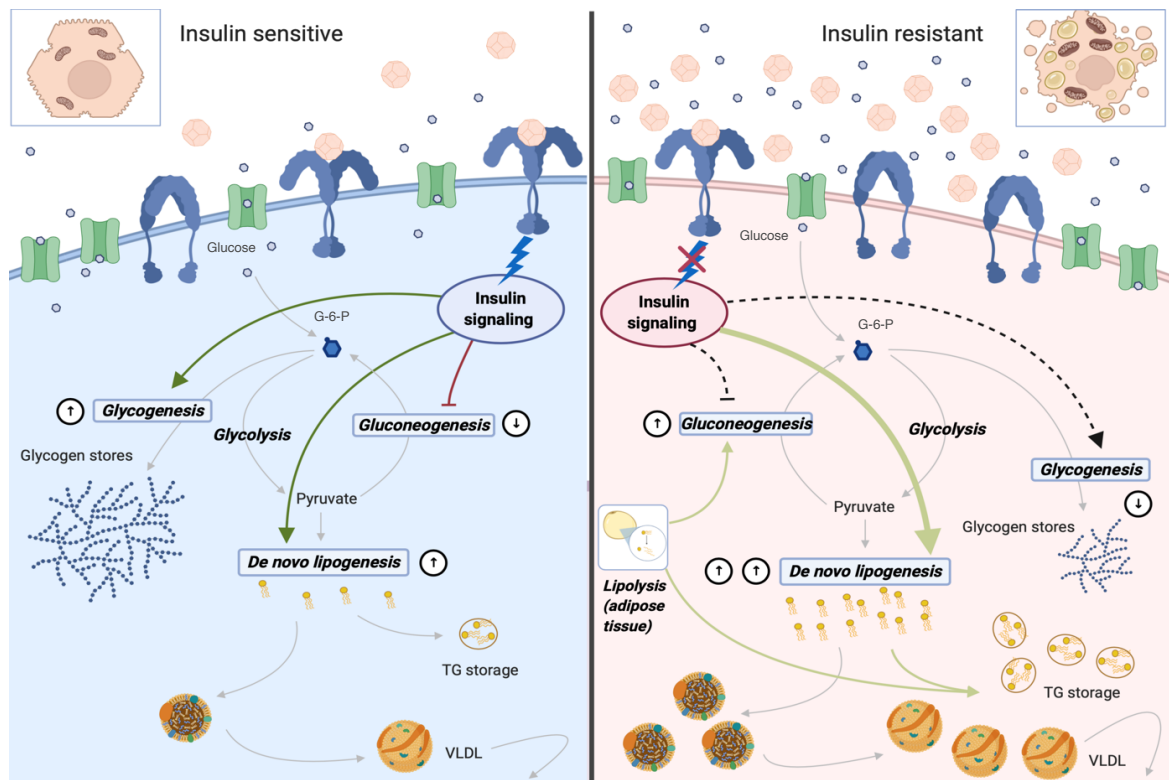


Figure 1 8 - Metabolic consequences of intact (left) and impaired (right) insulin signaling in hepatocytes. [Figure created with BioRender.com].

Molecular basis of insulin resistance

The impairment of insulin regulatory actions causes a multitude of metabolic consequences that at times makes it difficult to separate the cause from the effect. For example, obesity, increased appetite, hepatic steatosis, and diabetes might all coexist in the same individual. However, the sequence at which these different pathologies manifested, as well as how they have influenced the pathogenesis and progression of each other, is extremely difficult to elucidate and pinpoint on a temporal scale.

Countless pathways have been found altered in the pathological setting of insulin resistance. Inferring causality in this context has been proven challenging and several hypotheses have been proposed in order to identify that primary insult that in turn explains the aberrant secondary effects stemming from it. Hereafter we will review some of the most investigated hypotheses of insulin resistance and the mechanistic events that lead to disturbed insulin signaling.

Lipid-induced insulin resistance

The relationship between ectopic lipid accumulation and insulin resistance is well established. Intrahepatic TG content is a strong predictor of hepatic insulin resistance in both humans and rodents [83], [84], [44], thus the hypothesis that a particular lipid moiety could interfere with insulin signaling ultimately causing insulin resistance was an early postulate. Although TG levels correlate with insulin resistance in the liver, TGs *per se* are not effectors of insulin resistance. Alongside TGs, a variety of other lipid species accumulate in the steatotic liver and, among them, several possess bioactive signaling properties. 1,2-Diacylglycerol (DAG), the penultimate intermediate of TGs biosynthesis, whose levels therefore track with TGs levels, also positively correlates with hepatic insulin resistance [85]. Because of its well-known signaling properties, DAG received much attention in this context and a clear mechanism linking DAG accumulation to insulin resistance was identified and corroborated in a variety of models.

DAG is composed of two fatty acid chains covalently bound to a glycerol backbone and is a natural component of plasma membranes. Several factors can drive the ectopic accumulation of DAG inside the liver, including dietary imbalances, the inability of adipose tissue to clear lipids from circulation, and oxidative stress [86]. The accumulation of DAG in the plasma membrane correlates with the translocation and activation of protein kinase C (PKC) and consequent decrease in insulin sensitivity. Specifically, PKC ϵ , the PKC isoform responsible for this process in the liver, directly phosphorylates the insulin receptor causing the impairment of its kinase activity and termination of insulin signaling [87].

Although the DAG/PKC ϵ /IRK axis is at the moment the only mechanism whose components have all been characterized, several other classes of lipids have been proven to impact insulin action, both negatively and positively. Ceramides are a family of lipids associated with poor insulin sensitivity [88] that possibly disrupt insulin signaling at the level of AKT. Quantitative levels of ceramides do not correlate with insulin resistance, suggesting that specific ceramides species rather than overall ceramides levels mediate insulin resistance, but data supporting this hypothesis are scarce and conflicting [89]. Saturated fatty acids (SFAs), which mediate pro-inflammatory pathways and serves as substrates for ceramides and DAGs synthesis, are detrimental for insulin sensitivity [90] while polyunsaturated fatty acids (PUFAs) and monounsaturated fatty acids (MUFAs) have anti-inflammatory properties and are associated with improved insulin sensitivity [91].

Particularly relevant is the effect that short-chain fatty acids (SCFAs), namely acetate, propionate and butyrate, have on insulin sensitivity. SCFAs are the products of complex carbohydrate fermentation mediated by the gut microbiota and exert an overall beneficial effect on insulin sensitivity. Thus, altered gut microbiota composition and/or metabolic activity possibly caused by dietary imbalances, lead to changes in SCFAs appearance rates that in turn result in diminished insulin sensitivity [92].

The unfolded protein response (UPR) and insulin resistance

The UPR is a cellular mechanism initiated in response to the accumulation of unfolded and misfolded proteins in the ER lumen. Overnutrition can drive the accumulation of aberrant proteins and therefore induce and sustain the activation of the UPR, whose markers appear increased in obese patients [93]. Several animal studies have investigated the hypothesis of a direct link between the UPR and insulin resistance and, although the nature of this association is still rather obscure, the notion that the UPR is involved in the pathophysiology of insulin resistance is now well established [94]. Initially, a direct interaction between effectors of the UPR and the insulin signaling pathway was postulated. The c-Jun NH₂-terminal kinase (JNK) and the I κ B kinase (IKK), key downstream effectors of the UPR, were shown to directly impair insulin signaling at the level of IRS through inhibitory serine phosphorylation [95]. However, this model alone was later proven to be insufficient to explain the insurgence of insulin resistance, hence other additional UPR-mediated mechanisms were explored. The discovery that the UPR up-regulates DNL in the liver [96], offered an alternative explanation and animal studies aimed to investigate this new paradigm immediately followed [97], [98]. Taken together, these studies support a model in which UPR-mediated lipogenesis is involved in the progression of insulin resistance, leading to hepatic lipid accumulation and consequent activation of the DAG/PKC ϵ /IRK axis. Whether the UPR causes ectopic lipid accumulation or, as reported by some studies [99], lipids accumulation triggers the UPR, is difficult to assess. However, the available data draw a picture in which the UPR potentiates a primary lipotoxic mechanism.

Hepatic inflammation and insulin resistance

Overnutrition can induce inflammatory processes in insulin-sensitive tissues. Proinflammatory states are often associated with insulin resistance; both adipose tissue and liver are characterized by a chronic low-grade inflammation during pathological conditions such as obesity and NAFLD. On this basis, it was hypothesized that activation of the immune system could contribute to insulin resistance. The canonical model of inflammation-induced insulin resistance involves the activation of macrophages within insulin-sensitive tissues resulting in the secretion of proinflammatory cytokines such as TNF α , IL-6, and IL-1 β , and the consequent induction of inflammatory signaling cascades that overlap and impinge on the insulin signaling pathway resulting in disrupted insulin downstream effects. The serine kinases JNK and IKK are also effectors of the inflammatory response triggered by activated macrophages that, as it occurs during UPR-induced signaling events, directly interact with insulin signaling components and terminate insulin actions [100]. Although the adipose tissue is considered to be the primary site involved in this response, TNF α , IL-6, and IL-1 β that are secreted by afflicted adipose tissue impinge on other tissues as well [101]. The liver, which is populated by specialized hepatic macrophages known as Kupffer cells, can also be subject to cytokines derived from Kupffer cell activation.

Additionally, inflammation and hepatic insulin resistance are linked through an indirect lipotoxic effect. Early studies have demonstrated how cytokines in the inflamed adipose tissues enhance lipolysis [102], [103], thereby increasing the hepatic lipid burden that in turn leads to impaired hepatic insulin signaling and increased gluconeogenesis [73].

Although the association between inflammation and insulin resistance is well founded, it has not yet been established whether inflammation is the primary insult that eventually leads to insulin resistance. The mechanisms above described coexist alongside others in the pathological setting of insulin resistance and appear to be both inter-dependent and synergistic in terms of impairing insulin actions. For example, both lipid-enriched environments and the UPR induce inflammatory

responses. Inflammation might in turn induce lipid accumulation in the liver through adipose lipolysis, exacerbating insulin resistance. Lipid accumulation then aggravates both the UPR and inflammation in a positive feedback loop. Numerous efforts have been made to integrate these highly interconnected mechanisms in a unified model of insulin resistance, but to date there is no consensus.

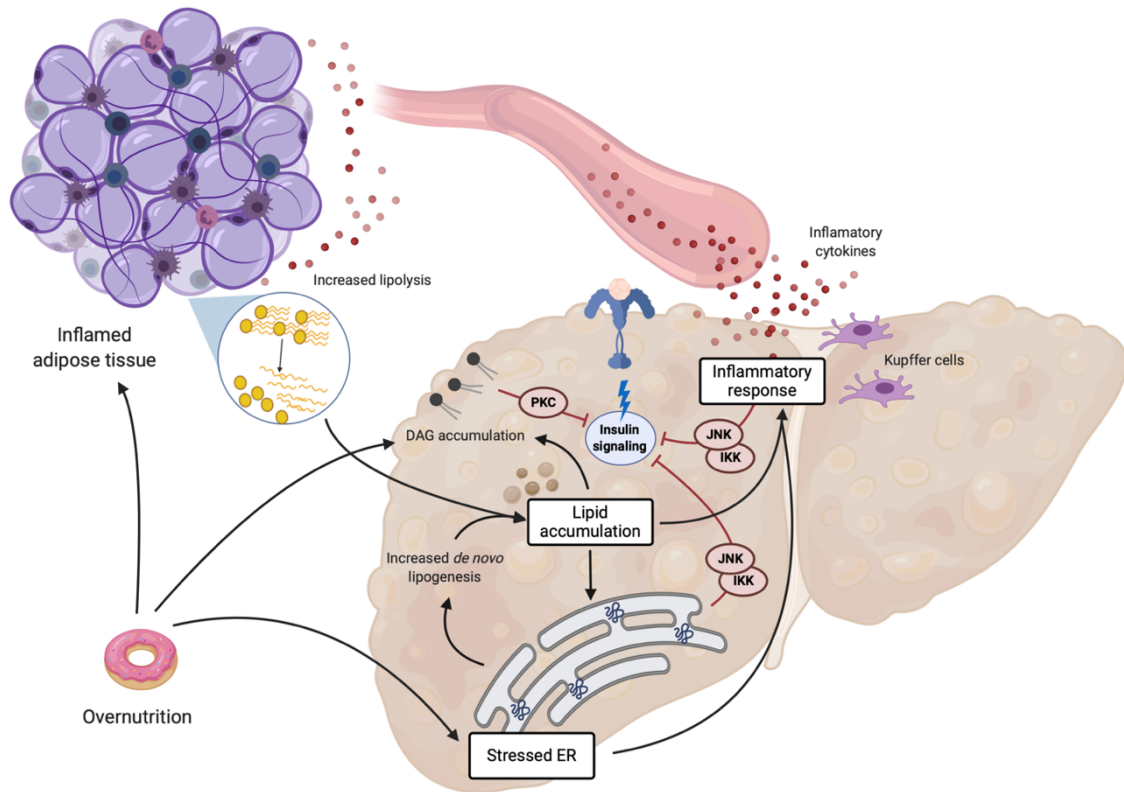


Figure 1.9 - Some of the most investigated molecular mechanisms of hepatic insulin resistance. Hepatic ectopic lipid accumulation, inflammation and ER stress often coexist and enhance each other in the pathological setting of insulin resistance. [Figure created with BioRender.com].

Insulin resistance and related diseases

Each insulin resistance mechanism that we have so far reviewed is strongly associated with and potentiated by nutrient oversupply. The finely tuned metabolic physiology that humans have developed over the course of evolution reflects an adaptation to an environment where nutrients are generally scarce with only intermittent availability. Thus, the evolved capacity for efficient utilization and storage of excess nutrients during rare times of plenty is ill-suited to Western dietary habits, characterized by a continuous supply of highly palatable, calorically dense, and easily available food, accompanied by a sedentary lifestyle. The technological advances in food processing allowed large-scale production of refined food and, as a consequence, the types of food that we consume profoundly changed over the last 100 years. The average daily caloric intake has increased by 205 calories since the 1960s [104] and today approximately 2.1 billion individuals are considered overweight or obese [105]. Obesity and obesity-related diseases such as NAFLD and T2DM are now endemic in both developed and undeveloped countries, impacting societies on multiple levels and causing long-term negative socioeconomic consequences.

Although the current surge in metabolic diseases is for the major part driven by unhealthy behavioral habits encouraged by the current capitalistic economic developmental model, it is fair to remember that a metabolic dysfunction results from a complex interplay between genetic and disparate environmental factors, which include socioeconomic status, cultural influences, comorbid conditions and related pharmacological treatments. Hereby we will analyze the pathophysiology of two of the most common metabolic diseases, NAFLD and T2DM, both characterized by insulin resistance, and also review a less studied case of metabolic disturbance, the one induced by certain classes of medication.

Nonalcoholic fatty liver disease (NAFLD)

When lipids are stored in tissues that are not designed to accumulate fat, (liver and muscle), a lipotoxic environment is progressively generated, leading to disturbed insulin signaling. This is the case of NAFLD, which is diagnostically defined as the presence of >5% hepatic fat accumulation in the absence of any other cause of fatty liver (i.e., viral, alcoholic, drug-induced). For NAFLD to develop, the rate of fatty acids input (fatty acids uptake and DNL) has to be greater than the rate of fatty acids output (fatty acids oxidation and VLDL export). The resulting continuous ectopic accumulation of lipids, accompanied by minor inflammatory processes, inevitably gives rise to hepatic insulin resistance. Glycogen synthesis decreases and excess glucose is diverted towards DNL instead aggravating lipid accumulation, whereas a concomitant insulin resistance in other organs such as adipose tissues, contributes to increased FFA fluxes towards the liver and indirectly stimulates hepatic gluconeogenesis. A series of factors deriving from the lipotoxic environment generated within and outside the liver, mediates the molecular switch that induces the progression toward nonalcoholic steatohepatitis (NASH), characterized by hepatic chronic inflammation, hepatocellular damage and fibrosis. In the long term, NASH might further advance towards hepatic cirrhosis which, in 2% of the cases, ultimately results in hepatocellular carcinoma [106].

NAFLD has an estimated global incidence of 25% [107] and, although not all people with NAFLD are obese, it is strongly associated with obesity. Moreover, NAFLD increases substantially the risk of developing T2DM and approximately 70% of people with T2DM also have NAFLD [108]. This association places lifestyle factors as the major putative cause implicated in the pathogenesis of NAFLD. Consumption of sugar-sweetened beverages and food has been especially scrutinized, as the industrialized production and diffusion of such food coincides with the modern times raise in obesity and related metabolic diseases. Genetic factors are also involved. The most studied example of genetic variant in this context is the single nucleotide polymorphism (rs738409, I148M) in the lipid droplet protein patatin-like phospholipase domain-containing protein 3 (PNLPA3),

which has been shown to significantly predispose to NAFLD [109]. Several other polymorphisms present in genes involved in both lipid and glucose metabolism have been associated with NAFLD, and the incidence of the disease is greater in ethnic groups that carry specific genetic variants, confirming that genetic factors play an important role in the pathogenesis of NAFLD.

Dysfunctional adipose tissue is implicated in the development of NAFLD and its transition to NASH. Visceral adipose tissues (VAT) in particular has a well-defined role in the progression of the disease, and increased waist circumference and VAT deposition is a common visible marker of NAFLD [110]. According to a well-accepted view, the increased lipolytic rate in VAT observed in obese patients, in part stimulated by inflammatory processes and sustained by defective insulin action, causes an overload of FFA in the portal vein promoting steatosis in the liver. In addition, inflammatory cytokines leaking from the inflamed VAT and released into the portal vein reach the liver, where they promote inflammatory processes that contribute to NASH transitioning [111].

Growing evidence points at the gut microbiota as one of the major players in the pathogenesis of metabolic diseases such as NAFLD and T2DM. A healthy gut microbiota has a number of beneficial functions for its host, which include body weight modulation. The discovery of an obesity-specific gut microbiota supported the idea that perhaps, is the gut microbiota itself that promotes obesity and associated diseases [112]. Diet, hygiene habits, medications, and numerous other factors regulate the microbiota composition and aberrant ratios of different species of microbiota can have deleterious consequences on the host. NAFLD patients and animal models have a different composition of gut microbiota that possibly contributes to the evolution of the disease through several mechanisms, including modulation of energy homeostasis, increased intestinal permeability and consequent “leakage” of pro-inflammatory agents, generation of toxic substances and decreased levels of secondary bile acids and choline (required for VLDL synthesis and export) whose metabolism is regulated by the gut microbiota [113].

Type 2 diabetes mellitus (T2DM)

T2DM is a heterogenic systemic disease characterized by three major metabolic defects: insulin resistance, dysfunctional insulin secretion that is not autoimmune-mediated, and increased hepatic glucose production. T2DM is also a slow disease: the initial metabolic disturbances that eventually lead to diabetes clinical manifestations are present years or even decades in advance. Diabetes onset begins with a state of generalized insulin resistance. Initially, pancreatic β -cells are able to compensate for this defect increasing insulin output (hyperinsulinemia), so that circulating glucose levels are kept under control. This initial stage is known as “pre-diabetes” and, apart from a mild postprandial hyperglycemia, no clinical symptoms are present. Over time however, β -cell function and number decline, resulting in decreased insulin secretion and consequent severe hyperglycemia. The cause for such decline is not completely understood, but it seems to involve a combination of genetic factors and toxic effects resulting from chronic exposure to high glucose and fatty acid levels [114]. Glucose in circulation becomes so high that it spills into the urine followed passively by a significant volume of water, leaving the patient to experience polyuria and intense thirst. The fasting hyperglycemia, also aggravated by the chronically increased hepatic gluconeogenic flux sustained by insufficient insulin action, is at this point severe enough to cause long-term damage to endothelial tissues, predisposing the diabetic patient to both macrovascular and microvascular diseases. Alongside hyperglycemia, dyslipidemia is another common outcome of diabetes. Diabetic patients manifest hypertriglyceridemia, decreased HDL cholesterol and elevated levels of the atherogenic LDL cholesterol [115]. These features are already in place years before the establishment of a fully developed diabetic phenotype and are observed to a more or less extent in all insulin resistance-related diseases, reflecting in part the failure of insulin to suppress adipose lipolysis.

Obesity, physical inactivity, weight gain in adulthood and ageing are all environmental factors involved in the progression of T2DM, affecting its speed and gravity during its whole continuum.

Early intervention before the metabolic derangements of glucose and lipids become manifest is of crucial importance. Identifying individuals that have impaired fasting glucose levels and/or impaired glucose tolerance that have not reached the clinical thresholds that define T2DM - often referred to as “pre-diabetic” - and treating them either pharmacologically or through behavioral correction can reduce the incidence of long-term complications such as cardiovascular diseases. Prevention is by far the most effective measurement in the management of T2DM. Despite the variety of lifestyle and/or pharmacological options for treatment, T2DM has proven to be difficult to reverse and only a small percentage of diabetic patients eventually achieve glycemic control [116].

Drug-induced metabolic dysfunctions

Several classes of medications commonly used in clinical practice are known to induce metabolic abnormalities such as hyperglycemia, dyslipidemia, weight gain and diabetes. These co-morbidities occur with a fairly high incidence and the underlying mechanism varies among the different drug agents. Some medications impact insulin sensitivity, other insulin secretion, while some others impact both of these aspects. In the following section, three classes of widely used drugs that list metabolic dysfunctions among their significant side effects will be reviewed.

Glucocorticoids (GCs)

GCs are natural hormones that control energy homeostasis. They normally liberate energy substrates to help the organism to cope with a stressor. Their actions include stimulating protein breakdown in the muscle, adipose tissue lipolysis and hepatic gluconeogenesis. All of these actions oppose those of insulin. GCs are also immunomodulators and a powerful tool in medical practice: synthetic GCs are administered to counteract uncontrolled inflammatory processes. However chronic exposure to pharmacological concentrations of GCs is associated with insulin resistance, diabetes and weight gain with disfiguring fat deposition primarily in visceral and interscapular

depots [117].

In abdominal adipose tissue, where the GCs receptor is predominately expressed, GCs facilitate the maturation of pre-adipocytes into differentiated adipose cells. Meanwhile, lipolysis is stimulated in existing subcutaneous depots, causing a systemic FFA elevation which, among other things, promotes ectopic lipid accumulation in muscle and liver and aggravates insulin resistance. This differentiated regulatory effect that GCs have on the different adipose depots results in an overall relocation of lipids, from the periphery (arms and legs) towards the trunk. Moreover, GCs directly interfere with insulin signaling, attenuating insulin action not only in adipose tissue, but also in the liver and muscle.

Finally, GCs affect both pancreatic α - and β -cells secretory activity and, by enhancing the former and restraining the latter, they worsen hyperglycemia and might ultimately induce diabetes [118].

Antihyperglycemic agents

Certain classes of medications used in the management of diabetes promote weight gain. Insulin, sulfonylureas (SU), and thiazolidinediones (TZDs) are the three antihyperglycemic medications most associated with this undesired effect. Insulin is currently the only treatment option for type 1 diabetic patients and is also administered to advanced-staged type 2 diabetics when other treatments no longer work. Insulin therapy is often associated with appetite stimulation triggered by fluctuating glycaemia which causes increased caloric intake and a consequent increase in body fat. Calories are also better retained as glycosuria is reduced and insulin-stimulated anabolic processes are potentiated, leading to an increase in lean body mass as well [119].

SU, which ameliorate hyperglycemia by stimulating insulin secretion, also promote similar metabolic changes, although the increase in body weight occurs mostly in the initial months of treatment [119].

TZDs lower hyperglycemia by improving insulin sensitivity rather than increasing its secretion. The weight gain observed in patients administered with TZDs is associated with a better recovery

of glycemic control. Fluid retention caused by reduced renal excretion of sodium and altered intestinal ion transport is also partially responsible for TZD-weight gain. In contrast to GC, the increased adiposity induced by TZDs is almost entirely observed in subcutaneous depots, whereas visceral adiposity remains unaltered [120].

Second-generation antipsychotics (SGAs)

SGAs have proven to possess a superior efficiency in treating both negative and positive symptoms of schizophrenia compared to first-generation antipsychotics (FGAs) [121]. One of the major advantages of SGAs over FGAs is their low propensity in causing extrapyramidal symptoms (EPS), the main FGA side effect [122]. Nowadays, SGAs are increasingly being prescribed not only to schizophrenic patients but also as treatment for a number of other psychiatric diseases such as bipolar disorder, autism and depression [123], [124], [125]. However, SGA therapy does have serious side effects which include weight gain and associated metabolic abnormalities such as hyperglycemia, insulin resistance, T2DM, dyslipidemia and cardiovascular diseases [126]. Considering the already debilitating impact that psychiatric diseases have, the additional complications of weight gain and associated co-morbidities might end up worsening the patient's quality of life as well as inducing social withdrawal and isolation.

The mechanisms by which SGAs cause their metabolic side effects are currently not well understood. The prevalence of metabolic abnormalities among schizophrenic patients is higher compared to the normal population [127] and the question of whether these metabolic abnormalities are already in place during the first episode of the disease or develop along the course of the illness following SGA treatment, is difficult to resolve. Drug-naive schizophrenics are not easy to recruit in human studies and, although available in the research market, animal models of schizophrenia are particularly difficult to characterize. Despite the difficulty in inferring causality on this subject, there is evidence suggesting that reward mechanisms are impaired in schizophrenic patients, which tend to indulge in addictive behaviors, including preference for and excessive consumption of high-

palatable food. SGAs attempt to correct the reward system but, by doing so, also better motivate the patient to seek and “come back for more” food, especially the type he/she has been conditioned to prefer, calorie-dense and highly palatable [128]. Moreover, the hedonic experience that comes with the act of eating such food (already enhanced in schizophrenic patients), is amplified by certain SGA treatments [129]. This proposed mechanism implies that disease and treatment have to co-exist for the full manifestation of SGAs side effects. On this basis, studies of SGA effects in animal models might be flawed, as demonstrated by the fact that in several of them, no or very little weight gain is observed following SGA administration.

However, the notion that SGAs uniquely contribute to the metabolic abnormalities observed in these patients is widely accepted and was corroborated by acute studies on healthy volunteers administered SGAs for few days. In these studies, early indications of dysregulated glucose and lipid metabolism, such as impaired glucose uptake, hyperinsulinemia and elevated circulating leptin and TGs were observed at the end of short treatment periods [130], [131]. These studies were especially useful, not only to understand the role of SGAs independently of the disease, but also to pinpoint some of the early metabolic changes, which appear to involve direct tissue and organ effects, rather than being secondary to weight gain.

SGAs exert their therapeutic actions through a number of receptors: dopamine (D), serotonin (5-HT), adrenergic (α , β), histamine (H), muscarinic (M), NMDA and GABA_A receptors. These receptors are expressed in regions of the brain that control food intake and in peripheral organs. Several studies have suggested that SGAs have antagonizing effects on certain central nervous system pathways involved in food intake, energy expenditure and food reward systems [132], [133]. Other studies have demonstrated that SGAs have a direct impact on certain peripheral tissues involved in body energy homeostasis. However, both of these sites and mechanisms of action need further validation and they do not necessarily exclude each other. Some of the most investigated mechanisms include SGA-induced impairment of α - and β -cells secretory activities [134], disturbed insulin signaling in organs such as liver and muscle [135], [136], and abnormal metabolic activities

mediated by the descending sympathetic and parasympathetic systems activated via central mechanisms [137]. In addition, SGAs seem to interfere with the immune system, gut microbiota and hormonal action [138] through mechanisms that are still unclear.

Different SGAs have different levels of affinity for each receptor and generally the SGAs with more therapeutic power are also the ones inducing the most severe metabolic side effects, suggesting common mechanisms for both outcomes [139]. Independently from central or peripheral modes of action, affinities for the H₁, D₂, 5-HT_{1A}, 5-HT_{2C} receptors are most closely linked to increased weight gain, and affinity for the H₁, M₃ and 5-HT_{2C} receptors correlates with increased risk for diabetes [140]. However, despite the large number of studies conducted to date, there is no consensus on how SGAs promote obesity and its metabolic complications.

Interventions in the management of metabolic diseases

Overnutrition is a common underlying link to almost all metabolic complications hereby analyzed; thus, behavioral intervention - in particular caloric restriction and increased physical activity - is considered to be a key strategy. Obesity drives the evolution of both NAFLD and T2DM and studies conducted in humans and rodents demonstrated that even a small but sustained proportion of weight loss is capable of ameliorating, or even reversing NAFLD and T2DM [141]. However, sustained weight loss has been found to be a difficult task to achieve for obese subjects who tend to relapse to their original body weight after a prescribed diet/lifestyle program [142]. Bariatric surgery currently offers the best chances of weight loss among obese patients with beneficial metabolic effects persisting over several years [143]. However, not all patients qualify for this intervention and therefore pharmacological treatment is an essential accompaniment to diet/lifestyle changes.

While there is no current licensed drug for the treatment of NAFLD, many are available in the market for T2DM. Metformin is the first drug of choice for all T2DM patients: it is associated with a good safety profile and, unlike other antihyperglycemics, does not include weight gain and hypoglycemia among its side effects. Through a not-so-well defined mechanism, metformin restores normal glycaemia by down-regulating hepatic gluconeogenesis, decreasing intestinal glucose absorption and enhancing peripheral glucose uptake [144]. Overall, metformin ameliorates insulin action without affecting insulin secretion, hence the term “insulin sensitizer”. Although metformin remains the best first-line antidiabetic drug in current use, metformin monotherapy tends to become less effective over time and second-line agents are therefore required. Second-line drugs include several other insulin sensitizers, insulin secretagogues (a class of drugs that enhances insulin secretion), GLP-1 analogues/DPP4 inhibitors (which act at the level of incretins: gut hormones that promote insulin secretion and reduce glucagon release) and insulin [145].

Despite the large number of medications for T2DM treatment, the majority of patients with long-term T2DM fail to achieve effective glycemic control, therefore new medications acting on different targets are urgently needed. Some of the therapies currently being tested and particularly further along in development, target the sodium-glucose cotransporter (SGLT-2), the major transporter in the kidneys responsible for glucose reabsorption whose inhibition should lower plasma glucose concentration, and 11 β -hydroxysteroid dehydrogenase type 1 (11 β -HSD1), the enzyme that converts cortisone into cortisol, its active form. Other promising drugs in the pipeline target hepatic metabolism. In particular, glycogen phosphorylase and glucokinase; the phosphatases involved in the attenuation of the insulin signaling pathway, first and foremost PTP-1B; and insulin counteracting hormone, glucagon, through glucagon receptors antagonists [116].

***Insulin Resistance and Metabolic
Perturbations: Common Methods and
Experimental Approaches***

Broadly, insulin sensitivity can be described as the ability of insulin to prompt a series of responses in its target tissues which ultimately result in clearance of excessive circulating glucose and reestablishment of euglycemia. A complete evaluation of insulin sensitivity has to take into account that this phenomenon depends on two factors: how abundant insulin is in circulation and how effective tissues respond to insulin. The gold standard method for the assessment of insulin sensitivity *in vivo* is the hyperinsulinemic-euglycemic clamp, a technique developed several decades ago [146] and still widely used in both humans and animals. Essentially, after an overnight fast, the subject's circulating insulin is raised and maintained for few hours to a concentration similar to that of postprandial levels while, to maintain euglycemia, glucose is infused. As long as insulin concentrations are kept steady, the quantity of glucose required to maintain euglycemia reflects insulin sensitivity, the more sensitive tissues are to insulin, the more glucose needs to be infused. Over the years several variations have been introduced to this standard technique and different other clamps have been optimized in order to address specific research questions. For example, the hyperglycemic clamp is used to assess β -cells responsiveness to hyperglycemia. In this setting, glucose is acutely infused to reach a target hyperglycemia, which is kept steady, while insulin is secreted by the subject in a variable amount, according to the individual's capacity to secrete insulin. Glucose clamps provide in principle very accurate measurements; however, they are very elaborate, expensive and technically difficult to perform. Unsuitable as a clinical diagnostic tool, their use is limited to research purposes. In this regard, discrepancies among studies have been reported due to the difficulty of the technique and lack of a standardized protocol [147].

The oral glucose tolerance test (OGTT) is the most commonly used clinical test for the diagnosis of diabetes and, with some adaptations, can also be performed in rodents. The OGTT measures the ability of an individual to dispose of a glucose load administered after an overnight fast. Glycaemia is measured at different time points before and after the glucose challenge, and

these measurements provide an approximate indication of the capacity to maintain euglycemia without, however, distinguishing between insulin sensitivity and insulin secretion contributions. The insulin tolerance test (ITT) and the pyruvate tolerance test (PTT) are variants of the OGTT in which the bolus of glucose is substituted by a dose of insulin in the first case, and of pyruvate in the second. Similarly, glucose excursion is measured over time, but the ITT provides an approximate indication of whole-body insulin sensitivity, whereas the PTT reflects the rate of hepatic gluconeogenesis [147].

A less direct method for the assessment of insulin resistance involves the use of mathematical models. The Homeostasis model assessment (HOMA) and the quantitative insulin sensitivity check Index (QUICKI) are two mathematical indices used to quantify insulin resistance [148], [149]. The main advantage of this approach is that only a single blood sample is required to calculate both indices as the only variables in their formulas are fasting glucose and insulin levels, however their precision is poor and ideally the integration of another method for insulin sensitivity assessment is required [150].

From a pure research perspective, the study of insulin action, or more in general, metabolism in the context of insulin resistance, can be approached from different angles. Molecular biology methods have been widely used to investigate perturbation of the insulin signaling pathway and alterations of gene expression in a given pathological state. Measurement of metabolite concentrations by metabolomics has revealed important associations between specific metabolites and disease progression, incidence, severity, and has contributed to the unraveling of new mechanistic links in the pathogenesis of metabolic diseases [151]. For example, dysregulated metabolism of branched-chain amino acids (BCAAs) has been shown to strongly correlate with insulin resistance states, a discovery largely corroborated by metabolomic studies, suggesting possible implications of BCAAs in the pathogenesis of insulin resistance [152]. However, information regarding metabolic pathway activity cannot be solely inferred by metabolite concentrations since changes in these parameters do not necessarily align with alterations in

metabolite fluxes, defined as the flow of carbons per unit time through a metabolic pathway. Given that the control of systemic glucose levels ultimately involves dynamic alterations in metabolic fluxes through the pathways of glucose synthesis and disposal, direct measurement of these fluxes is a fundamental parameter for understanding the disruption of glucose homeostasis in diabetes. This approach also applies for understanding the changes in systemic lipid levels and tissue distributions that accompany those of glucose.

The use of stable isotope tracers in metabolic research made possible the quantification of metabolic fluxes through pathways involving carbohydrate, lipid and protein synthesis and degradation. Isotopes are chemically identical atoms that differ in mass because of different numbers of neutrons in their nuclei; in metabolic research, two commonly used isotopes are ^2H (or deuterium) and ^{13}C . Isotopes can be incorporated into substrates of interest (i.e. $^2\text{H}_2\text{O}$, [1- ^{13}C]glucose) and administered to the subject or animal model at the beginning of an experiment. These substrates are called tracers and are metabolically indistinguishable from the tracee, their naturally occurring counterpart. Once inside the organism, the tracer participates in the metabolic reaction of interest, “isotope-labeling” the product of the reaction in specific positions. The amount of isotope present in a metabolic intermediate or a pathway end-product can then be quantified through nuclear magnetic resonance (NMR) or mass spectrometry. By applying these data to stoichiometric models of metabolic pathways or networks, metabolic estimates can be obtained. Tracers can also be used to estimate appearance rates of circulating metabolites such as glucose by the isotope dilution method. For example, in the case of glucose, [6,6- $^2\text{H}_2$]glucose, is infused into the blood at a constant rate. Once isotopic steady-state is achieved, blood from a contralateral vein is sampled for [6,6- $^2\text{H}_2$]glucose enrichment. The extent to which the [6,6- $^2\text{H}_2$]glucose enrichment was diluted relative to that of the infusate informs the rate of glucose appearance.

Isotopic tracers have a variety of applications and are used in several experimental set-ups in combination with other techniques. Glucose tracers can be administered during hyperinsulinemic-euglycemic clamps to provide information regarding the rate of appearance (R_a) and the

contribution of endogenous glucose production to R_a [153]. Insulin-mediated suppression of lipolysis can also be assessed during hyperinsulinemic-euglycemic clamps infusing labeled palmitate or glycerol [154]. $^2\text{H}_2\text{O}$ administration to enrich body water has provided relative quantification of both lipid and glucose fluxes; for example, in an animal model, $^2\text{H}_2\text{O}$ alone can resolve the contributions of direct and indirect pathway to hepatic glycogenesis, as well as measure the rate of DNL, desaturation, elongation and glycerol synthesis in a liver or adipose TG sample [155], [156].

Rodents in metabolic research: experimental considerations

The use of rodent models to draw inferences about human metabolism has proven to be an invaluable experimental tool. The anatomical, physiological and genetic similarities with humans, small size, easy maintenance, short life cycle, and ease of genetic modification are among the most appreciated advantages that rodents offer over other animal models. During decades of biomedical research, a vast number of human diseases have been successfully transposed to mice models, potential treatments have been quality- and safety-checked in mice before humans, and there is no doubt that our basic scientific knowledge has greatly advanced since mice became a widespread model of investigation. However, mice are not miniature humans, and it is critical that every test and experimental protocol developed in humans to study aspects of human pathophysiology, is validated in rodents each and every time an animal study is considered. When conducting a study in mice, the researcher needs to interpret the obtained data in the light of certain caveats. Hereby we will review some important considerations that need to be taken into account when approaching the study of certain metabolic conditions such as insulin resistance, obesity and T2DM in a rodent model.

The most striking difference between human and rodents metabolism is that, because of their small size, rodents possess a much greater basal metabolic rate than humans. Mice require approximately seven times more energy per gram of body weight to function while at rest in a neutrally temperate environment [157]. Among other things, it means that the fasting interval for establishing “baseline” metabolic state is much shorter than overnight fasting (~12 hr without food) typically used for humans. For a mouse, a 12 hour fast causes a ~ 15% loss of lean body mass, which results in a state of metabolic stress that is characterized, among other things, by improved insulin-stimulated glucose utilization [158]. A second important point to consider is that mice have a very different feeding behavior when compared to humans. Rodents do not possess the concept of “meal” and they rather feed themselves continuously over their metabolically active period, the dark cycle. They occasionally eat their own feces and small changes in temperature might alter their caloric intake. On the other hand, humans fulfil their total caloric intake in the form of meals (approx. 3 per day), their feeding behavior is influenced by their psychological status and is characterized by a strong “volitional” component, in the sense that humans can deliberately choose whether to eat or not. Some of these caveats can be successfully circumvented, for example rodents can be trained to eat their food in the form of discrete meals or placed in metabolic cages, special cages that enable accurate metabolic monitoring.

Proper animal handling is another factor that should never be neglected, especially when performing metabolic tests. Many common procedures require the animal to be physically restrained, something that rodents particularly dislike. “Tail-picking” is a common handling method but picking a mouse by the tail simulates the act of being captured which is cause of great discomfort for the animal [159]. Blood sampling can also be a source of considerable stress; blood is normally withdrawn by cutting a small portion of tissue from the tip of the tail and by “milking” the blood into a collecting tube. This procedure, although easy to perform, can only provide a small amount of blood, and the attempt of withdrawing more blood from the same animal, cutting the tail at several points continuously “squeezing” it while the animal is kept restrained, is cause of pain

and distress [158]. All of these procedure-associated stressors are potentially significant metabolic confounders affecting plasma cortisol, glucose and lipid levels among other things [160]. To minimize this effect, the researcher is encouraged to positively habituate the animal to human contact, exposing it to standard handling procedures each day over a prolonged period of time before the planned experimental test.

Some of the most common experimental biases that characterize all animal studies in general, independently of the research area of interest, are in relation to the animal age and gender. The vast majority of animal studies are conducted in young male rodents. This is mostly due to practical reasons; young animals are always preferred over old ones as their maintenance is less costly, and because of the estrous cycle where hormones vary periodically, females are considered “more variable” than males. However, insulin resistance and associated diseases strongly relate to age and studies on young animals might not mimic the evolution of metabolic diseases as they are observed in humans [161]. Likewise, exclusion of the female gender has important implications. In the context of metabolism, females are generally less prone to metabolic disturbances, in part due to estrogen protective effects [162]. The concept of “control animal” has been also largely scrutinized in this context. What is normally called “control” in a standard laboratory environment might not exactly reflect human physiological normality: laboratory control animals fed *ad libitum* living a sedentary lifestyle might in reality be metabolically morbid and therefore not representative of healthy human controls [163].

Rodent phenotypes representing obesity, insulin resistance and metabolic diseases can be achieved by diet interventions and/or drug administration. Genetic mouse models of obesity and diabetes are also widely used and comprise of mice bearing naturally occurring mutations that induce the development of metabolic dysfunctions, as well as genetically engineered mice where expression of a specific protein is altered. Among the former, one of the most commonly used animal models of obesity is the leptin-deficient ob/ob mouse. This mouse strain develops obesity, hyperinsulinemia and hyperglycemia after 4 weeks of age, a phenotype entirely due to a recessive

null mutation in the leptin gene which spontaneously arose in the Jackson laboratory several decades ago [164]. This mouse was one of the first to be used in the study of diabetes and has provided much fundamental knowledge about T2DM pathogenesis. However, the metabolic profile of the ob/ob mouse, as well as of all the other strains whose phenotype is a direct consequence of a singular mutation, can be correctly described as “monogenic” while T2DM is not a monogenic disease. The sequence of clinical manifestations that builds up during the progression of diabetes in humans is not correctly represented in these animals; nonetheless they are still to this day considered valuable mouse models commonly used in pharmacological studies.

A better representation of the evolutionary path of the metabolic syndrome in humans is perhaps depicted by animals whose metabolic dysfunctions are induced by hypercaloric diets that mimic modern Western diets. Although different strains of mice respond differently to such diets, combinations of high-fat or high-sugar diets are well known to induce metabolic phenotypes. A normal rodent diet contains 10% fat, whereas a high-fat diet (HFD) and a very-high-fat diet (VHFD) contain respectively 45% and 60% fat by calories [165]. Both HFD and VHFD induce obesity accompanied by impaired glucose tolerance, hyperinsulinemia, hepatic steatosis, increased circulating TGs and FFAs [166]. VHFD induces more rapid and exaggerated metabolic responses, but HFD better represents the fat content of modern Western diets, which are also rich in refined sugars. Of note, early metabolic abnormalities can be observed after just a few days of high-fat feeding in rodents, and such initial manifestations include hepatic steatosis and increased hepatic glucose output, whereas skeletal muscle insulin resistance requires few weeks to develop. This timeline differs in humans, whose first abnormal metabolic alteration is the impairment of glucose disposal due to defective insulin signaling in skeletal muscle [167].

High fructose/sucrose diets contain 50-60% calories from fructose or sucrose. Fructose, a very much abundant component of modern western diets, is for the most part responsible for the metabolic outcomes associated with such diets. High fructose/sucrose feeding induces insulin resistance, fatty liver and dyslipidemia; however, a substantial period of time is required to induce

considerable weight gain in rodents [168]. Rats better manifest this metabolic phenotype, which requires approximately two weeks to develop after initiating the feeding regime, whereas most common mice strains require a considerably longer time to develop insulin resistance in response to high fructose/sucrose diets [169].

To conclude, rodent studies and especially those performed in mice, offer important advantages which, among other things, include the extensive knowledge that we came to acquire over the years in several aspects of their biology and behavior. However, critical thinking and careful reading of pertinent literature are fundamental during each study design. Information regarding animal age, gender, strain, and protocols of all the undertaken experimental procedures must always be detailed when an animal study is described and, in order to avoid false outcomes and fictitious phenotypes, interpretation of data and extrapolation to humans must take into account the intrinsic limitations and uniqueness of the animal model

AIM OF THE WORK

Aim of the Work

Metabolism is by definition the sum of all the chemical events that take place within an organism. Metabolism is a dynamic and adaptative process whose well-functioning relies on the coordinated control of metabolic fluxes by a diverse set of regulatory mechanisms.

The metabolic status of an organism is often defined in terms of intermediary metabolite steady-state concentrations and/or levels of storage products such as lipids or glycogen. However, these parameters are blind to key aspects of metabolic regulation and adaptation such as futile cycling activity and the sources of carbons utilized for oxidative or biosynthetic activities.

Steady-state metabolite concentrations in a given cell or tissue represents a balance between their rates of appearance and disposal. These underlying metabolic fluxes may be regulated by several different mechanisms, often concurrently. Aberrant regulation gives rise to altered flux rates, which in turn explain abnormal metabolite profiles and/or imbalances in substrate utilization and biosynthetic activities observed in many pathological settings.

The use of isotopic tracers allows the resolution of these metabolic fluxes, while informing about the utilization of specific substrates by catabolic or anabolic pathways. In some cases, this information explains the observed changes in intermediary metabolite and/or product concentrations in certain physiological or pathophysiological conditions. In other cases, it reveals compensatory alterations in metabolic fluxes that allow stable metabolite concentrations to be maintained in these settings.

In the liver, the principal metabolic axis encompassing carbohydrate and lipid metabolism can be defined as connecting glycogen, glucose-6-phosphate, pyruvate, acetyl-CoA and triglyceride. Along this axis are catabolic pathways such as glycolysis and β -oxidation and anabolic pathways such as gluconeogenesis, glyceroneogenesis, glycogenesis and lipogenesis.

In this work, we employed isotopic tracers to study various component pathways of this axis in response to putative perturbations in hepatic insulin actions by three different types of interventions:

high sugar feeding, second-generation antipsychotic medications, and genetic deletion of PTP-1B - a phosphatase that negatively regulates insulin signaling.

In Study 1, a combination of $^2\text{H}_2\text{O}$ and ^{13}C -enriched fructose and glucose was utilized to study hepatic glycogen synthesis in animals fed a high-fructose corn syrup formulation for a prolonged period of time. Our main goal was of assessing the metabolic fate of fructose and glucose in the context of hepatic glycogenesis during high-sugar feeding.

In Study 2, we administered for the first time $^2\text{H}_2\text{O}$ to mice chronically treated with second-generation antipsychotics. The goal in this case was different; by measuring hepatic glycogen and lipid synthetic fluxes, we aimed at inferring the presence of any aberrant regulatory mechanism that governs the rates at which altered pathways function.

Finally, in Study 3, we employed the use of $^2\text{H}_2\text{O}$ in a genetically modified mouse to better understand the role of a much-studied enzyme involved in the perturbation of insulin signaling - PTP-1B - a promising drug target for the reversal of insulin resistance and its associated pathologies.

To pursue these stated objectives, advances in the stable isotope tracer methodologies developed for the assay of glycogenesis were made, in particular towards resolving the metabolic conversion of fructose to glycogen and determining its overall contribution to hepatic glycogen synthesis. These method developments nevertheless maintained a critical aspect of the metabolic measurements developed in the lab: that they are always performed in animals that are allowed to feed *ad libitum* in their usual environment.

THEORY AND METHODS

***Stable Isotope Tracers for the Analysis of
Hepatic Glycogen and Lipid Synthetic
fluxes: Theoretical Aspects***

A general protocol

Each of the three studies presented in this thesis was conducted in mice according the following general protocol.

Briefly, mice of each study were subjected for a determined period of time to a specific intervention (i.e., alteration in the diet, drugs), that could potentially induce a perturbation in the metabolic fluxes under study, in our case hepatic glycogen and lipid synthetic fluxes.

At the end of the intervention period, mice were administered with one or more stable isotope tracers provided at the beginning of the final evening. During this interval (~ 16 hours), the animals were allowed to feed normally in order to promote hepatic glycogen deposition and *de novo* synthesis of lipids. At the end of the dark cycle, mice were sacrificed.

Post-mortem, hepatic glycogen and lipids were purified from livers and later analyzed for tracer incorporation. Glycogen was first digested into glucose and then derivatized to monoacetone glucose (MAG) prior further analysis. Isotopes' enrichments in the biological samples were then detected with nuclear magnetic resonance techniques (NMR). Finally, NMR data were processed, and glycogen and lipid synthetic fluxes quantified.

NMR spectroscopy: basic principles

Because of their nuclear spin properties (spin $\neq 0$), ^2H (spin =1) and ^{13}C (spin = $\frac{1}{2}$) enrichment of metabolites can be detected and quantified by NMR spectroscopy.

Atoms with a nuclear spin also possess a magnetic moment, meaning that in the absence of an external magnetic field they behave as tiny magnets spinning at random directions. When a strong external static magnetic field such as the one generated by a NMR spectrometer is applied to such nuclei, their magnetic moments align with respect to the external magnetic field. Under these conditions, quantum mechanical rules dictate that the alignments are restricted to limited numbers of orientations, each corresponding to a specific energy level and whose number is related to the

nuclear spin number by $2I + 1$, where I is the spin number. Thus, ^{13}C with $I = \frac{1}{2}$ has two possible orientations corresponding to two different energy levels. ^2H on the other hand, being characterized by a quadrupolar nuclear spin moment ($I = 1$), has three possible orientations corresponding to three different energy levels. The difference between energy levels is proportional to the strength of the magnetic field applied.

In these conditions, if an additional weak oscillating magnetic field (radio-frequency pulse) is applied, nuclei absorb energy and transiently swing out of alignment moving to higher energy states. Only an oscillatory magnetic field that matches the energy difference between energy states can cause the nuclear spin population to transition from lower to higher energy levels. When the radio-frequency pulse is turned off, nuclei return to the lower energy state, emitting non-radiative energy in the form of radio waves at the same frequency of the one absorbed. Radio waves emitted by the nuclei are then detected by a receiver coil, yielding an NMR spectrum.

Resonating nuclei of a given element in a molecule can be distinguished in the NMR spectrum because they experience slightly different magnetic field strengths depending on the intramolecular environment of the atom. This is due to the “shielding” effect caused by the surrounding electrons that produce magnetic moments opposing that of the applied field. Generally, high electron density around a specific nucleus causes reduced magnetic field at the nucleus and thus the energy required to transit from lower to higher energy level is also reduced. Because of this, different nuclei in a molecule resonate at different frequencies (chemical shift) producing distinctive peaks in the NMR spectrum that can be resolved from one another and quantified.

Of note, in comparison to other atomic transitions, for example those involving electron spin states that are coupled with the absorption of visible light, the nuclear spin transitions are very weak. This means that according to the Boltzmann distribution, the population difference between low and high spin states under ambient conditions is very small, even with the strongest available magnets. A direct outcome of this is that the inherent sensitivity of NMR is considerably less compared to other spectroscopic methods based on visible light or UV absorption/emission.

Tracing hepatic glycogen metabolism with stable isotopes

²H₂O for quantification of direct and indirect pathway contributions to hepatic glycogen synthesis

Glycogen synthetic fluxes were measured using ²H₂O as metabolic tracer in all three studies described in this thesis.

²H₂O is an inexpensive and widely used metabolic tracer that presents several advantages. First, ²H₂O rapidly equilibrates with total body water, thus the water precursor enrichment can be easily and precisely determined from body fluids such as plasma or urine. Second, ²H₂O rapidly distributes throughout all tissues and allows the simultaneous assessment of biological processes in different sites of the body such as liver and adipose tissue. On distribution into body water, ²H₂O participates in numerous biochemical reactions involving hydrogen exchange or addition between water and metabolites that are almost all catalyzed by metabolic pathway enzymes. These reactions are ubiquitous and are found in almost all metabolic pathways, including those that converge on glycogen synthesis.

Hepatic glycogen synthesis can occur from intact hexose precursors (direct pathway) or from gluconeogenic precursors (indirect pathway). As previously explained, direct pathway activity is highly regulated by insulin, thus any perturbation in hepatic insulin signaling is expected to disproportionately affect direct pathway glycogen deposition. Incorporation of ²H from ²H₂O into glycogen allows the quantification of the individual contributions of direct and indirect pathways to hepatic glycogen synthesis in rodents during natural overnight feeding [155], [170], [171].

Figure 2.1 schematically shows how glycogen monomers become enriched with ²H in specific positions according to the glycogenic source. Following exchange with ²H₂O, both direct and indirect pathway precursors of glycogen become enriched with ²H.

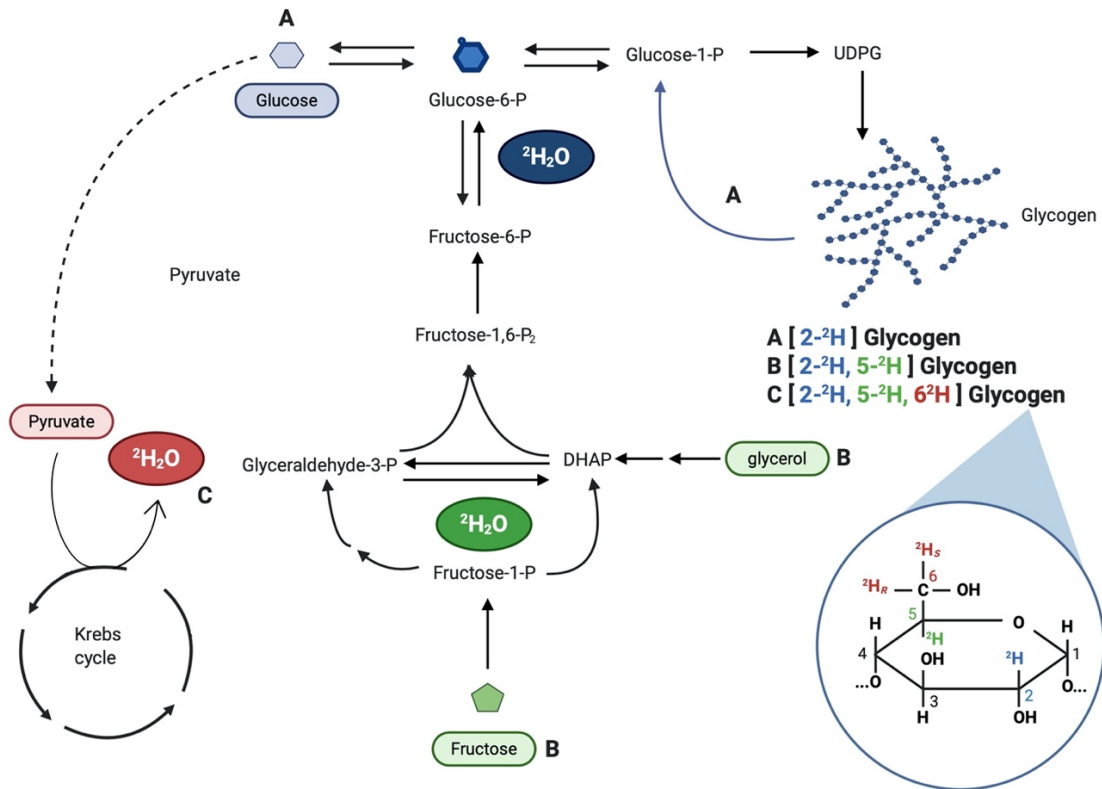


Figure 2.1 - Schematic representation of glycogen synthesis and positional enrichment of glycogen units from $^2\text{H}_2\text{O}$. Direct pathway precursors deriving from intact hexoses (Glucose \rightarrow Glu-6-P \rightarrow Glu-1-P \rightarrow Uridine diphosphate glucose (UDPG) \rightarrow Glycogen) become enriched with ^2H only in position 2 (represented in blue). Glycogen cycling (blue arrow) also results with position 2 enrichment of previously unlabeled glycogen monomers. Triose-P precursors, which include glycerol and fructose, become enriched in positions 2 and 5 (green), whereas anaplerotic Krebs cycle substrates become additionally enriched on the methylene hydrogens of carbon 6 (red). On the bottom right, a glycogen unit with positions 2, 5 and 6 highlighted in the corresponding color as above described. [Figure created with BioRender.com].

All direct and indirect pathway precursors become enriched in position 2 as a result of extensive exchange between glucose-6-phosphate and fructose-6-phosphate catalyzed by G6P-isomerase. This includes hitherto unlabeled glycogen units that participated in futile cycling with glucose-6-phosphate.

While glucose metabolized by the direct pathway results in glycogen enriched exclusively in position 2, indirect pathway precursors have the possibility of becoming enriched in additional positions. Besides position 2, all indirect pathway precursors become enriched in position 5 via triose phosphate isomerase. Indirect pathway contributions can be further resolved into substrates

metabolized via the anaplerotic pathways of the Krebs cycle and substrates that enter at the level of triose-P, which include fructose and glycerol. In fact, besides position 2 and 5, anaplerotic Krebs cycle precursors become enriched also in position 6 following exchange of hydrogens with $^2\text{H}_2\text{O}$ -enriched body water at the level of pyruvate and Krebs cycle intermediates.

Neither intact glycogen nor its glucose product following glucosidase digestion, are well suited for NMR analysis of ^2H -enrichment due to limited solubility and/or poor signal dispersion. However, the glucose derivative monoacetone glucose (MAG) provides fully resolved NMR signals for all seven carbon-bound ^2H [172]. Hence, hepatic glycogen was digested into glucose and converted into MAG prior NMR analysis.

Figure 2.2 shows a ^2H -NMR spectrum of MAG obtained from mouse hepatic glycogen. A typical ^2H -MAG spectrum gives rise to well resolved peaks, each representing a specific positional ^2H -enrichment of the MAG molecule. Based on the principle that the area under a peak is proportional to the number of the resonating nuclei; by integrating the different peaks, ^2H -enrichment of all positions in the molecule can be inferred.

The two methyl groups of MAG (orange arrows in Figure 2.2) are incorporated during the derivatization process from acetone enriched with ^2H to a specific known percentage and are therefore used as intramolecular standards for the quantification of ^2H -enrichments of all other positions.

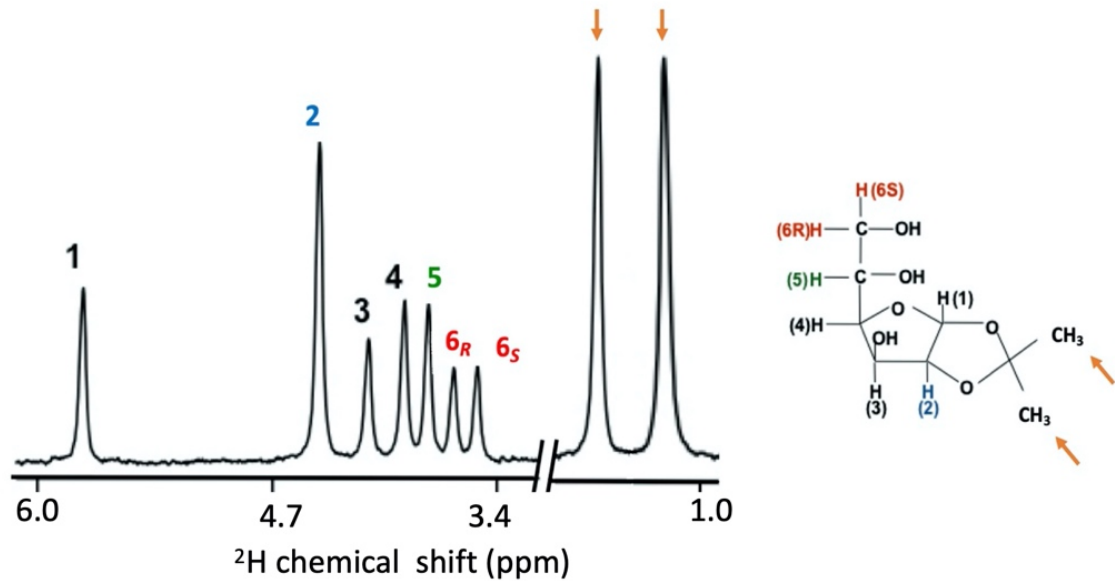


Figure 2.2 - Representative ^2H -NMR spectrum of monoacetone glucose obtained from mouse hepatic glycogen. On the right, a molecule of monoacetone glucose. Position 2, 5 and 6 are highlighted in colors as in figure 2.1. The orange arrows indicate the two methyl positions whose hydrogens enrichments are used as intramolecular standard for the quantification of all other positions' enrichments.

Once ^2H -enrichments of MAG positions 2, 5, and 6_S, along with body water (BW) ^2H -enrichment, were obtained from ^2H -NMR spectra analysis, the fraction of overall glycogen appearance and the contributions of direct and indirect pathway, the latter further resolved into Krebs cycle and triose-P contributions, were determined as illustrated in Table 2.1.

Table 2.1 - Formulas employed in Study 1, 2, and 3 for the estimation of different glycogenic sources to hepatic glycogen deposition during nocturnal feeding in mice administered with $^2\text{H}_2\text{O}$. BW corresponds to ^2H -enrichment of body water derived after analysis of ^2H -NMR spectra obtained from urine or plasma. ^2H -enrichment of MAG positions 5 and 6_S are represented by $^2\text{H}_5$ and $^2\text{H}_{6_S}$, respectively. Enrichment of position 2, after correction for 64% exchange between glucose-6-phosphate and fructose-6-phosphate, is represented by $^2\text{H}_{2_{\text{corr}}}$.

Newly-synthesized glycogen (%) (f_{GLY})	$100 \times ^2\text{H}_{2_{\text{corr}}}/\text{BW}$
Fraction of pre-existing, non-cycled glycogen (%)	$100 - f_{GLY}$
Indirect pathway, all sources (%)	$100 \times ^2\text{H}_5 / ^2\text{H}_{2_{\text{corr}}}$
Indirect $_{Kc}$ (%)	$100 \times ^2\text{H}_{6_S} / ^2\text{H}_{2_{\text{corr}}}$
Indirect $_{TP}$ (%)	$100 \times (^2\text{H}_5 - ^2\text{H}_{6_S}) / ^2\text{H}_{2_{\text{corr}}}$
Direct pathway + glycogen cycling (%)	$100 - (\text{indirect pathway})$

Exchange between body water and position 2 hydrogens mediated by G6P-isomerase is only 64% complete in mice, hence the measured enrichment level is corrected by $1/0.64$ ($^2\text{H}_{2_{\text{corr}}}$) [170]. As $^2\text{H}_{2_{\text{corr}}}$ does not distinguish between newly synthesized glycogen and pre-existing unlabeled glycogen that underwent cycling with glucose-6-phosphate, “newly synthesized glycogen” also includes this recycled fraction.

As result of “backwards scrambling” between oxalacetate malate and fumarate, glycogenic precursors originating via Krebs cycle are postulated to be more fully exchanged with body water in their position 6_S hydrogen compared to 6_R . $^2\text{H}_{6_S}$ was therefore selected for representing Krebs cycle precursors in our calculations [173].

¹³C-labeled glycogenic precursors and ¹³C-isotopomers quantification: analysis of ¹³C-MAG spectra

In Study 1, uniformly labeled glycogenic substrates ([U-¹³C]glucose and [U-¹³C]fructose) were given to mice alongside ²H₂O. After administration, a fraction of the labeled substrates was recruited in the liver for glycogen synthesis. As [U-¹³C]glucose and [U-¹³C]fructose are metabolized for glycogen synthesis, each generates distinctive glycogen ¹³C-isotopomers. The relative abundance of the different ¹³C-isotopomers found in hepatic glycogen provides information on the relative amount of each labeled substrate incorporated into hepatic glycogen as well as the route of incorporation.

¹³C is present in nature at an abundance of 1.1%, thus each hexose carbon will generate a ¹³C signal independently of any ¹³C-enrichment from [U-¹³C]glucose or [U-¹³C]fructose. Since the natural abundance ¹³C is distributed equally among all carbons, the probability of a hexose with two or more neighboring natural-abundance ¹³C is very low. As a result, each hexose carbon signal yields a singlet signal representing the 1.1% natural abundance ¹³C-enrichment. In contrast, essentially all ¹³C glycogen atoms derived from the [U-¹³C]sugar precursors will be connected to at least one other ¹³C as a consequence of the metabolic processing of the hexose carbon skeletons during the conversion of glucose or fructose to glycogen. As a result of homonuclear ¹³C-¹³C spin coupling (*J*-coupling), these ¹³C-NMR signals appear as flanking multiplets that are fully resolved from the natural-abundance singlet (Figure 2.3).

J-coupling arises from the interaction of two spinning nuclei through the chemical bond of a molecule. Such interaction results in the splitting of NMR signals: interactions between “*n*” equivalent nuclei, splits the signal into “*n*+1” multiplets. The appearance of multiplets permits the quantification of the different ¹³C-isotopomers generated either from [U-¹³C]glucose or [U-¹³C]fructose during glycogenesis.

Figure 2.3 shows a representative ^{13}C -MAG spectrum derived from rodents administered with a bolus of $[\text{U-}^{13}\text{C}]$ glucose. Carbon 1 (C1) signal, shown in expanded form in the figure, is composed of a central signal S, corresponding to the isotopomer shown on the right. As explained above, this isotopomer is naturally present in glycogen and its relative abundance is assigned to 1.1%, serving as reference for the quantification of all other isotopomers.

When $^{13}\text{C}1$ is flanked by another ^{13}C in position 2 such as in the isotopomers $[1,2\text{-}^{13}\text{C}_2]$ - and $[1,2,3\text{-}^{13}\text{C}_3]$ glycogen, corresponding in our study to labeled $[\text{U-}^{13}\text{C}]$ glucose that underwent PPP cycling before being converted into glycogen, the NMR signal of $^{13}\text{C}1$ splits forming a doublet (D). Further splitting occurs when $^{13}\text{C}1$ also couples with $^{13}\text{C}5$, giving rise to the multiplet indicated in the figure as M and whose integration provides the relative abundance of the isotopomer corresponding to $[\text{U-}^{13}\text{C}]$ glycogen.

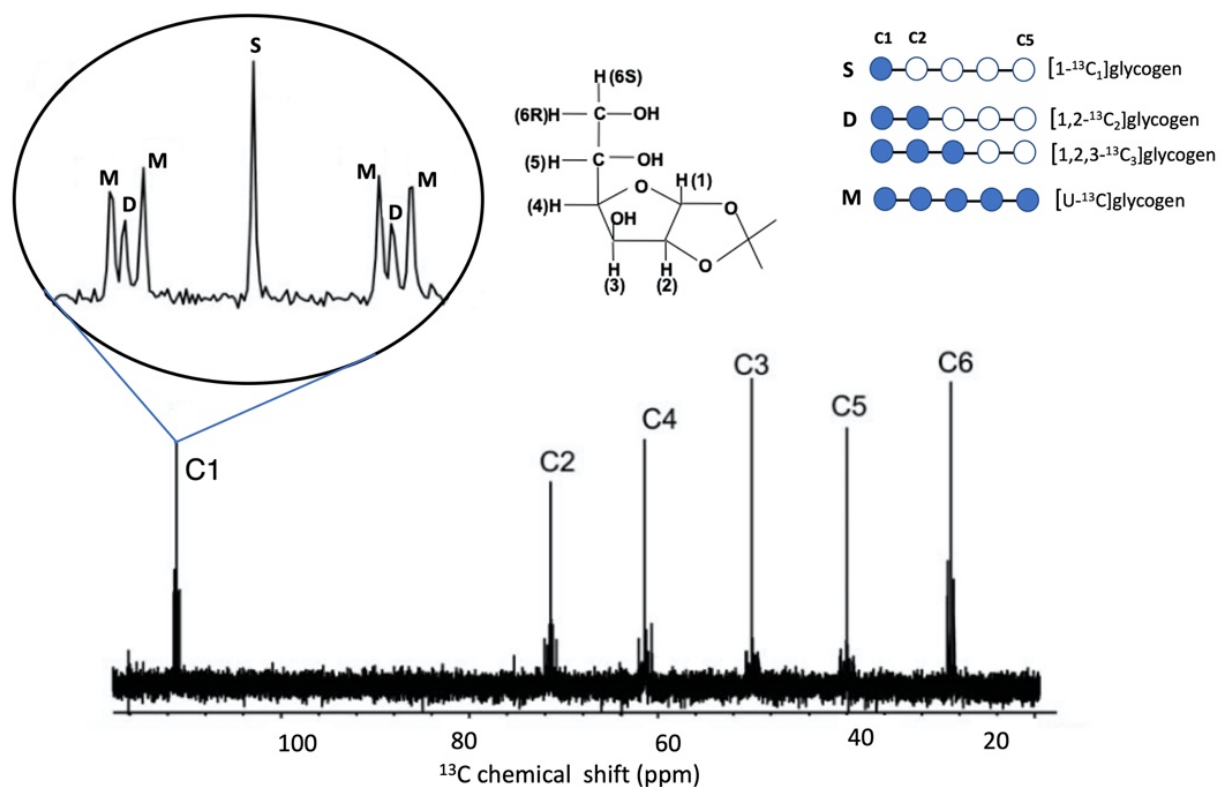


Figure 2.3 - Example of ^{13}C -MAG spectrum derived from rodents administered with a $[\text{U-}^{13}\text{C}]$ glucose load. Resonance of C1 is shown in expanded form. Figure adapted from [174].

The isotopomers useful for our analysis are [U-¹³C]glycogen generated via direct pathway, and [4,5,6-¹³C₃]glycogen and [5,6-¹³C₂]glycogen generated from triose-P and Krebs cycle anaplerosis. A more detailed overview on how these isotopomers are metabolically generated and how they are detected from analysis of C1 and C5 of ¹³C-NMR spectra, is described in detail in Study 1. Formulas employed in Study 1 are summarized hereafter.

Table 2.2 - Formulas employed in the calculation of exogenous [U-¹³C]glucose and [U-¹³C]fructose contributions to glycogen synthesis in Study 1.

Exogenous [U-¹³C]glucose contribution via direct pathway (%)	$100 \times ([U-^{13}C]glycogen \times 5) / f_{GLY}$
Exogenous [U-¹³C]glucose contribution via Krebs cycle (%)	$(100 \times ([5,6-^{13}C_2]glycogen \times 1.67) \times 1.5 \times 5) / f_{GLY}$
Exogenous [U-¹³C]fructose contribution via trioses-P (%)	$(100 \times [4,5,6-^{13}C_3]glycogen_{TP} \times 5) / f_{GLY}$ where: $[4,5,6-^{13}C_3]glycogen_{TP} = [4,5,6-^{13}C_3]glycogen_{total} - [4,5,6-^{13}C_3]glycogen_{KC}$ and: $[4,5,6-^{13}C_3]glycogen_{KC} = [5,6-^{13}C_2]glycogen \times 0.67$
Exogenous [U-¹³C]fructose contribution via Krebs cycle (%)	$(100 \times ([5,6-^{13}C_2]glycogen \times 1.67) \times 1.5 \times 5) / f_{GLY}$

Krebs cycle anaplerosis generates both [4,5,6-¹³C₃]glycogen and [5,6-¹³C₂]glycogen isotopomers, however, due to PEP-pyruvate-OAA-PEP futile cycling, the yield of [4,5,6-¹³C₃]glycogen is lower. The factor of 1.67 accounts for this lower yield: for every [5,6-¹³C₂]glycogen, 0.67 [4,5,6-¹³C₃]glycogen is formed. The factor of 1.5 accounts for dilution of both isotopomers by exchange at the pyruvate cycling [175] and the factor of 5 accounts for the [U-¹³C]glucose load being 20% enriched. f_{GLY} corresponds to the fraction of newly synthesized glycogen calculated as illustrated in Table 2.1.

Tracing hepatic lipid metabolism with stable isotopes

¹H-NMR for lipidomic analysis

Since proton nuclei also possess a spin of $\frac{1}{2}$, they yield sharp NMR signals characterized by extensive splitting arising from multi-bond *J*-coupling with ¹H attached to the same or adjacent carbons. In ¹H-NMR spectra, *J*-coupling provides information on the immediate molecular environment of a specific hydrogen, including the number of neighboring hydrogens and the nature of the C-H bonds. Because ¹H has high natural abundance (> 99.98%) and since almost all metabolites contain protons, ¹H-NMR is widely used to identify and quantify metabolite concentrations in biological samples.

In Studies 2 and 3, we assessed the lipidomic profile of TGs purified from the liver of mice. By applying the same principles, in Study 2, TGs purified from adipose tissue were also analyzed. Percentages of different fatty acids species can mutate following metabolic perturbations. Thus, we employed ¹H-NMR analysis to assess the relative abundance of different lipid classes such as ω -3 fatty acids, saturated fatty acids, mono-, and poly-unsaturated fatty acids, in liver and adipose tissue.

Figure 2.4 shows a representative ¹H-NMR spectrum obtained from purified TGs of mouse liver, while Table 2.3 summarizes the functional groups assigned to each peak in the ¹H spectrum.

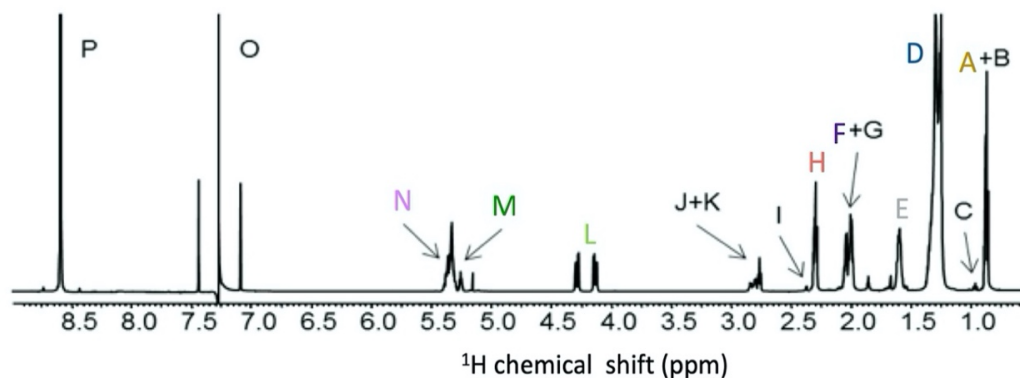


Figure 2.4 - Representative ^1H -NMR spectrum of hepatic mouse TGs. Functional groups and chemical shifts corresponding to each peak are listed in detail in Table 2.3. Each peak was quantified in relation to the ^1H intensity of a pyrazine standard (P). Figure adapted from [156].

Table 2.3 - Functional groups and chemical shift corresponding to each peak in the ^1H spectrum obtained from mice TG showed in Figure 2.4. Colored letters are associated with peaks highlighted with the same color in Figure 2.4. **MU**: monounsaturated; **PU**: polyunsaturated, **DHA**: docosahexaenoic acid.

Signal	Functional Group	Chemical Shift (ppm)	Assignment
A + B	Non n-3 + partial n-6 methyls	0.88	$\text{CH}_3\text{-CH}_2\text{-}$
C	n-3 Methyls	0.98	$\text{CH}_3\text{-CH}_2\text{-CH=}$
D	Aliphatic chain methylenes	1.26	$\text{CH}_3\text{-(CH}_2\text{)}_n\text{-}$
E	β Methylenes	1.62	$\text{-CH}_2\text{-CH}_2\text{-COO-}$
F	MU allylic hydrogens	2.02	$\text{-CH}_2\text{-CH=CH-}$
G	PU allylic hydrogens	2.06	$\text{-CH}_2\text{-CH=CH-}$
H	α Methylenes	2.32	$\text{-CH}_2\text{-CH}_2\text{-COO-}$
I	DHA α and β methylenes	2.40	$\text{-CH}_2\text{-CH}_2\text{-COO-}$
J + K	Bisallylic methylenes	2.80	$\text{-CH=CH-CH}_2\text{-CH=CH-}$
L	<i>sn</i> -1, <i>sn</i> -3 of TG-glycerol	4.15	$\text{HOCH}_2\text{-CHOH-CH}_2\text{OH}$
M	<i>sn</i> -2 of TG-glycerol	5.27	$\text{HOCH}_2\text{-CHOH-CH}_2\text{OH}$
N	Olefinic hydrogens	5.37	-CH=CH-
O	Chloroform	7.25	Solvent
P	Pyrazine	8.60	Standard

After integrating each peak in the ¹H-NMR spectra, different species of lipids were quantified employing the mathematical formulas illustrated in detail in Table 2.4. All formulas were previously validated in mice by Duarte et al., [156].

Table 2.4 - Mathematical equations utilized in Study 2 and 3 to quantify the relative amount of different lipid species in mouse liver and adipose tissue. Alphabetical letters correspond to the same letters used to indicate peaks and functional groups in Figure 2.4 and Table 2.3. Functional groups in each equation are anyway referred on the side. **ω-3 FAs**: omega-3 fatty acids, **non-ω-3 FA**: non-omega-3 fatty acids; **SFA**: saturated fatty acids; **MUFA**: monounsaturated fatty acids; **PUFA**: polyunsaturated fatty acids; **DHA**: docosahexaenoic acid. Equations previously validated by Duarte et al., [156].

ω-3 FAs (%)	$100 \times \frac{C_{1Ha}}{C_{1Ha} + AB_{1Ha}}$	<i>C</i> _{1Ha} : ¹ H area of ω-3 methyls <i>AB</i> _{1Ha} : ¹ H area of non ω-3 methyls
Non-ω-3 FAs (%)	100 - (% ω-3 FAs)	
MUFA (%)	$100 \times \frac{F_{1Ha}}{(2 \times H_{1Ha}) + I_{1Ha}}$	<i>F</i> _{1Ha} : ¹ H area of MU allylic hydrogens <i>H</i> _{1Ha} : ¹ H area of α methylenes <i>I</i> _{1Ha} : ¹ H area of DHA α and β methylenes
PUFA (%)	$100 \times \frac{(G_{1Ha} + I_{1Ha})}{(2 \times H_{1Ha}) + I_{1Ha}}$	<i>G</i> _{1Ha} : ¹ H areas of PU allylic hydrogens <i>I</i> _{1Ha} : ¹ H area of DHA α and β methylenes <i>H</i> _{1Ha} : ¹ H area of α methylenes
SFAs (%)	100 - (%MUFA +%PUFA)	
Linoleic acid (%)	$100 \times \frac{J_{1Ha}}{H_{1Ha} + \frac{I_{1Ha}}{2}}$	<i>J</i> _{1Ha} : ¹ H area of linoleic acid bisallylic hydrogens <i>H</i> _{1Ha} : ¹ H area of α methylenes <i>I</i> _{1Ha} : ¹ H area of DHA α and β methylenes
DHA (%)	$100 \times \frac{\frac{I_{1Ha}}{2}}{H_{1Ha} + \frac{I_{1Ha}}{2}}$	<i>H</i> _{1Ha} : ¹ H area of α methylenes <i>I</i> _{1Ha} : ¹ H area of DHA α and β methylenes

$^2\text{H}_2\text{O}$ for the quantification of lipid synthesis fluxes

As mentioned above, $^2\text{H}_2\text{O}$ administration allows the simultaneous assessment of several biological processes. Thus, in addition to quantifying hepatic glycogen fluxes, we also analyzed the incorporation of deuterium into lipid moieties to obtain information regarding fatty acid (FA) and TG biosynthesis in liver (Studies 2 and 3), and adipose tissue (Study 2).

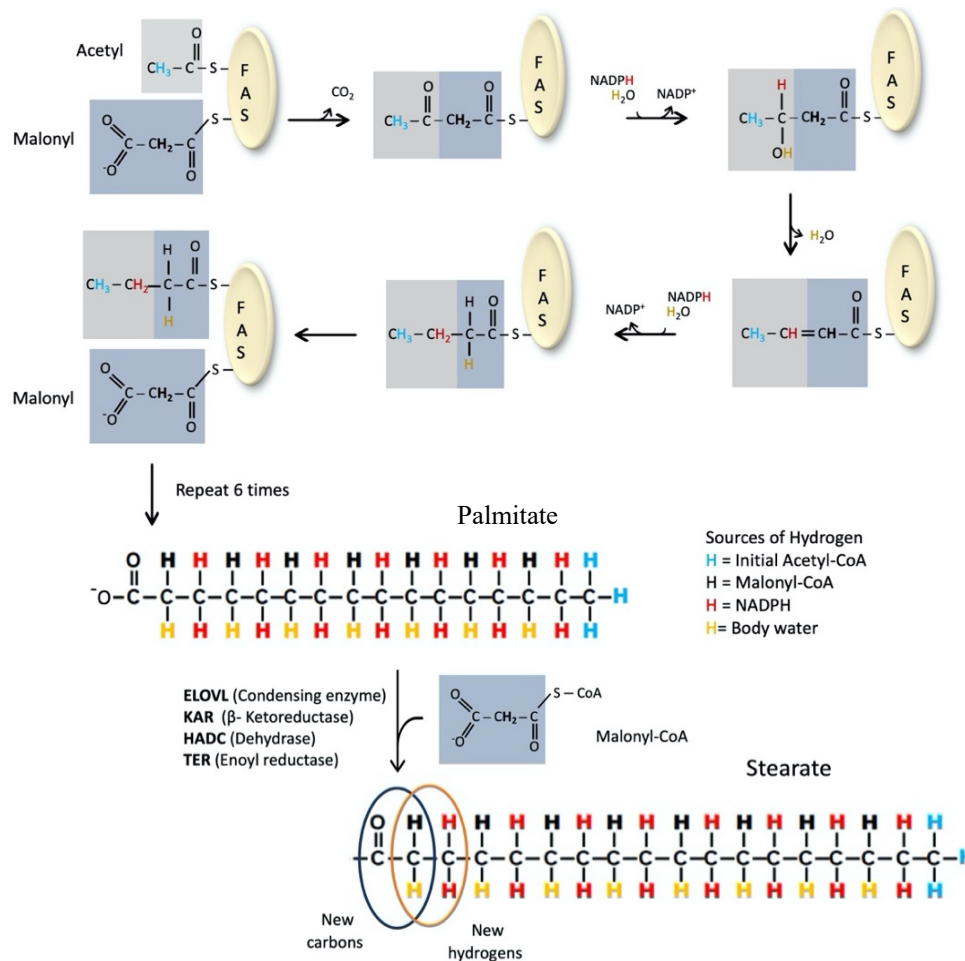


Figure 2.5 - Schematic representation of palmitate synthesis operated by the fatty acyl synthase complex FAS. Two-carbon units donated by activated malonate are repetitively added to the acyl chain in a sequence of 4 reactions consisting of decarboxylation and subsequent condensation of the malonyl subunit to the nascent acyl chain, reduction by NADPH, dehydration and second reduction by NADPH. Hydrogens in the final product palmitate are highlighted in different colors according to their source. Hydrogen highlighted in black and bold originate from malonyl units, hydrogens in red are donated by NADPH and hydrogen in yellow are provided by body water. The three hydrogens in the methyl group are highlighted in blue and originate from the initial acetyl group used in the process. Newly synthesized and pre-existing chains can undergo elongation in the ER where an additional malonyl subunit is condensed to the fatty acyl chain, elongating it of two additional carbons (stearate in the picture).

During DNL, nascent acyl chains acquire their hydrogens from different sources.

Odd-numbered carbons receive both hydrogens from NADPH, whereas even-numbered carbons receive one hydrogen from water, and one from malonyl-CoA. The only exception is the methyl group of the chain, whose three hydrogens originate from the first acetyl unit used to prime the process (Figure 2.5).

In the presence of $^2\text{H}_2\text{O}$, deuterium progressively accumulates in the FA chain, enriching these positions in a region-specific manner and at a rate proportional to lipid synthesis. Enrichment in the fatty acid methyl position occurs only during DNL, but enrichment of the hydrogens at position 2 occurs during both DNL and elongation of existing FAs. Desaturation *per se* occurs without incorporation of hydrogens, but deuterium enrichment in allylic positions is indicative of desaturation activity in newly synthesized FA chains. Finally, the TG glycerol moiety also becomes enriched with deuterium while being synthesized and, because glycerol-3-phosphate synthesis occurs before esterification to FAs, TG-bound glycerol enrichment tracks with the rate of FA esterification. (Figure 2.6).

After $^2\text{H}_2\text{O}$ administration and incorporation into TGs, the deuterium contents of these positions can be resolved by ^2H -NMR.

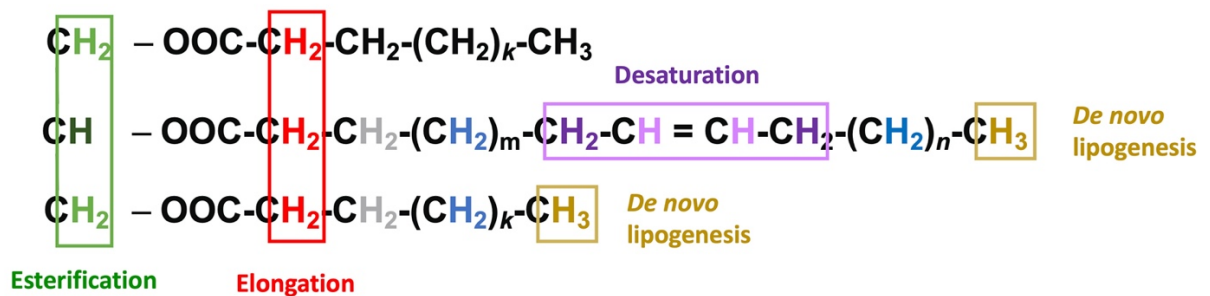


Figure 2.6 - Positional ^2H -enrichment of TG. In the presence of $^2\text{H}_2\text{O}$, ^2H progressively enriches the fatty acyl chains and glycerol moiety of TGs. Enrichment in specific positions of the different TG components allows the quantification of rates of several TG-FA synthetic fluxes. Enrichment of methyl positions (yellow) occurs only during DNL, whereas enrichment in alpha positions (red) can also occur during elongation. Enrichment in allylic position (purple) appears in newly synthesized chains that underwent desaturation. Finally, glycerol enrichment (green) provides information on the rate of fatty acid esterification, and thus of TG synthesis.

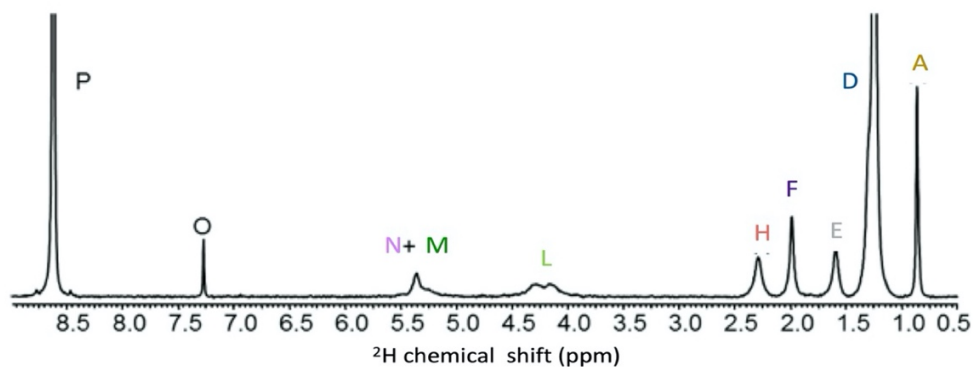


Figure 2.7 - ^2H -NMR spectrum of hepatic mouse TGs. Functional groups and chemical shifts corresponding to each peak are listed in detail in Table 2.3. Colored letters are associated with peaks corresponding to hydrogens highlighted with the same color in Figure 2.6 and Table 2.3. Each peak was quantified in relation to the ^2H intensity of a pyrazine standard (P). Figure adapted from [156].

Figure 2.7 shows a representative ^2H -NMR spectrum obtained from hepatic mouse TG. ^1H - and ^2H -signals are isochronous, thus chemical shifts and corresponding functional groups in ^2H spectra, match their ^1H counterparts (Figure 2.4)

Lipids synthetic fluxes such as DNL, elongation, desaturation and glycerol synthesis were determined from ^1H -/ ^2H -NMR analysis as described by Duarte et al., [156]. All formulas employed are summarized hereafter in Table 2.5.

Table 2.5 - Mathematical equations utilized in Study 2 and 3 to measure lipid fractional synthetic rates (% per overnight) in mice liver and adipose tissue from ¹H-²H-NMR analysis. All Mathematical formulas hereby provided were previously validated in mice by Duarte et al., [156]. Alphabetical letters (also referred below each formula) correspond to the same letters used to indicate peaks and functional groups in Figures 2.4 and 2.7, and Table 2.3. ²H-enrichments of the methyl site are always corrected for linoleic acid contribution, an essential fatty acid that does not get labeled with ²H.

	<p>After integration of the corresponding peaks in the NMR spectrum, all positional enrichments are calculated as follows:</p> $X_{eC} = 100 \times \frac{X_{2Ha} \times \% 2HS \times P_{1Ha}}{(X_{2Ha} \times \% 2HS \times P_{1Ha}) + (X_{1Ha} \times \% 1HS \times P_{2Ha})} - NA$ <p>where:</p> <p>X_{1Ha}: ¹H area of X X_{2Ha}: ²H area of X %2HS: % of ²H labelled pyrazine %1HS: % of ²H unlabelled pyrazine P_{1Ha}: ¹H area of the pyrazine standard P_{2Ha}: ²H area of the pyrazine standard NA: natural abundance (0.012%)</p> <p>Methyl positions (A) are additionally corrected per linoleic acid contribution whose relative abundance was calculated from ¹H-NMR analysis as shown in Table 2.4</p> $A_{eC} = 100 \times \frac{X_{2Ha} \times \% 2HS \times P_{1Ha}}{(X_{2Ha} \times \% 2HS \times P_{1Ha}) + (X_{1Ha} \times [1 - \frac{\% \text{ linoleic acid}}{100}] \times \% 1HS \times P_{2Ha})} - NA$
<p>New FAs or DNL rate (%)</p>	$100 \times \frac{A_{eC}}{\% \text{ body water enrichment}}$ <p>A_{eC}: ²H enrichment of non ω-3 fatty acids methyl hydrogens</p>
<p>Elongated FAs (%)</p>	$100 \times \left[1 - \frac{A_{eC} \times 2}{H_{eC} \times 3} \right] \times \frac{H_{eC}}{\% \text{ body water enrichment}}$ <p>A_{eC}: ²H enrichment of non ω-3 fatty acids methyl hydrogens H_{eC}: ²H enrichment of hydrogens in position 2</p>
<p>Desaturated new FAs (%)</p>	$100 \times \frac{F_{eC}}{\% \text{ body water enrichment}}$ <p>F_{eC}: ²H enrichment of the MUFAs' allylic hydrogens</p>
<p>New glyceryl (%)</p>	$100 \times \frac{L_{eC}}{\% \text{ body water enrichment}}$ <p>L_{eC}: average ²H enrichment of the four hydrogens on glycerol C1 and C3.</p>

Materials and Methods

Animals

Study 1

Twenty-one adult male C57BL/6J mice obtained from Charles River Labs, were housed at the University of Coimbra UC Biotech Bioterium. They were maintained in a well-ventilated environment and a 12h light/12h dark cycle. Mice were provided with free access to water and standard chow, comprising of 54% mixed carbohydrate, 19% protein and 3% lipid by weight. All Animal studies performed in Study 1 were approved by the University of Coimbra Ethics Committee on Animal Studies (ORBEA) and the Portuguese National Authority for Animal Health. In addition, all animal procedures hereby described were performed in full accordance with DGAV guidelines and European regulations (European Union Directive 2010/63/EU).

Study 2 and 3

In Studies 2 and 3, a total of thirty-three adult male mice of a mixed genetic background C57BL/6J x 129/sv, were maintained in a well-ventilated environment and a 12h light/12h dark cycle at the animal facilities of the Instituto de Investigaciones Biomédicas Alberto Sols (CSIC-UAM, Madrid). These mice were obtained from PTP-1B heterozygous mice originally received from Abbott laboratories; that were inter-crossed to yield three genotypes of mice (wild-type, heterozygous, knockout). In Study 2, only wild-type animals were used, whereas in Study 3 wild-type and PTP-1B knockout animals were used.

Mice were given ad libitum access to water and standard chow (60% mixed carbohydrate, 16% protein and 3% lipid by weight).

All animal experimentation described in Study 2 and 3 was approved by the Consejo Superior de Investigaciones Científicas and Comunidad de Madrid Animal Care and Use. All animal

procedures hereby described were performed in full accordance with DGAV guidelines and European regulations (European Union Directive 2010/63/EU).

Reagents

$^2\text{H}_2\text{O}$ at 99.8% isotopic enrichment used in Study 1, 2 and 3, was manufactured by Cambridge Isotopes Limited; Cambridge, MA, USA. $[\text{U-}^{13}\text{C}]$ Fructose at 99% enrichment and $[\text{U-}^{13}\text{C}]$ glucose at 99% enrichment used in Study 1 were obtained from Omicron Biochemicals Inc., IN, USA; and Cambridge Isotopes Limited respectively.

Olanzapine used in Study 2 was purchased from Glentham Life sciences, Wiltshire, United Kingdom (Gp8311, 132539-06-1,); while Aripiprazole was purchased from Acros Organics, Thermo Fisher Scientific, Massachusetts, USA (457990000, 129722-12-9).

Liver processing

Frozen liver samples weighing between 0.5 and 1 g were powdered under liquid nitrogen and then rapidly mixed with HPLC-grade methanol (4.6 mL/g) followed by methyl-tert-butyl ether (MTBE) (15.4 mL/g). The mixture was placed in a shaker for 1.5 hour at room temperature then centrifuged at 13,000 x g for 10 min. After centrifugation, the insoluble pellet containing hepatic glycogen was separated from the upper phase of the mixture. The upper phase was further separated into an aqueous fraction and an organic fraction. The organic fraction proceeded further processing for TG extraction. When relevant, the aqueous fraction was neutralized, lyophilized and analyzed directly by ^{13}C NMR (Study 1).

Hepatic glycogen extraction and monoacetone glucose (MAG) synthesis

All glycogen analyzed was converted to MAG prior NMR analysis. Glycogen from the insoluble pellet was extracted with 30% KOH (2 mL/g of liver) at 70°C for 30 minutes. The solution was then treated with 6% Na₂SO₄ (1 mL/g of liver) and glycogen was precipitated with ethanol (7 mL/g of liver). After centrifugation, the solid residue was dried and resuspended in acetate buffer (50 mM, pH 4.5). 200 U of amyloglucosidase from *Aspergillus niger* (Glucose-free preparation, Sigma-Aldrich, Germany) were added and the solution incubated for 8 hours at 55°C. The supernatant was lyophilized and mixed with 5 mL ²H-enriched acetone and 4% sulphuric acid enriched to 2% with ²H₂SO₄ (v/v). The mixture was stirred overnight at room temperature. The reaction was quenched with 5 mL water, the pH adjusted with HCl (pH 2.0) and the mixture incubated at 40°C for 5 hours. The solution pH was then adjusted to 8 with NaHCO₃ and the samples evaporated to dryness. MAG in the residue was extracted with boiling ethyl acetate. Ethyl acetate was evaporated, the residue dissolved in H₂O and purified by solid phase Discovery DSC-18 3 mL/500 mg disposable columns (Sigma-Aldrich) [176].

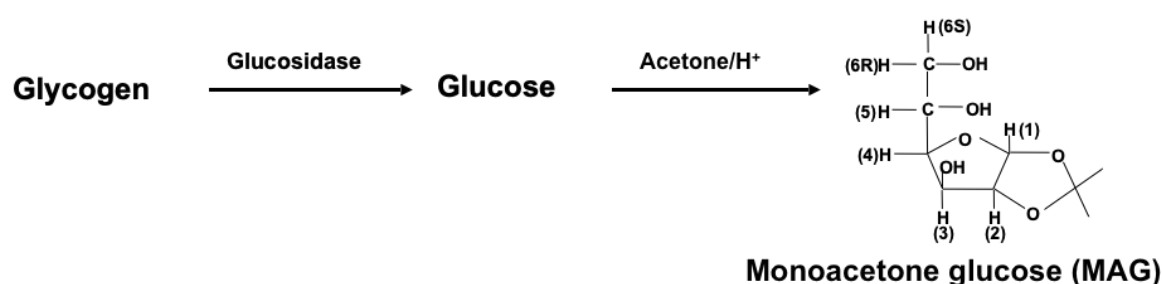


Figure 2.8 - Schematic representation of monoacetone glucose (MAG) synthesis from glycogen. MAG's two methyl groups are incorporated during the derivatization process from acetone enriched with ²H to a specific percentage and are therefore used as intermolecular standard for the quantification of ²H-enrichment of all other positions.

Hepatic glycogen quantification

After hepatic glycogen was digested, an aliquot of 20 μL was kept for liver glycogen quantification. Total hepatic glycogen content was quantified with a fully automated analyzer Miura 200 (I.S.E, S.r.l. Guidonia, Italy) using a dedicated glucose reagent kit (ref. A-R010000060, n=2).

Liver TG extraction and purification

The upper phase of the liver mixture contained hepatic lipids. After separation from the aqueous fraction, the organic fraction of the upper phase was dried under hood in an amber glass vial. TGs from the dried organic fraction were purified with a solid phase extraction (SPE) process as described by Silva *et al.*, [177]. Briefly, Discovery DSC-Si SPE cartridges (2g/12 mL) were washed with 8 mL of hexane/MTBE (96/4; v/v) followed by 24 mL of hexane. The dried lipids were re-suspended in 500 μL of hexane/MTBE (200/3; v/v) and loaded into the column after washing. The lipid vials were washed with a further 500 μL of solvent to quantitatively transfer the lipids to the column. TGs were eluted with 32 mL of hexane/MTBE (96/4; v/v), collected in 4 mL fractions. Fractions containing TGs were identified by thin-layer chromatography. A few microliters of the eluted fractions were spotted on the TLC plate and the plate was developed with petroleum ether/diethyl ether/acetic acid (7.0/1.0/0.1; v/v/v). After drying, lipid spots were visualized under iodine vapor. The TG-containing fractions were pooled, dried under hood and stored at -20°C until NMR analysis.

TG extraction from adipose tissue

Adipose tissues samples were processed for TG extraction using a combination of HPLC-grade methanol and MTBE as already described for liver samples. The upper organic phase containing TG was then dried in an amber vial under hood and stored at -20°C until NMR analysis.

NMR spectra acquisition

^1H - and proton-decoupled ^2H -NMR spectra were acquired with an 11.7 T Bruker Avance III HD system using a dedicated 5 mm ^2H -probe with a ^{19}F -lock channel and ^1H -decoupling coil, whereas proton-decoupled ^{13}C -NMR spectra were obtained with a Varian VNMRS 600 MHz NMR (Agilent) spectrometer equipped with a 3-mm broadband probe. ^1H -, ^2H - and ^{13}C -NMR spectra were processed and analyzed with ACD/NMR Processor Academic Edition software (ACD/Labs, Advanced Chemistry Development, Inc.).

Body water ^2H -enrichment

Body water ^2H -enrichments were determined from 10 μL of urine (Study 1) or 10 μL plasma (Study 2 and 3). Samples were mixed with 1 mL acetone and ~ 0.5 mL of this mixture were loaded in a 5 mm NMR tube to which 50 μL hexafluorobenzene were added. Each sample was tested in duplicate and analyzed by ^2H -NMR as previously described [178]. ^2H -NMR spectra were acquired at 25°C with a 23° pulse angle, 922 Hz spectral width, 4 s acquisition time and 8 s interpulse delay. The number of free induction decay (f.i.d.) collected for each spectrum was sixteen and water ^2H -enrichment was determined from a calibration curve calculated from ^2H -enriched water standards, assuming the water fraction to be 95% in urine and 92% in plasma. The summed f.i.d. was processed with 1 Hz line-broadening before Fourier transform.

MAG

²H - NMR spectra

Samples were dissolved in 0.5 mL 90% acetonitrile/10% ²H-depleted water to which 50 µL of hexafluorobenzene were added. ²H-NMR spectra were acquired at 50 °C with a 90° pulse angle, 1.6 s of acquisition time and a 0.1 s interpulse delay. The number of f.i.d. collected ranged from 2,000-10,000. Positional ²H-enrichments were determined using the MAG methyl signals as an intramolecular standard [179]. The summed f.i.d. was processed with 0.2 Hz line-broadening before Fourier transform.

¹³C-NMR spectra

¹³C-NMR spectra were obtained after ²H-NMR acquisition and evaporation of the acetonitrile/water solvent mixture. MAG residue was then resuspended in 0.5 mL 99.9% ²H₂O. ¹³C-NMR spectra were acquired at 25 °C using a 60° pulse angle, 30.5 kHz spectral width and 4.1 s of recycling time (4.0 s of acquisition time and 0.1 s pulse delay). The number of acquisitions ranged from 2,000 to 18,000. The summed f.i.d. was processed with 0.2 Hz line-broadening before Fourier transform.

TG

¹H-NMR spectra

Purified TGs were reconstituted in ~0.4 mL CHCl₃, with the addition of 25 µL of a pyrazine standard (enriched to 1% with pyrazine-d₄ and dissolved in CHCl₃; 0.07g pyrazine/g CHCl₃), and 50 µL of hexafluorobenzene. ¹H- and ²H- NMR spectra were then acquired in tandem. ¹H spectra at 500.1 MHz were acquired at 25 °C with a 90° pulse angle, 10 kHz spectral width, 3 s of acquisition time and 5 s of pulse delay. Sixteen f.i.d. were collected for each spectrum. The summed f.i.d. was processed with 0.2 Hz line-broadening before Fourier transform.

²H-NMR spectra

²H-NMR spectra at 76.7 MHz were obtained at 25 °C with a 90° pulse angle, a 1230 Hz spectral width, an acquisition time of 0.37 s and a pulse delay of 0.1 s. Approximately 20,000 f.i.d. were acquired for each spectrum. Correction factors for partially saturated ²H signals were obtained from a set of seven samples where for each sample, a spectrum was acquired with the described parameters and immediately followed by a spectrum acquired under the same parameters with the exception of the acquisition time and pulse delay, which were set to 1 s and 8 s, respectively. The summed f.i.d. was processed with 1 Hz line-broadening before Fourier transform.

Statistics

All results are presented as means ± standard error of the mean (SEM). GraphPad Prism 8 was used to analyze the data and to create graphs.

Study 1

Shapiro-Wilk normality test was applied to every dataset to check for normality of residuals, while a homoscedasticity test (F test for equality of variances) was used to test for equality of variances.

If both groups presented a normal distribution, an unpaired Student t-test was applied (Welch corrected if variances were unequal). Otherwise, the Mann-Whitney U-test was employed.

Study 2

Shapiro-Wilk normality test was applied to check for normality of residuals while Bartlett's test was used to test for equality of variances. If datasets fulfilled assumptions of normality and equality of variances, an ordinary one-way ANOVA followed by multiple comparison of each study group vs control group, (*p* values adjusted with Dunnett's correction) was applied. Otherwise, a Kruskal-

Wallis test, followed by multiple comparison of each study group vs control group (p values adjusted with Dunn's correction) was used.

Study 3

Shapiro-Wilk normality test was applied to check for normality of residuals. All groups analyzed presented a normal distribution of residuals but due to different sample sizes between the two groups and the high variability of many of the dataset generated during our analysis, unequal variances were assumed *a priori*, and a Welch's t test was performed for each statistical comparison.

STUDY 1

Study 1

Determining the Contribution of a High-Fructose Corn Syrup Formulation to Hepatic Glycogen Synthesis During Ad-Libitum Feeding in Mice

This chapter is based on:

G. Di Nunzio, G.D. Belew, A.N. Torres, J.G. Silva, L.P. Silva, C. Barosa, L. Tavares, J.G. Jones. “Determining the contribution of a high-fructose corn syrup formulation to hepatic glycogen synthesis during ad-libitum feeding in mice”. *Sci Rep*, vol. 10, no. 1, p. 12852, 2020.

Study 1

Introduction

The continuous increase in refined sugar consumption over the last few decades has coincided with the modern surge of metabolic diseases. Not only overconsumption of food and beverages rich in refined sugars constitutes a copious caloric surplus, but a growing body of evidence points at the fructose component of sugars as one of the major culprits in the pathogenesis and progression of such diseases [24].

Fructose and glucose metabolisms differ substantially from each other in that fructose metabolism is not subjected to insulin regulation nor to any negative feedback regulatory mechanism within the cell. Ingestion of a fructose load results in the unrestrained production of triose phosphates (triose-Ps) in the liver, the organ most responsible for fructose extraction and metabolism. Rapid accumulation of triose-Ps in hepatocytes leads to increased substrate flux towards insulin-regulated anabolic pathways in the liver, such as DNL and glycogen synthesis.

The role of fructose is however controversial: if large doses of fructose have detrimental effects on the overall metabolism and promote obesity and associated diseases, discrete amounts of fructose are not deleterious, on the contrary, fructose metabolites possess signaling properties that enhance glucose disposal through several routes [21].

In rodents, high-sugar feeding causes increase in fat mass, glucose intolerance, dyslipidemia, and a substantial decrease in both liver and muscle insulin sensitivity [180], [181], [182]. Sugar-induced increase in DNL rates appear to be closely associated with fructose adverse effects, and numerous studies in humans and rodents have addressed this association [183], [184], [185]. High levels of ingested fructose enhance hepatic lipid synthesis not only by providing substrates for fatty acids and TGs production but also by transcriptional mechanisms that potentiate the lipid synthetic machinery [186].

Few studies have explored the role of high fructose intake in the context of hepatic glycogen synthesis. Glycogen synthesis via direct pathway plays an important role in glucose homeostasis

maintenance: insulin promotes glycogen deposition especially via direct pathway, stimulating glucokinases transcription and activity [187]. Moreover, hepatic glycogen levels regulate food intake and thus any alteration in hepatic glycogen metabolism may influence systemic energy balance [31].

The effects of fructose on glycogen synthesis are unclear: on the one hand fructose is a potent glycogenic substrate that competes with glucose for glycogen deposition, on the other hand, catalytic amounts of fructose enhance glucose conversion to glycogen via glucokinases activation [188].

The aim of this study was to examine hepatic glycogen synthesis in the context of chronic high-sugar feeding in mice whose standard chow was supplemented with high-fructose corn syrup-55 (HFCS-55) in the drinking water. HFCS-55 is the most common form of HFCS, a widespread food and drinks additive consisting of 55% fructose and 45% glucose and with the same level of sweetness as sucrose. $^2\text{H}_2\text{O}$ was administered alongside ^{13}C -tracers of the glucose and fructose present in the drinking water: the former allowed the estimation of direct and indirect pathway contributions to hepatic glycogen synthesis in mice fed HFCS-55 versus mice fed standard chow only, whereas the latter were used to assess the individual contributions of the glucose and fructose components of HFCS-55 to hepatic glycogenesis.

Due to the differences in hepatic glucose and fructose metabolism, and given the excess of fructose over glucose, we hypothesized the fructose component of HFCS-55 to contribute a significantly higher fraction of glycogen synthesis than the glucose component. Since fructose is converted into glycogen exclusively via indirect pathway, we also predicted the indirect pathway to contribute a larger fraction of glycogen deposition in mice fed HFCS-55. This scenario was expected also in light of the fact that mice had been continuously exposed to HFCS-55 for a period of eighteen weeks and thus, as a consequence of altered hepatic insulin signaling following chronic sugar intake, glucose recruitment via direct pathway was anticipated to be less responsive than normal.

Animals and experimental set-up

A total of twenty-one adult male mice (C57BL/6J) were used in this study. Mice were randomly divided in two groups: control animals (n = 9), hereby referred to as NC, and animals receiving HFCS-55, (n = 12), hereby referred to as HS.

Intervention

While fed a standard chow diet, HS mice were provided with a drinking water solution containing HFCS-55. HFCS-55 was present at a concentration of 30% w/v and was administered for a period of eighteen weeks. The remaining mice, NC, were maintained on a standard chow diet and normal drinking water for the same period.

Tracers administration:

At the beginning of the final evening, all mice were administered with an intraperitoneal loading dose of 99% $^2\text{H}_2\text{O}$ containing 0.9 mg/mL NaCl (4 mL/100 g body weight) and the drinking water was enriched to 5% with $^2\text{H}_2\text{O}$. For the HS mice that during the intervention period were provided with HFCS-55 in their drinking water, this was replaced with a mixtures of identical composition but with 20% enriched [U- ^{13}C]glucose for six of the animals (HS1), and 20% enriched [U- ^{13}C]fructose for the remaining six mice (HS2).

Sacrifice

At the end of the dark cycle, mice were deeply anesthetized with ketamine/xylazine and sacrificed by cardiac puncture. Urine, collected overnight using a special collection apparatus in the cage, was stored at -80°C . Livers were freeze-clamped and stored at -80°C until further analysis.

Study 1

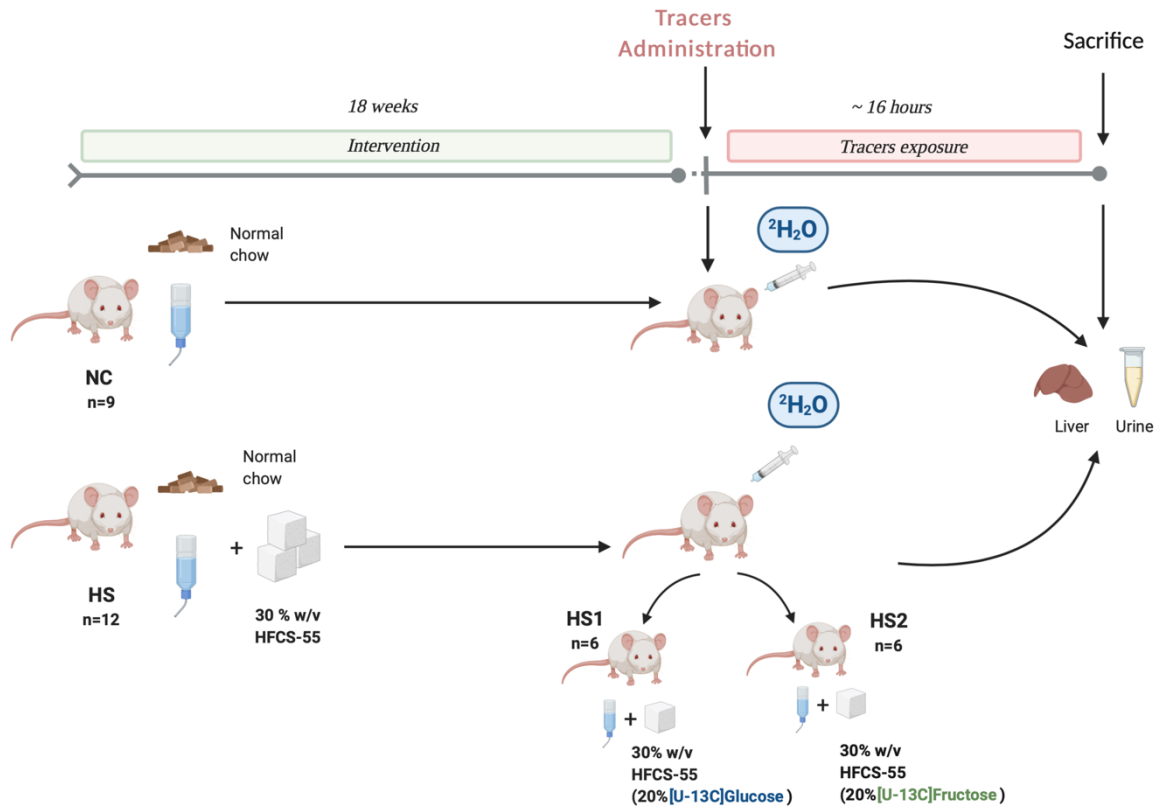


Figure 3.1 - Graphical representation of the timeline and experimental set-up employed in Study 1. Control animals maintained on a normal chow diet are referred to as NC, whereas animals administered HFCS-55 are referred to as HS. At the beginning of the final evening, all mice were administered with an intraperitoneal injection of $^2\text{H}_2\text{O}$ (4 mL/100 g body weight) and the drinking water was enriched to 5% with $^2\text{H}_2\text{O}$. HS animals were additionally provided with the ^{13}C tracers: HFCS-55 in the drinking water was substituted with a mixture of identical composition but 20% enriched with either $[\text{U-}^{13}\text{C}]\text{glucose}$ (HS1, n=6) or $[\text{U-}^{13}\text{C}]\text{fructose}$ (HS2, n=6). [Figure created with BioRender.com].

Results

Body weight and body water ^2H -enrichment

By the 18th week, no difference in body weight was observed between mice fed normal chow, and mice whose chow was supplemented with HFCS-55 in the drinking water, (34.0 ± 3.5 g versus 35.7 ± 4.2 g, $p = 0.34$).

However, body water ^2H -enrichments estimated from urine were significantly higher in HS mice (Table 3.1). Following intraperitoneal injection, $^2\text{H}_2\text{O}$ rapidly equilibrates with total body water in all cells within an organism and in mice, plasma water ^2H -enrichment reaches isotopic steady state within minutes. The bolus of $^2\text{H}_2\text{O}$ (4 mL/100 g body weight) was adjusted to the weight of each animal taking into account that normally, 70% of the animal's body weight is constituted of water. Thus, this difference in body water ^2H -enrichment likely reflects different body compositions between the two groups, with HS mice having a higher fraction of adipose tissue, hence a lower fraction of water.

Hepatic glycogen enrichment from $^2\text{H}_2\text{O}$

As illustrated in the previous chapter (page 87), the fraction of overall hepatic glycogen appearance and the contributions of direct and indirect pathways (further resolved into Krebs cycle and triose-P contributions) to hepatic glycogen deposition, can be calculated from positional ^2H -enrichments of MAG derivatized from hepatic glycogen. Briefly, in the presence of $^2\text{H}_2\text{O}$, glycogen monomers become enriched with ^2H during glycogen deposition, and the enrichment occurs in a region-specific manner according to the route of incorporation. All newly incorporated glycogen units and pre-existing units that underwent cycling, get enriched in position 2. This exchange operated by G6P-isomerase is incomplete and in mice occurs for a fraction 0.64 [170]. While direct pathway units become enriched exclusively in position 2, units incorporated via indirect pathway

might become enriched in all other positions; however, enrichments of position 5 and 6 accurately discriminates between indirect glycolytic sources: triose-P precursors such as fructose get labeled in position 2 and 5 and precursors deriving from Krebs cycle anaplerosis get labeled in position 2, 5 and 6.

Figure 3.2 shows representative NC and HS ^2H -NMR spectra of MAG, while in Table 3.1 all positional ^2H -enrichments of MAG derived from hepatic glycogen of NC and HS mice, and those of body water (BW), are reported.

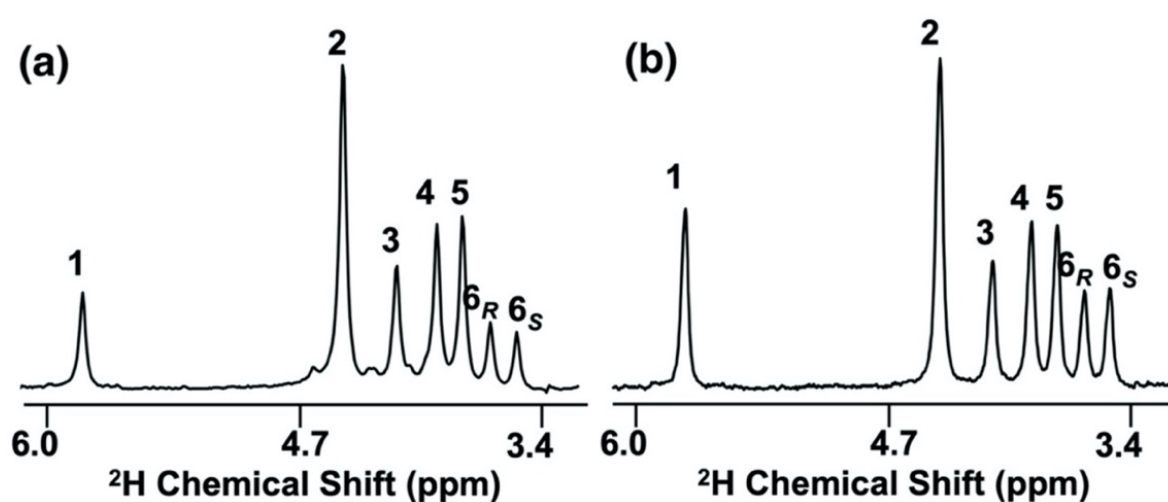


Figure 3.2 - Representative ^2H -NMR spectra of monoacetone glucose derived from liver glycogen of a mouse fed standard chow supplemented with 30% HSCS-55 in the drinking water (a) and a mouse fed standard chow only (b). Figure adapted from [176].

Table 3.1 - Liver glycogen positional ^2H -enrichments (H1-H6) and body water ^2H -enrichments (BW) for mice fed normal chow (NC, n=9) and mice fed normal chow supplemented with 30% HFCS-55 in the drinking water (HS, n=12). Data are expressed as percentages (%) and are presented as mean (SEM). (***) = $p < 0.001$. We hereby refer to H2_{corr} to indicate enrichment of H2 after correction for incomplete exchange with body water ($\text{H2}_{\text{corr}} = \text{H2} \times 1.57$) as previously described [170].

	BW	H1	H2	H2 _{corr}	H3	H4	H5	H6 _R	H6 _S
<i>NC</i>	4.46 (0.25)	1.56 (0.21)	3.28 (0.21)	5.14 (0.33)	1.26 (0.08)	1.65 (0.10)	1.74 (0.12)	1.15 (0.09)	1.20 (0.09)
<i>HS</i>	5.88 *** (0.14)	0.82 *** (0.06)	2.85 (0.17)	4.47 (0.27)	1.27 (0.11)	1.56 (0.13)	1.63 (0.15)	0.58 *** (0.06)	0.55 *** (0.06)

After employing the mathematical formulas illustrated on page 91, Table 2.1; the fraction of newly synthesized glycogen and the relative contributions of different glycolytic sources to overnight glycogen deposition were quantified (Table 3.2).

Table 3.2 - Fraction of newly synthesized glycogen expressed as $H2_{corr} / BW$ and fractional contributions of different glycolytic sources to overnight glycogen appearance for mice fed normal chow (NC, n=9) and mice fed normal chow supplemented with a 30% HFCS-55 in the drinking water (HS, n=12). Data are presented as mean (SEM). ** = $P < 0.01$, *** = $P < 0.001$.

	<i>$H2_{corr} / BW$</i>	<i>Direct and/or cycling (%)</i>	<i>Indirect Krebs cycle (%)</i>	<i>Indirect Triose-P (%)</i>
NC	1.14 (0.10)	66.21 (0.67)	23.19 (0.83)	10.60 (0.43)
HS	0.76 (0.04) **	64.19 (1.27)	12.01 (0.83) ***	23.80 (1.23) ***

For NC mice, average $H2_{corr}$ was not smaller than body water 2H -enrichment, indicating that all glycogen examined was synthesized or underwent cycling following 2H_2O administration, as shown by the ratio $H2_{corr}/BW \geq 1$. On the other hand, $H2_{corr}$ is significantly lower than body water 2H -enrichment in HS mice and $H2_{corr}/BW$ equals 0.76. This indicates that in HS mice approximately one-quarter of the glycogen analyzed was pre-existing, hence synthesized before 2H_2O administration.

Direct pathway + glycogen cycling contributed for about two-thirds to glycogen synthesis in both NC and HS mice. The remaining one-third was synthesized via indirect pathway. As explained above, the difference between position 5 and 6 enrichments can further resolve the indirect pathway into triose-P and Krebs cycle contributions. In HS mice, enrichment of H6 was more relatively diluted compared to H5 enrichment (Figure 3.2, Table 3.1), thus a much bigger load of substrates entered at the level of triose-P, suggesting that fructose was abundantly utilized for glycogen synthesis. This effect was offset by diminished contribution from Krebs cycle sources (Table 3.2).

¹³C-isotopomer analysis of hepatic glycogen enrichment from exogenous [U-¹³C]glucose and [U-¹³C]fructose

We next aimed to quantify the individual contributions of the glucose and fructose components of HFCS-55 to glycogen synthesis. During the final night, HFCS-55 enriched to 20% with either [U-¹³C]glucose (HS1, n=6) or [U-¹³C]fructose (HS2, n=6) was provided to HS mice in place of the regular HFCS-55 administered during the previous eighteen weeks.

Figure 3.3 illustrates the main ¹³C-isotopomers generated during glycogen synthesis in the presence of uniformly labeled ¹³C glycolytic substrates. [U-¹³C]glucose entering via the direct pathway is easily quantifiable as it retains uniform ¹³C- enrichment in all six carbons. On the other hand, only half of the hexose molecule displays ¹³C-enrichment when labeled glycolytic substrates ([U-¹³C]fructose) enter at the level of triose-P. Labeled glycolytic precursors entering the Krebs cycle become, in quantities corresponding to a specific ratio, enriched in either one half or one-third of the molecule.

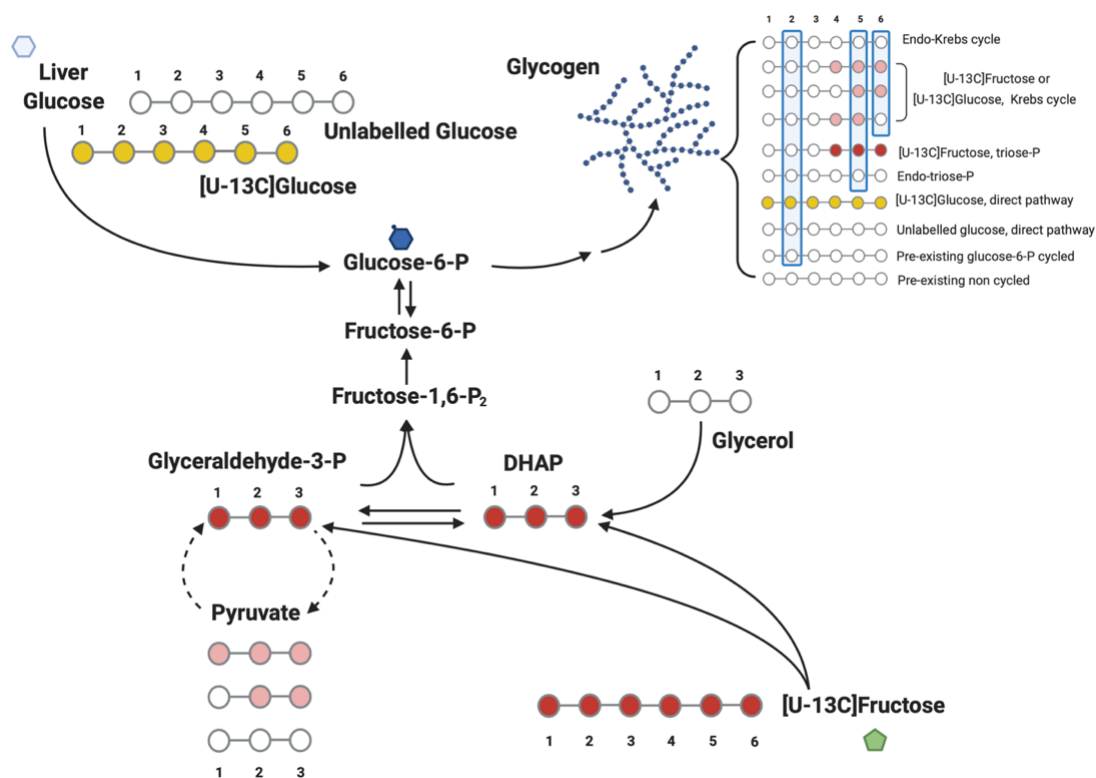


Figure 3.3 - Schematic of glycogen synthesis from unlabeled endogenous sources, and exogenous $[U-^{13}C]$ glucose and $[U-^{13}C]$ fructose. ^{13}C -isotopomers of triose-P intermediates and glycogen originating from $[U-^{13}C]$ fructose are shown by red circles while glycogen ^{13}C -isotopomers that originated via the Krebs cycle are shown as pink. Glycogen formed from $[U-^{13}C]$ glucose via the direct pathway is shown as yellow. Unlabeled glycogen and unlabeled precursors are represented by unfilled circles. For simplicity, some metabolic intermediates were omitted and only those ^{13}C -isotopomers within the 456-triose moiety of glycogen are shown. Positions 2, 5 and 6s enriched from 2H_2O are also highlighted (blue shading). [Figure created with BioRender.com].

^{13}C -NMR spectra of MAG obtained from hepatic glycogen of mice provided with $[U-^{13}C]$ glucose and $[U-^{13}C]$ fructose are shown in Figure 3.4. The contributions of exogenous glucose and fructose to glycogen synthesis were estimated from the analysis of carbon 1 and 5, shown in expanded form.

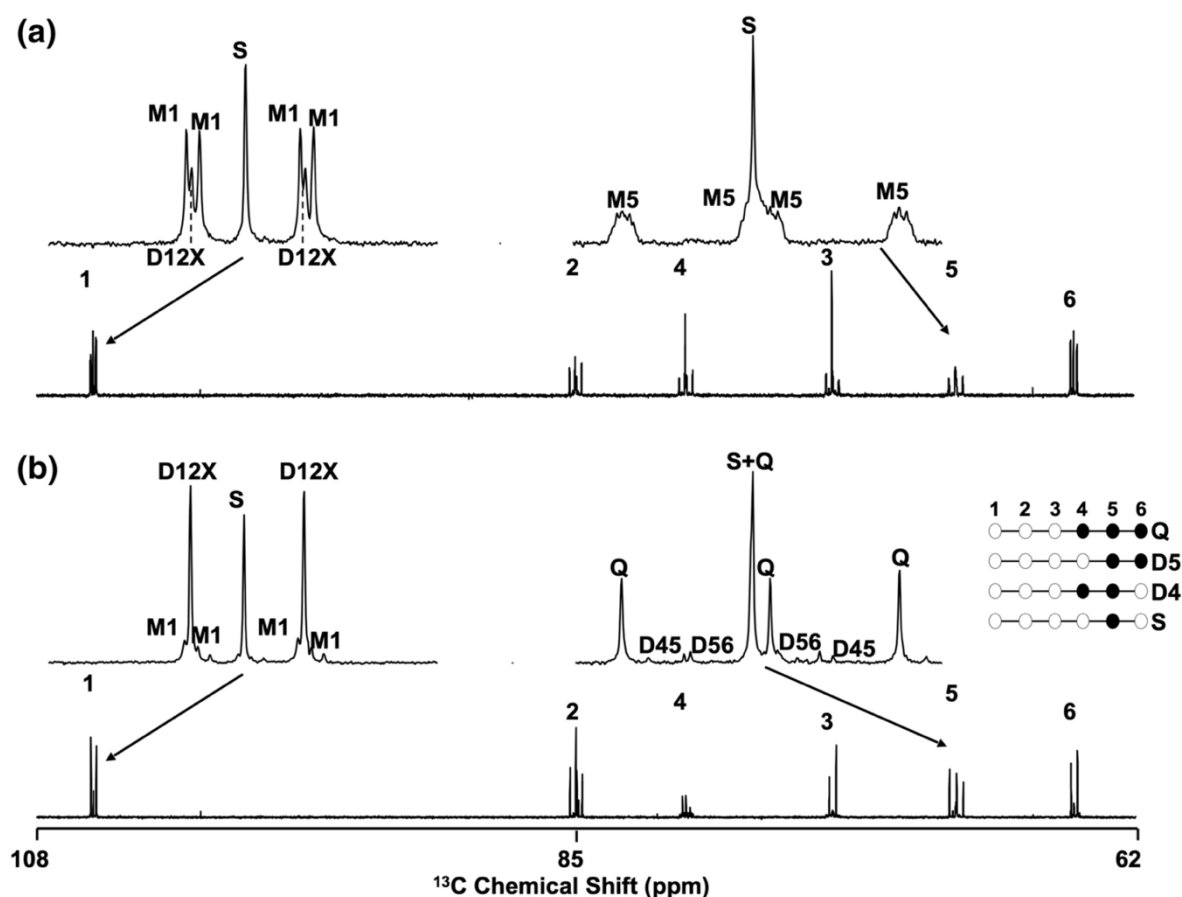


Figure 3.4 - ^{13}C -NMR spectra of hepatic glycogen following derivatization to monoacetone glucose obtained from a mouse fed a HFCS-55 enriched with $[\text{U-}^{13}\text{C}]$ glucose (a) and $[\text{U-}^{13}\text{C}]$ fructose (b). For the ^{13}C -NMR multiplets, S = carbon singlet resonance; **D12X** = carbon 1 doublet from ^{13}C - ^{13}C -coupling between carbon 1 and carbon 2 and \pm ^{13}C in carbon 3; **M1** = carbon 1 multiplet from ^{13}C - ^{13}C -couplings between carbon 1, carbon 2 and carbon 5; **M5** = carbon 5 multiplet from ^{13}C - ^{13}C -couplings between carbon 5, carbon 6, carbon 3 and carbon 1; **D56** = carbon 5 doublet from ^{13}C - ^{13}C -coupling between carbon 5 and a neighboring ^{13}C in position 6; **D45** = carbon 5 doublet from ^{13}C - ^{13}C -coupling between carbon 5 and a neighboring ^{13}C in position 4; **Q** = carbon 5 quartet from ^{13}C - ^{13}C -coupling between carbon 5 and neighboring ^{13}C in both positions 4 and 6. To the right of the carbon 5 multiplet of spectrum (b) are shown the ^{13}C -isotopomers represented by the S, **D45**, **D56** and **Q** components. Figure adapted from [176].

As previously explained, each of the hexose six carbons gave rise to a signal composed of a central singlet (S) from background ^{13}C (natural ^{13}C abundance, approximately 1.1%), and multiplets on both sides originating from the exogenous $[\text{U-}^{13}\text{C}]$ tracers.

For mice that received $[\text{U-}^{13}\text{C}]$ glucose (Figure 3.4a), resonance of carbon 1 shows intense M1 signal, corresponding to $[\text{U-}^{13}\text{C}]$ glucosyl units metabolized via direct pathway. Signals

Study 1

corresponding to [1,2-¹³C₂]- and/or [1,2,3-¹³C₃]glucose, (D12X), were also detected from carbon 1 resonance, consistent with pentose phosphate pathway activity [189].

On the other hand, ¹³C-isotopomers generated via indirect pathway metabolism (corresponding to D45 or D56 signals) were not observed or barely detectable from analysis of carbon 5 resonance.

For mice that received [U-¹³C]fructose (Figure 3.4b), carbon 5 resonance was dominated by the quartet C5Q corresponding to [4,5,6-¹³C₃]glycogen. [4,5,6-¹³C₃]glycogen accounted for ~95% of the total multiplet signals, consistent with the glycogenic metabolism of [U-¹³C]fructose. The D45 and D56 components, representing passage of the ¹³C-label through the Krebs cycle were detected to a very moderate extent.

Resonance of carbon 1 revealed the presence of some minor M1 signals in the ¹³C-NMR spectra of mice provided with [U-¹³C]fructose. [U-¹³C]fructose normally generates discrete ¹³C-isotopomers for each of the triose halves of glucose-6-phosphate and thus, a small proportion of glucose-6-phosphate is predicted to be synthesized with ¹³C in both triose moieties, hence the modest M1 signal. Consistent with this, a close inspection of carbon 5 Q signals revealed some residual clusters of M5 at their base.

Quantification of the different liver glycogen ¹³C-isotopomers for the two groups of mice is reported in Table 3.3.

Table 3.3 - Liver glycogen ¹³C-isotopomer enrichments from six mice fed normal chow plus HFCS-55 in the drinking water enriched with [U-¹³C]glucose (HS1), and six mice fed normal chow plus HFCS-55 in the drinking water enriched with [U-¹³C]fructose (HS2). Data are expressed as percentages (%) and are presented as mean (SEM), n.d. = non detected.

	<i>[U-¹³C]glycogen</i>	<i>[4,5,6-¹³C₃]glycogen</i>	<i>[5,6-¹³C₂]glycogen</i>	<i>[4,5-¹³C₂]glycogen</i>
HS1 <i>HFCS-55[U-¹³C]Glu</i>	2.57 (0.41)	n.d.	0.04 (0.02)	0.03 (0.02)
HS2 <i>HFCS-55[U-¹³C]Fru</i>	0.55 (0.06)	2.59 (0.14)	0.10 (0.01)	0.10 (0.01)

Estimates of exogenous glucose, fructose and other substrate contributions to hepatic glycogen synthesis

By integrating $^2\text{H}_2\text{O}$ measurements of hepatic glycogen sources with quantifications of glycogen ^{13}C -isotopomers deriving from $[\text{U-}^{13}\text{C}]\text{glucose}$ and $[\text{U-}^{13}\text{C}]\text{fructose}$ in the drinking water, contributions from various sources to hepatic glycogen synthesis during a single night were estimated in NC and HS mice. Figure 3.5 comprehensively summarizes our findings. Contributions of the exogenous glucose and fructose components of HFCS-55 to glycogen synthesis via different glycolytic routes were calculated by employing the mathematical equations previously illustrated (page 94, Table 2.2).

Positional ^2H -enrichments of MAG provided information on the fractional contributions of direct and indirect pathways to overnight glycogen deposition as well as the fraction of glycogen synthesized overnight following $^2\text{H}_2\text{O}$ administration.

For NC mice, all glycogen examined was synthesized or underwent cycling during the night. On the contrary, a significant proportion of glycogen was pre-existing in HS mice. As Hepatic glycogen concentration, measured in NC and HS mice (Materials and Methods, page 108), tended to be higher in HS mice (38 ± 3 versus 30 ± 3 mg/g wet weight of liver, $p = 0.07$), we estimated the absolute fraction of newly synthesized glycogen deposited overnight to be approximately equal in both groups.

For NC mice, two-thirds of the newly synthesized glycogen were incorporated via direct pathway + cycling and one-third was synthesized via indirect pathway, with the Krebs cycle accounting for the majority of indirect pathway sources. Similarly, in HS mice two-thirds of the newly synthesized fraction were synthesized via direct pathway + cycling and one-third was incorporated via indirect pathway. However, in this case the majority of indirect pathway precursors originated from triose-P substrates, supplying twice that of Krebs cycle sources.

^{13}C -tracers enabled to assess the individual contributions and the routes of incorporation into hepatic

glycogen of the glucose and fructose components of HFCS-55, each independently from the other. The glucose and fructose components of HFCS-55 contributed approximately in equal measures to glycogen synthesis (16% and 17% respectively), but while the glucose component was almost exclusively incorporated into glycogen via direct pathway, fructose entered almost exclusively at the triose-P level. Both components of HFCS-55 contributed to glycogen synthesis via Krebs cycle anaplerosis only to a minimal proportion.

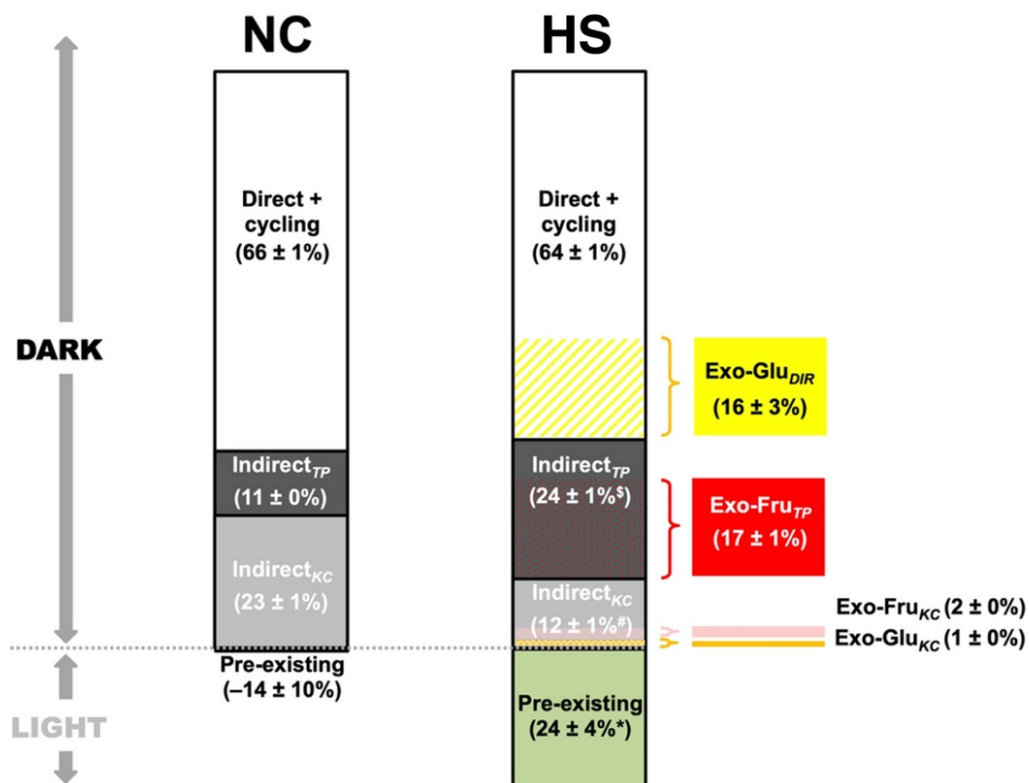


Figure 3.5 - Sources of hepatic glycogen synthesis in mice fed normal chow (NC, n=9) and mice fed normal chow plus a mixture of fructose and glucose in the drinking water (HS, n=12). Pre-existing glycogen was assumed to have been present at the end of the light phase of the previous day while all newly synthesized glycogen, arbitrarily set to 100%, was defined as having been formed entirely during the following dark period. For NC mice these include the fraction of pre-existing glycogen that had not undergone cycling with glucose-6-phosphate; direct pathway + cycling, indirect pathway via the Krebs cycle (Indirect_{KC}), and indirect pathway via triose-P (Indirect_{TP}). For the HS mice, these parameters are accompanied by direct pathway contribution of exogenous glucose shown in yellow (Exo-Glu_{DIR}), indirect pathway Krebs cycle contribution of exogenous glucose shown in orange (Exo-Glu_{KC}), exogenous fructose contribution via triose-P shown in red (Exo-Fru_{TP}) and exogenous fructose contribution via the Krebs cycle shown in pink (Exo-Fru_{KC}). Data are presented as mean ± SEM. *p < 0.005 versus NC, #p < 10⁻⁵ versus NC, §p < 10⁻⁷ versus NC. Figure adapted from [176].

¹³C-isotopomer analysis of liver aqueous fraction

The aqueous fraction of liver obtained during the processing of liver tissues (Materials and Methods, page 106); contained glucose and other gluconeogenic metabolites such as lactate and several amino acids, immediately prior to their incorporation into hepatic intermediary metabolism. Therefore, after analysis of liver glycogen, we briefly assessed the appearance of ¹³C-isotopomers from the labeled components of HFCS-55 in the liver aqueous fractions of the animals administered with [U-¹³C]glucose and [U-¹³C]fructose.

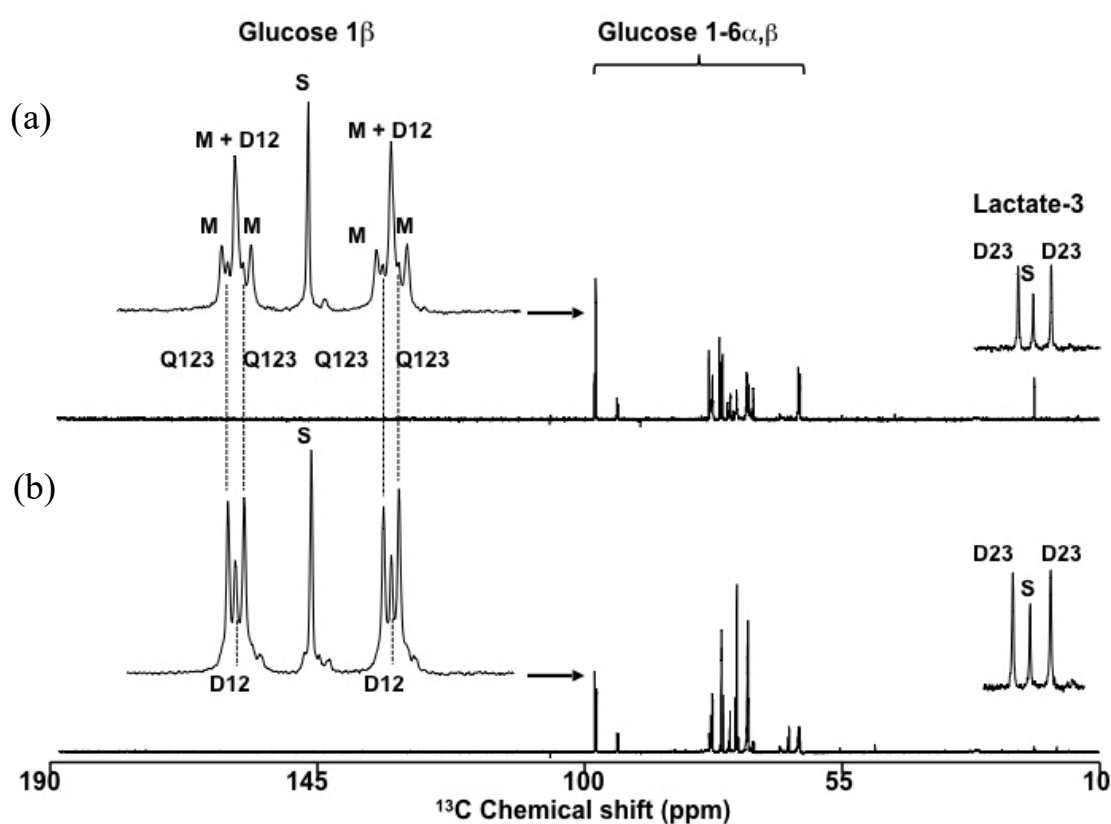


Figure 3.6 - ¹³C-NMR spectra of liver aqueous fractions from mice provided with glucose/fructose mixtures enriched with [U-¹³C]glucose (a) and [U-¹³C]fructose (b). The lactate carbon 3 and glucose carbon 1β signals are shown in expanded form and the multiplet components are indicated as follows: S = natural-abundance singlet, D23 = doublet from ¹³C-¹³C coupling between lactate carbon 3 and carbon 2; M = multiplet from coupling of glucose carbon 1β with carbons 2β, 3β and 6β, and representing [U-¹³C]glucose; Q123 = quartet from coupling of glucose carbon 1β with carbons 2β and 3β and representing [1,2,3-¹³C₃]glucose; D12 = doublet from coupling of glucose carbon 1β with carbon 2β and representing [1,2-¹³C₂]glucose. Figure adapted from [176].

The representative ^{13}C -NMR spectra shown in Figure 3.5 exhibit several peaks whose splitting patterns inform about the isotomeric abundance of the various metabolites present in liver aqueous fractions.

Glucose was the most abundant ^{13}C -enriched metabolite found in the spectra of both mice administered with exogenous $[\text{U-}^{13}\text{C}]$ glucose (3.5a) and $[\text{U-}^{13}\text{C}]$ fructose (3.5b). ^{13}C -Lactate isotopomers, present in less amounts, were observed in similar quantities in the two groups, whereas peaks corresponding to alanine, glutamate and other amino acids were barely detectable.

For the spectra of mice administered with exogenous $[\text{U-}^{13}\text{C}]$ glucose, the most abundant glucose isotopomer was intact $[\text{U-}^{13}\text{C}]$ glucose (multiplet M in Figure 3.5a), consistent with absorption and transport of exogenous glucose to the liver, whereas partially enriched glucose isotopomers generated via Cori cycle or pentose phosphate pathway were present but with relatively less abundance (D12 and Q123). Overall, enrichment of $[\text{U-}^{13}\text{C}]$ glucose in liver tissue was estimated to be 4.6%, an approximately four-fold dilution compared to the original $[\text{U-}^{13}\text{C}]$ glucose precursor enrichment.

Interestingly, intact $[\text{U-}^{13}\text{C}]$ fructose was not detected in the spectra of mice provided with $[\text{U-}^{13}\text{C}]$ fructose as seen by a complete lack of resolvable ^{13}C signals resonating at 104.2 and 100.8 ppm (Figure 3.5b), representing the fructose carbons 1α and 1β , respectively. For these mice, glucose present in the aqueous fraction showed strong enrichment from ^{13}C -isotopomers such as $[1,2,3\text{-}^{13}\text{C}_3]$ - and $[4,5,6\text{-}^{13}\text{C}_3]$ glucose (Q123 in figure 3.5b) - the expected products of fructose metabolism to triose-P followed by gluconeogenesis to form glucose.

Discussion

In this study, the effect of HFCS-55 supplementation on hepatic glycogenesis was studied in mice under *ad libitum* feeding. Using a combination of $^2\text{H}_2\text{O}$ and ^{13}C -tracers, we examined the consequences of high-sugar intake on the overall glycogenic process, and we assessed the individual metabolic fates of the glucose and fructose components of HFCS-55 in the context of hepatic glycogen synthesis.

At the beginning of the dark cycle, HS mice exhibited a significant amount of pre-existing non-cycled glycogen ($24 \pm 3 \%$). This effect is likely attributed to certain experimental caveats that were unavoidable in our set-up. As HFCS-55 was provided in the drinking water, HS mice ingested a significant amount of glucose and fructose every time they drank water, which most likely had occurred also during the light phase, hence the residual unlabeled glycogen at the beginning of the dark phase. On the other hand, NC displayed a negative nominal value ($-14 \pm 10 \%$). Our estimates of pre-existing glycogen fractions are dependent on position 2 enrichment after adjustment for incomplete exchange with body water (H_2_{corr}). Given that the correction factor employed for such adjustment was derived from mice fed fructose/glucose loads that resembled those given to HFCS-55 mice [170], it is possible that it understates the extent of H_2 -body water exchange in mice fed normal chow, thereby resulting in a systematic underestimate of pre-existing glycogen in NC mice. Moreover, as shown by some longitudinal studies on hepatic glycogen excursion measured in mice fed normal chow over a 12/12h light and dark cycle, glycogen levels can normally drop to 10-15% of their maximal post-absorptive values [190], [191]. We therefore consider the obtained negative value not incompatible with our system and/or experimental set-up.

Absolute hepatic glycogen measurements revealed that HS mice exhibited on average one-quarter more hepatic glycogen than NC mice. Since the fraction of pre-existing non-cycled glycogen in HS was also estimated to be one-quarter of the total, we concluded that, despite differences in

baseline glycogen content, net hepatic glycogen synthesis during the dark phase was approximately equal in the two groups.

Analysis of the ²H-enrichment distribution of hepatic glycogen revealed that direct and indirect pathways contributed two-thirds and one-third respectively of the newly synthesized glycogen fraction in both NC and HS mice. In HS mice, however, indirect pathway precursors contributed mainly via triose-P, whereas Krebs cycle substrates were the dominant indirect source in NC mice. Such expansion of triose-P contributions was expected in mice fed HFCS-55 and already described in previous studies conducted in rodents using similar experimental set-ups [170], [171].

Nonetheless, in one of our initial hypotheses we also anticipated indirect pathway to contribute a bigger fraction to glycogen synthesis in HS mice, in part because of the large fructose supply likely entering the glycogenic pool via triose-P, and in part because of possibly attenuated direct pathway activity following chronic high-sugar feeding. ¹³C-isotopomer analysis later confirmed that the larger triose-P contribution in HS mice was indeed caused by the glycogenic metabolism of the fructose component of HFCS-55, but this effect was offset by a reduction in Krebs cycle substrates contribution. Moreover, direct pathway activity was found intact in HS mice. Consequently, the proportion between direct and indirect pathway was maintained the same in the two groups, disproving our theory.

The ¹³C-isotopomer data provided new insights on how exogenous glucose was converted to glycogen in the presence of fructose. The role of fructose in this context is ambiguous. Whilst fructose is a highly glycogenic substrate that, when ingested in high doses, competes with glucose for all anabolic pathways in the liver and promotes hepatic insulin resistance, which among other things, would be expected to decrease insulin-mediated activation of glucokinase; low dietary levels of fructose potentiate glucokinases activation [188], [192], [193] and contribute to the activation of ChREBP [184], a transcription factor that promotes the transcription of glycolytic pathway enzymes and acts synergistically with glucokinase to potentiate glucose phosphorylation to glucose-6-phosphate. Considering that in our study fructose was provided as part of a chronic high-sugar diet,

Study 1

we expected fructose, whose conversion into glycogen bypasses glucokinase, to overthrow the glucose component of HFCS-55 as substrate for glycogen synthesis. However, our results did not support this prediction; albeit labeled fructose was in excess compared to labeled glucose (55% and 45% respectively), HFCS-55's fructose and glucose contributions to hepatic glycogenesis were similar (17% and 16% respectively). Labeled glucose entered almost exclusively via direct pathway and constituted approximately one-quarter of all direct pathway sources whereas, as already mentioned, labeled fructose entered almost entirely at the triose-P level.

On a separate note, analysis of liver glucose from HS mice aqueous fraction showed a ~ 4-fold dilution of the 20% enriched [U-¹³C]glucose in the drinking water by endogenous glucose sources. Assuming that these sources were entirely derived from absorbed glucose, an estimate of direct pathway contributions can be made from the ratio ($[U-^{13}C]glycogen/0.76$) / liver [U-¹³C]glucose. This estimate ($75 \pm 7\%$) exceeds the 64% obtained from the ²H₂O method and likely reflects an incomplete suppression of hepatic gluconeogenesis. This suggests that, upon high-sugar feeding in mice, metabolic dysregulations like unrestricted hepatic gluconeogenesis might have a faster progression compared to alterations in glycolytic fluxes, such as impairment in direct pathway activity. Unfortunately, we are unable to provide a more complete metabolic profile of these animals and further argument on this matter, a caveat that we acknowledge as one of the main limitations of this study.

Conclusions

This study was designed having two main objectives in mind. If on one hand we aimed at investigating the effect of chronic high-sugar feeding on hepatic glycogenesis in mice, on the other hand we also wanted to mechanistically resolve the metabolic fate of the sugar provided (HFCS-55) in the context of hepatic glycogen synthesis.

Despite the excess of exogenous fructose over glucose, both were utilized for glycogen synthesis to a similar extent, with exogenous glucose being incorporated almost exclusively via direct pathway and fructose mainly through the indirect pathway via triose-P. This flux was offset by a decreased Krebs cycle contribution to the indirect pathway.

Chronic high-sugar consumption did not however alter the overall rate of hepatic glycogen deposition during nocturnal feeding and direct pathway contribution to glycogen synthesis. Additional analysis to determine whether high-sugar feeding induces more systemic metabolic alteration in this animal model is required and will be the objective of further investigation.

STUDY 2

***Effects of Second-Generation
Antipsychotics on Hepatic Glucose and
Lipid Metabolic Fluxes***

Introduction

Second-generation antipsychotics (SGAs) have proven to be effective in the treatment of several psychiatric disorders, including schizophrenia. However, SGAs can cause significant side effects such as weight gain and T2DM that induce many patients to quit the treatment. The underlying molecular events that lead to such side effects are not well-described and their onset might be triggered by a complex interplay between central and peripheral systems.

Reconstructing the molecular evolution of SGA-induced side effects in their whole continuum can provide insights into the mechanism of action of SGAs and help the research around the development of more clinically safe therapeutic agents.

Acute studies on healthy subjects have shown how certain SGAs disrupt glucose and lipid homeostasis even after short-term administrations [131], [194], [195], [196], suggesting that some of the early events involved in the pathogenesis of SGA-associated metabolic diseases are independent of weight gain. Several studies point at hepatic insulin resistance as the putative cause behind these defects [197], [198], [199]. Marked hepatic insulin resistance, either peripherally induced or resulting from SGAs action via central mechanisms, is believed to persist during chronic SGAs treatment contributing to the progression towards more metabolically dysfunctional phenotypes, which ultimately result in weight gain and T2DM. Although SGAs-associated metabolic diseases are a multifactorial phenomenon involving several tissues, this theory places central importance on the liver as a key target organ in the pathogenesis and evolution of SGA-induced metabolic diseases.

With the intent of validating previous studies around this matter and of establishing whether the liver is a key target organ during this process, we administered two commonly used SGAs, olanzapine and aripiprazole, to mice over a period of seven months. Using $^2\text{H}_2\text{O}$ as a metabolic tracer and measuring ^2H -enrichment distribution by ^2H -NMR, we quantified hepatic glycogen and lipid synthetic fluxes. As hepatic lipid metabolism is strongly connected to adipose tissue lipid

inflows and outflows, lipid synthesis was also briefly investigated in adipose tissue by analysis of ²H-enrichment present in visceral adipose depots. To our knowledge, this is the first study examining the relative changes in metabolic fluxes following chronic administration of SGAs in an animal model.

In line with some of the current research literature, we expected SGAs to cause hepatic insulin resistance, impacting both hepatic glycogen and lipid synthetic fluxes. Furthermore, as olanzapine is clinically associated with more detrimental metabolic side effects [200], we predicted olanzapine to induce more damaging effects when compared to aripiprazole, especially after such long-term exposure, in which dysregulated glucose metabolism is at this point believed to be accompanied by changes in lipid synthesis rates and distribution, consequence of a more advanced metabolically morbid phenotype.

Animals and experimental set-up

Twenty-six adult male mice (wild type of mixed genetic background C57BL/6J x 129/sv) were used in this study. Mice were randomly divided in three groups: control animals (n = 9), hereby referred to as CTL; mice receiving olanzapine, referred to as OLA (n = 9); and mice receiving aripiprazole, referred to as ARI (n = 8).

Intervention

All mice were provided with a standard chow diet and regular drinking water. OLA and ARI mice chow diet was supplemented with olanzapine and aripiprazole respectively for a period of seven months, whereas CTL animals were fed standard chow only. Olanzapine and aripiprazole were incorporated in the food at a concentration that allowed the animals to assume a daily dose of 5mg/Kg for a mean food intake of 4 g/day/mice.

Tracer administration:

All animals received $^2\text{H}_2\text{O}$ as tracer, provided at the beginning of the final evening as an intraperitoneal loading dose of 99% $^2\text{H}_2\text{O}$ containing 0.9 mg/mL NaCl (4 mL/100 g body weight). The drinking water was enriched to 5% with $^2\text{H}_2\text{O}$.

Sacrifice

Mice were approximately eleven months old at the time of sacrifice. At the end of the dark cycle, all animals were sacrificed by decapitation. Plasma was isolated and stored at -80°C , livers and epididymal adipose tissue were freeze-clamped and stored at -80°C until further analysis.

Results

In vivo analysis

During the intervention period, mice underwent a series of metabolic assessments conducted at the animal facilities of the Instituto de Investigaciones Biomédicas Alberto Sols (CSIC-UAM, Madrid) where the animals were kept until sacrifice. The data described in this section were not directly produced by the author of this thesis and therefore are not examined in detail. The conclusions drawn from these initial *in vivo* metabolic assessments (summarized in Table 4.2) are hereby reported with the only purpose of facilitating the interpretation of the overall metabolic status of the animals under study in relation to liver metabolism, the main object of our investigation.

Food intake and body composition:

By the 5th month of treatment, food intake was significantly increased in both OLA and ARI animals (data not shown). However, no significant difference in body weight was reported for any of the groups the night before the sacrifice. Post-mortem, liver and epididymal fat depots were weighted and while no difference was observed in liver weights, animal treated with SGAs showed a significant increase in adiposity (Table.4.1).

Table 4.1 - Body, liver and visceral depots weights in control mice and mice treated with OLA or ARI over a period of seven months. Weights were recorded upon tissue collection. Data are expressed as Mean \pm SEM. CTL: n=9, OLA: n=9, ARI: n=8. * = $p < 0.05$, ** = $p < 0.01$.

	CTL	OLA	ARI
Body weight (g)	34.37 \pm 1.33	36.79 \pm 1.23	35.23 \pm 2.00
Liver weight (g)	1.42 \pm 0.06	1.49 \pm 0.04	1.49 \pm 0.09
Epididymal fat weight (g)	0.46 \pm 0.04	0.87 \pm 0.15*	1.07 \pm 0.13**

Glucose tolerance and insulin sensitivity

Five months into the treatment, a GTT was performed to assess overall glucose tolerance. ARI animals exhibited significant glucose intolerance. OLA mice exhibited a similar trend, although to a less and not significant extent (data not shown).

An ITT was performed in order to assess whole body insulin sensitivity. ARI animals manifested signs of insulin resistance, while OLA mice showed similar but less pronounced and not significant effects (data not shown).

After five months of treatment, ARI animals presented significantly higher fasting glucose levels. A PTT was performed to elucidate the contribution of hepatic gluconeogenesis to the observed fasting hyperglycemia. Neither group exhibited a significant glycemic excursion in response to a pyruvate bolus, suggesting that hepatic gluconeogenesis does not play a role in the observed glycemic dysregulations (data not shown).

Table 4.2 - In vivo assessment of different metabolic features in OLA and ARI animals. All metabolic tests and measurements were conducted at the animal facilities of the Instituto de Investigaciones Biomédicas Alberto Sols (CSIC-UAM, Madrid). OLA and ARI higher (↑), lower (↓) or not significant (X) trends were assessed in relation to CTL animals.

	<i>OLA</i>	<i>ARI</i>
<i>Food intake</i>	↑	↑
<i>Fasted glucose concentration</i>	X	↑
<i>Glucose tolerance (GTT)</i>	X	↓
<i>Insulin resistance (ITT)</i>	X	↑
<i>Pyruvate tolerance (PTT)</i>	X	X

Hepatic glycogen metabolism

Body water, hepatic glycogen enrichment from $^2\text{H}_2\text{O}$, and fractional contributions of direct and indirect pathways to hepatic glycogenesis

Body water (BW) ^2H -enrichments were determined from plasma by ^2H -NMR spectroscopy whereas hepatic glycogen was digested and derivatized to MAG as previously described (Materials and Methods, page 107). ^2H -NMR spectra were obtained for each MAG and positional ^2H -enrichments were determined (Table 4.3). The fraction of newly synthesized glycogen, and the fractional contributions of direct and indirect pathways to overnight hepatic glycogen appearance were calculated as already described (page 91, Table 2.1). Results are illustrated in Table 4.4.

Table 4.3 - BW and liver glycogen positional ^2H -enrichments (H1-H6) in control mice and mice that underwent a treatment of 7 months with either OLA or ARI. Enrichment of glycogen position 2 was adjusted by multiplication to a correction factor of 1.57 (H2_{corr}) to correct for incomplete exchange of body water and position 2 hydrogens [170]. Data are expressed as percentages (%) and are presented as mean (SEM). CTL: n=9, OLA: n=9, ARI: n=8.

	BW	H1	H2	H2_{corr}	H3	H4	H5	H6_R	H6_S
<i>CTL</i>	4.35 (0.19)	1.49 (0.17)	2.72 (0.29)	4.27 (0.46)	1.02 (0.14)	1.44 (0.18)	1.52 (0.19)	1.12 (0.15)	1.18 (0.15)
<i>OLA</i>	4.82 (0.13)	1.25 (0.18)	3.36 (0.19)	5.28 (0.29)	1.01 (0.12)	1.44 (0.15)	1.52 (0.15)	1.07 (0.13)	1.14 (0.12)
<i>ARI</i>	4.76 (0.14)	1.52 (0.15)	3.24 (0.19)	5.08 (0.35)	1.02 (0.13)	1.45 (0.16)	1.53 (0.17)	1.04 (0.12)	1.09 (0.13)

Table 4.4 - Fraction of newly synthesized glycogen expressed as $\text{H2}_{\text{corr}} / \text{BW}$ and fractional contributions of different glycolytic sources to overnight glycogen appearance in control mice and mice treated with either OLA or ARI over a period of 7 months. Data are shown as means (SEM). CTL: n=9, OLA: n=9, ARI: n=8. * = $p < 0.05$.

	<i>H2_{corr} / BW</i>	<i>Direct and /or cycling (%)</i>	<i>Indirect Krebs cycle (%)</i>	<i>Indirect triose-P (%)</i>
<i>CTL</i>	0.99 (0.10)	65.06 (1.42)	27.18 (1.22)	7.76 (0.34)
<i>OLA</i>	0.97 (0.09)	68.27 (1.93)	23.54 (1.85)	8.19 (0.30)
<i>ARI</i>	1.06 (0.06)	70.11 (1.24)	21.13 (1.09) *	8.66 (0.35)

As previously explained, differences in body water enrichment from $^2\text{H}_2\text{O}$ are indicative of differences in body composition. No differences in body water enrichment were detected between groups, although both OLA and ARI animals presented a non-significant tendency towards more enriched body waters ($p = 0.08$), in line with the more abundant visceral adiposity observed in these groups.

The ratio $\text{H2}_{\text{corr}} / \text{BW}$, representing the fraction of newly synthesized glycogen following $^2\text{H}_2\text{O}$ administration, was not significantly different and approximately equal to 1 in each group, indicating that all glycogen analyzed was newly synthesized or underwent cycling during the night. Compared to CTL animals, ARI mice presented a not significant tendency towards increased direct pathway + cycling fractional contribution to glycogen synthesis ($p = 0.06$), compensated by a statistically significant reduction in Krebs cycle intermediates fractional contribution ($p = 0.02$). OLA mice followed the same trend as ARI animals, although none of the observed differences in fractional contributions reached statistical significance in OLA mice.

Glycogen content and absolute contribution of glycogenic sources to hepatic glycogenesis

Total hepatic glycogen content was quantified as illustrated in Materials and Methods (page 108). Absolute contributions of various glycogenic sources were calculated by hepatic glycogen content (mg per g of liver) multiplication to the respective fractional contributions (Figure 4.1).

Although hepatic glycogen content was on average higher in ARI and OLA animals, no statistical difference has been reported between groups.

Similar to what previously observed from relative numbers, the absolute contribution of direct pathway + cycling to hepatic glycogen synthesis was on average (but not significantly) higher in ARI and OLA animals. On the other hand, after normalization per glycogen content, the absolute contribution of indirect pathway sources (Krebs cycle intermediates + triose-P sources) emerged as

approximately equal in each group, suggesting that possible variations in glycogen concentrations are a sole consequence of direct pathway activity.

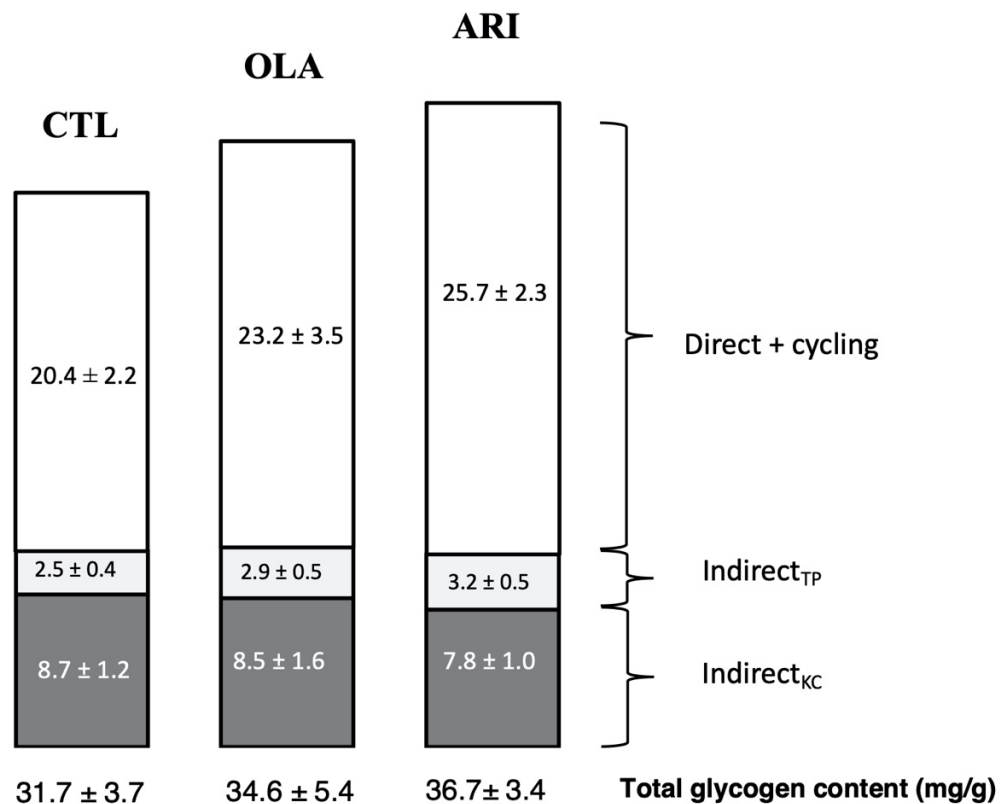


Figure 4.1 - Total glycogen content and absolute contributions of various glyco-genic sources to overnight glycogen appearance in control mice and mice treated with either OLA or ARI over a period of seven months. Results are expressed as mean ± SEM (mg per g of liver). CTL: n=9, OLA: n=9, ARI: n=8. Indirect_{TP}: indirect pathway via triose-P; Indirect_{KC}: indirect pathway via the Krebs cycle.

Overall, these results point towards metabolically functional hepatic glycogen synthesis in both OLA and ARI animals. The ability of synthesizing glycogen via direct pathway, which plays an important role in glucose homeostasis maintenance, appears intact and even potentiated in OLA and ARI mice. This is especially visible in ARI mice, whereas OLA mice present a similar, but less significant trend.

Hepatic lipid metabolism

In order to assess hepatic lipid profiles as well as to measure TG-associated fractional synthetic fluxes in the liver, which include *de novo* synthesis of FA chains from acetyl CoA, chain elongation of existing and newly synthesized FAs, desaturation of newly synthesized FA, and synthesis of the TG glyceryl moiety; we extracted and purified TGs from the liver of CTL, OLA, and ARI animals (Materials and Methods, pages 108) and acquired TG ¹H- and ²H-NMR spectra. Percentages of different lipid species and fractional rates of lipid synthetic fluxes were then estimated applying the mathematical equations illustrated in Tables 2.4 and 2.5 (pages 97 and 101).

Lipidomic analysis

Percentages of fatty acid species can be determined from ¹H-NMR spectra of TG. The lipidomic profiles of hepatic TGs obtained from CTL, OLA and ARI mice are summarized in Table 4.5.

Table 4.5 - Percentages of different lipid species in the livers of CTL mice and mice that underwent a 7-months treatment with either OLA or ARI. Results are expressed as mean \pm SEM. CTL: n=9, OLA: n=9, ARI: n=8. **ω -3 FA**: omega-3 fatty acids; **non- ω -3 FA**: non-omega-3 fatty acids; **SFA**: saturated fatty acids; **MUFA**: monounsaturated fatty acids; **PUFA**: polyunsaturated fatty acids, **DHA**: docosahexaenoic acid.

	CTL	OLA	ARI
ω-3 FA (%)	1.36 \pm 0.25	1.31 \pm 0.21	1.20 \pm 0.17
Non-ω-3 FA (%)	98.64 \pm 0.25	98.69 \pm 0.21	98.80 \pm 0.17
SFA (%)	35.48 \pm 1.61	35.25 \pm 0.89	36.08 \pm 2.11
MUFA (%)	48.84 \pm 1.12	51.82 \pm 1.53	51.81 \pm 1.61
PUFA			
Linoleic acid (%)	14.65 \pm 1.29	12.24 \pm 1.27	11.52 \pm 1.17
DHA (%)	1.03 \pm 0.19	0.69 \pm 0.15	0.59 \pm 0.10

Lipid species profiles were similar across the three groups and comparable to expected reference values obtained in similar experiments previously conducted in mice [177].

Although not relevantly from a statistical point of view, linoleic acid and DHA, essential fatty acids ingested through the diet, presented a tendency towards reduced values in the livers of OLA and ARI animals. However, food intake was not decreased in OLA and ARI mice, on the contrary, was significantly increased in both groups.

We previously observed in similar set-ups that essential fatty acids such as linoleic acid, which serve as precursors for structural lipids, tend to be relatively more diluted in tissues that present increased lipid accumulation; while lipid species such as MUFA and SFA, that are preferentially destined to long-term storage within the cell, appear relatively more concentrated.

Based on this observation, together with the increased food intake and visceral adiposity observed in OLA and ARI mice, it is logic to assume that these animals possessed greater hepatic TGs contents. We are however unable to confirm this hypothesis with intrahepatic TG measurements, which will be the objective of future analysis.

Lipid synthetic rates

$^2\text{H}_2\text{O}$ administration allows the estimation of several metabolic fluxes, including hepatic lipid synthesis. As previously explained (page 98), the principle behind these estimations is that in TGs synthesized after $^2\text{H}_2\text{O}$ administration, only chains entirely synthesized *de novo* become progressively enriched with ^2H in all carbons, from position 2 until the methyl group. On the other hand, pre-existing chains undergoing elongation after $^2\text{H}_2\text{O}$ administration, do not become enriched on the methyl group but, as elongation takes place from the carboxyl-terminal, they get enriched in position 2. Hence, the enrichment of the methyl position is used to discriminate between chains synthesized during DNL and pre-existing chains undergoing elongation.

While position 2 and methyl position enrichments are employed for the quantification of DNL and elongation fluxes, enrichments in allylic positions are used to quantify the rate of desaturated newly synthesized chains.

Finally, the glycerol moiety of TG also becomes enriched during its synthesis which occurs before esterification to fatty acyl chains, and thus enrichment of the glycerol moiety not only correlates with glycerol synthesis, but also with the rate of TG esterification, and therefore with the rate of TG synthesis.

By analyzing the enrichment distribution of ^2H in TGs purified from livers of CTL, OLA and ARI mice, we could estimate the hepatic lipid synthetic fluxes above described.

The synthetic fluxes shown hereby are expressed as fractional synthetic rates (% overnight⁻¹), meaning as amount of labeled product synthesized per overnight over total product mass. DNL and elongation fluxes are expressed as percentages of new and elongated FAs respectively, over total liver FA content (in triglycerides) minus essential FAs that do not get labeled with ^2H . Desaturation fluxes refer to the percentages of *de novo* synthesized FAs that also underwent desaturation. Since we assume that the same proportion of non-essential FAs that were not newly synthesized (for example dietary palmitate) were also desaturated, desaturation rates can be

intended as percentages of desaturated FAs on total liver FA content (in triglycerides) minus essential FAs. Finally, glycerol synthetic rate represents the amount of newly synthesized TG-glyceryl over total TG-bound glycerol content.

Results are illustrated in Figure 4.2.

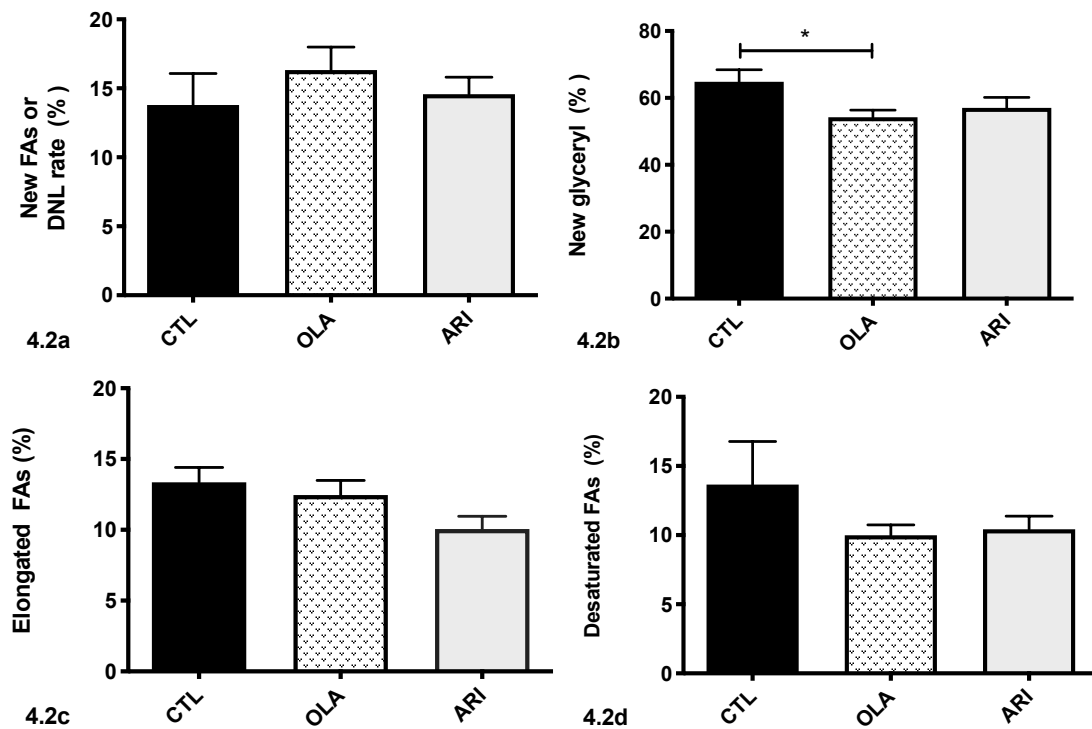


Figure 4.2 - Rates (% per overnight) of hepatic DNL (4.2a), glycerol synthesis (4.2b), elongation (4.2c) and desaturation (4.2d) in CTL mice and mice that underwent a 7-months treatment with either OLA or ARI. Results are expressed as mean \pm SEM. CTL: n=9, OLA: n=9, ARI: n=8. * = $p < 0.05$

The fractional synthetic rate of glycerol, and thus of TG, exceeded the fractional synthetic rate of FAs synthesized via DNL in all groups (Figure 4.2a and 4.2b). This is expected, as the glycerol moiety of TG, synthesized either via glycolysis or glyceroneogenesis, can become enriched with ^2H independently of DNL activity, and be esterified in the liver to unlabeled FAs deriving from adipose lipolysis (TG-FFA cycling) and/or dietary sources.

DNL, desaturation, and elongation rates were similar across the three groups, however OLA animals presented a significant reduction in glycerol synthetic rate, not accompanied by a

corresponding relative reduction in DNL rate, suggesting decreased glycerol esterification to unlabeled FAs.

Contributions of different lipid sources to overall hepatic TG content

Contributions of different lipid sources to overall hepatic TG content after one overnight feeding can be estimated from the rates of DNL and glycerol synthesis obtained from our previous analysis of TG ²H-enrichment, as follows:

- *Total Hepatic TG content (100%) = Pre-existing TGs + Newly synthesized TGs*
- *Newly synthesized TGs = TGs made from de novo synthesized FAs + TGs made from non-synthesized FAs*

Where:

- “*Newly synthesized TGs*” corresponds to the glycerol fractional synthetic rate and is defined as the percentage of hepatic TG made from both *de novo synthesized* and *non-synthesized FAs*.
- “*TGs made from de novo synthesized FAs*” is obtained as follows:
$$\text{DNL rate} / (1 + \% \text{ linoleic acid} + \% \text{ DHA})$$
and represents the percentage of hepatic TG made from FAs synthesized *de novo* via DNL.
- “*TGs made from non-synthesized FAs*” is obtained from:
$$\text{“Newly synthesized TGs”} - \text{“TGs made from de novo synthesized FAs”};$$
and represents the percentage of hepatic TG synthesized by esterification of unlabeled FAs. This includes TG-FFA cycling and/or esterification of dietary FAs.

Table 4.6 summarizes the contributions of the TG sources above described to total hepatic TG content after one overnight feeding in the three groups of mice.

Table 4.6 - Relative percentages of different lipid contributions to total hepatic TG content after one overnight feeding in CTL, OLA and ARI mice. Results are expressed as mean \pm SEM. CTL: n=9, OLA: n=9, ARI: n=8. * = $p < 0.05$

	<i>CTL</i>	<i>OLA</i>	<i>ARI</i>
<i>Pre-existing TGs (%)</i>	35.18 \pm 3.63	45.79 \pm 2.18	42.97 \pm 3.15
<i>Newly synthesized TGs (%)</i>	64.82 \pm 3.63	54.21 \pm 2.18 *	57.03 \pm 3.15
<i>TGs made from de novo synthesized FAs- DNL- (%)</i>	12.05 \pm 2.40	14.42 \pm 1.37	13.02 \pm 1.08
<i>TGs made from non-synthesized FAs- TG-FFA cycling and dietary sources- (%)</i>	52.77 \pm 5.42	39.80 \pm 2.19 *	44.00 \pm 3.38

Taken together, these results do not suggest any major dysfunctionality concerning hepatic lipid metabolism in OLA and ARI mice. The lipid synthetic rates examined, as well as the hepatic lipid profiles, were similar among the three groups.

The relative reduction in glycerol synthetic activity in OLA animals, and thus of TG synthesis, was the only exception. A closer look at the different contributions of various sources to total hepatic TG content confirmed a significant reduction in the percentage of TG esterified overnight from non-synthesized FAs in OLA mice. Such diminished levels of TGs synthesized from unlabeled sources might correlate with statuses of dyslipidemia. However, at this stage we are unable to complement these results with serum measurements of FFAs or TGs.

Food intake differences and the increased adiposity exhibited by OLA and ARI animals let us postulate that both OLA and ARI mice had larger hepatic TG contents and therefore, the absolute rates of DNL and TG synthesis in OLA and ARI groups might be greater. As previously stated, we are unable to measure hepatic TG content and validate this hypothesis; our most relevant result remains therefore the lack of any major perturbation in hepatic lipid metabolic fluxes.

Lipid metabolism in adipose tissue

Since hepatic lipid metabolism appeared relatively intact, we next investigated the lipid profile and lipid synthetic activities in epididymal adipose tissue. As previously explained, both OLA and ARI mice exhibited bigger adipose stores, therefore a larger lipid inflow is expected in the adipose tissue of these two groups of animals.

Lipidomic analysis

As for hepatic lipidomic profile, ¹H-NMR analysis was employed for the resolution of epididymal adipose tissue lipid species.

Table 4.7 - Percentages and absolute values (mg) of different lipid species in epididymal adipose tissue of CTL mice and mice that underwent a 7-month treatment with either OLA or ARI. Results are expressed as mean \pm SEM. CTL: n=9, OLA: n=9, ARI: n=8. * = $p < 0.05$, ** = $p < 0.01$; *** = $p < 0.01$; **** = $p < 0.001$. ω -3 FA: omega-3 fatty acids; non- ω -3 FA: non-omega-3 fatty acids; SFA: saturated fatty acids; MUFA: monounsaturated fatty acids; PUFA: polyunsaturated fatty acids, DHA: docosahexaenoic acid.

	(%)			(mg)		
	CTL	OLA	ARI	CTL	OLA	ARI
ω-3 FA (%)	1.11 \pm 0.11	0.99 \pm 0.07	0.94 \pm 0.04	0.49 \pm 0.05	0.91 \pm 0.19	1.01 \pm 0.15 *
Non-ω-3 FA (%)	98.89 \pm 0.11	99.01 \pm 0.07	99.06 \pm 0.04	45.51 \pm 4.91	86.42 \pm 15.15	105.49 \pm 12.64 *
SFA (%)	32.65 \pm 1.62	32.90 \pm 2.97	28.50 \pm 1.58	15.02 \pm 1.61	28.05 \pm 5.24	29.58 \pm 2.87 **
MUFA (%)	48.93 \pm 1.03	52.03 \pm 1.40	56.60 \pm 1.51****	22.63 \pm 2.36	45.90 \pm 8.47	60.97 \pm 8.14 **
PUFA						
Linoleic acid (%)	18.24 \pm 0.82	14.67 \pm 1.71	14.64 \pm 0.92	8.29 \pm 0.73	12.99 \pm 2.84	15.66 \pm 2.39
DHA (%)	0.24 \pm 0.03	0.39 \pm 0.07	0.25 \pm 0.03	0.12 \pm 0.04	0.38 \pm 0.03	0.27 \pm 0.39

Since OLA and ARI animals had significantly bigger adipose stores, almost all lipid species were present in larger amounts in the adipose tissue of OLA and ARI mice.

The relative amount of MUFA species was significantly higher in ARI animals whereas, although

to a not significant extent, concentrations of linoleic acid, were relatively diluted. Adipose tissue lipid profiles of OLA and ARI animals matched the corresponding lipid profiles of liver, where the observed changes likely reflect a status of increased adiposity that drives the accumulation within the cell of lipid species that are more suitable for storage, rather than fatty acid species such as linoleic acid which are for a significant amount employed for the synthesis of structural lipids.

Contribution of newly synthesized TGs to total adipose TG mass

Similar to hepatic lipid fluxes, ²H-enrichments of TGs obtained from adipose tissue can be used to quantify lipid synthetic fluxes such as DNL and glycerol synthetic rate, which in turn can be used to assess the contribution of different sources to total adipose TG content per overnight, calculated as explained in the previous paragraph (page 153).

Since under overnight feeding conditions the adipose tissue TG pool of mice can be considered as not having significant net loss of fatty acids, each contribution was normalized per total weight of epididymal adipose tissue in order to assess the absolute amount of lipid inflow from different sources into adipose tissue. Table 4.8 reports the absolute values of different contributions to total adipose TG mass per overnight.

Study 2

Table 4.8 – Different lipid contributions (per overnight) to total adipose TG mass in CTL, OLA and ARI mice, calculated as following:

Newly synthesized TGs = TGs made from *de novo* synthesized FAs + TGs made from non-synthesized FAs; where:

“Newly synthesized TGs” equals the amount of newly synthesized glycerol, and “TGs made from *de novo* synthesized FAs” equals the amount of TGs synthesized via DNL. Results are expressed as mean ± SEM. CTL: n=9, OLA: n=9, ARI: n=8. * = p < 0.05, ** = p < 0.01.

	<i>CTL</i>	<i>OLA</i>	<i>ARI</i>
<i>TG mass (mg)</i>	460.00 ± 40.00	870.00 ± 150.00 *	1070.00 ± 130.00 **
<i>Newly synthesized TGs (mg) per overnight</i>	8.95 ± 1.58	11.50 ± 2.60	9.27 ± 3.60
<i>TGs made from de novo synthesized FAs (mg) per overnight -DNL</i>	3.04 ± 0.71	2.79 ± 0.75	1.77 ± 0.34
<i>TGs made from non-synthesized FAs (mg) per overnight - TG-FFA cycling and dietary sources</i>	5.89 ± 1.43	8.71 ± 2.10	7.50 ± 3.69

No significant differences were reported between the overall amounts of newly synthesized TGs, as well as the amounts of TGs esterified from *de novo* synthesized FAs during nocturnal feeding. On average, the amounts of TGs esterified overnight from non-synthesized FAs originating from dietary source or from futile TG-FFA cycling within the adipocyte, were greater in the adipose tissues of OLA and ARI mice, possibly reflecting increased lipid inflow deriving from dietary sources; however, none of the differences reached statistical significance. We therefore concluded that, despite increased fat stores, no significantly increased lipogenic activity was detected in the adipose tissue of OLA and ARI mice.

Discussion

Among the advantages that come with the use of $^2\text{H}_2\text{O}$ as metabolic tracer, one of the most important is that, unlike substrate-specific tracers, deuterium is easily incorporated into several biological substrates and therefore allows the simultaneous quantification of multiple metabolic fluxes. In this study, we administered $^2\text{H}_2\text{O}$ as isotopic tracer to calculate flux through several metabolic pathways in mice under chronic SGAs treatment.

Although considered a first-line medications for many mental diseases, SGAs induce significant metabolic side effects, whose etiology is currently unknown. Unraveling the mechanisms behind such side effects has been proven particularly challenging because of the complexity of the many factors involved, which include the multisystemic effect that SGAs exert on various organs and the potential role that mental diseases have on the development of metabolic abnormalities. However, studies on healthy volunteers have clarified that SGAs induce certain metabolic disturbances acutely and independently of any underlying disease and before any increase in body weight. Moreover, specific SGAs are known to induce more detrimental metabolic consequences compared to others.

Glucose intolerance, dyslipidemia and postprandial hyperinsulinemia are among the early symptoms that manifest after short administration of certain SGAs which eventually progress into more chronic metabolically altered states, such as obesity and T2DM. Among the various hypotheses, several point at the liver as being the prime responsible organ in the generation and progression of such side effects, and hepatic insulin resistance is hypothesized to occur very early on and to persist along the whole process.

Hepatic insulin resistance has specific manifestations. The insulin-resistant liver is incapable of suppressing endogenous glucose production and induce glycogen synthesis efficiently. However, the insulin-resistant liver does not lose its ability of synthesizing lipids *de novo*, on the other hand, this process appears upregulated in advanced metabolically altered states.

Study 2

After seven months of treatment, mice treated with SGAs showed an increase in visceral adiposity, although the three groups of mice exhibited no significant differences in body weight. By the 5th month of treatment, food intake was significantly higher in both OLA and ARI animals, and ARI mice manifested glucose intolerance and insulin resistance, as proved by a GTT and an ITT respectively. OLA mice did not produce statistically different results but exhibited a non-significant tendency towards the same pattern as ARI mice. However, as confirmed by a PTT, all animals responded well to a pyruvate challenge, hinting towards functional hepatic metabolism. We next focused on hepatic glycogen and lipid metabolism. The use of ²H₂O as metabolic tracer allowed the quantification of both glycogen and lipid metabolic fluxes in this specific setting. Overall, our results showed us intact glucose and lipid metabolic fluxes in the liver of mice treated with SGAs. The small alterations detected in hepatic glucose and lipid metabolism are congruent with a modest state of overnutrition rather than a state of hepatic insulin resistance, consequence of the increased food intake observed in both OLA and ARI groups. Glycogen content in animals treated with SGAs was not diminished, but rather had a tendency to be increased via elevated direct pathway activity. For what concerns lipid metabolism, the fractional synthetic rate of each lipid flux analyzed was approximately equal among the three groups. However, we speculate that intrahepatic TG content, and therefore the absolute values of each of these fluxes, might have been greater in OLA and ARI animals, considering the greater adiposity and increased food intake recorded in these mice.

Although it is reasonable to assume that states of overnutrition correlate with increased intrahepatic TG content, we were surprised to discover that the only significant anomaly concerning hepatic lipid metabolism in these mice was the relatively lower glycerol synthetic rate (and thus, TG synthetic rate), in the livers of OLA animals. It has been consistently reported in the literature that olanzapine treatment in humans lowers circulating FFAs acutely and chronically [201], [202]. This finding was counterintuitive as obesity and insulin-resistant states are normally associated with elevated FFA levels. Following studies in rodents have elucidated how this phenomenon is

specifically linked to olanzapine mode of action, which appears to increase FA uptake and disposal into most peripheral tissues. In adipose tissue in particular, olanzapine promotes adiposity by increasing FA uptake and impairing lipolysis [203], [204]. This is in line with our findings: less hepatic synthesis of glycerol without a concomitant decrease in DNL, is indicative of less esterification of FAs deriving from unlabeled sources, a condition perhaps supported by such olanzapine-mediated lipid-lowering effects. Thus, by enhancing lipid clearance by peripheral tissues and reducing FFA release from adipose stores; olanzapine causes relatively fewer lipids to remain in circulation during both fed and fasted state, consequently impacting hepatic esterification rates.

Considering the significantly bigger adipose stores of OLA and ARI mice, we were expecting to detect significantly higher TG synthesis in their adipose depots. However, although on average both OLA and ARI mice esterified overnight higher amounts of unlabeled FAs likely due to larger dietary intakes, none of the differences reached statistical significance. Moreover, adipose DNL levels were comparable among the three groups.

In view of the well-documented effects that olanzapine exerts on adipose lipolysis [204], we speculate that the expansion of adipose stores observed in OLA mice might have been indeed a consequence not only of increased nutrient inflow, but also of a defect in adipose tissue lipid output, which was not assessed in our study and that possibly plays a fundamental role in the progression of SGAs side effects (Figure 4.3). While the olanzapine-mediated effects on adipose lipolysis are established, to our knowledge aripiprazole has never been associated with defects in lipolytic activity. However, ARI mice exhibited higher levels of adiposity which are difficult to explain in this context. Two possible elements, that do not necessarily exclude each other, might have contributed to this.

First, impaired adipose tissue dynamism possibly played a role in increasing the adiposity of ARI mice too, which in our set-up have been exposed to aripiprazole for an unprecedented period of

time. Additional studies on adipose tissue lipid inflows and outflows in ARI mice may reveal a more sluggish performance of adipose tissue in whole-body lipid homeostasis.

Second, an important factor that might help to explain the reduced adipose expansion of OLA mice compared to their ARI counterparts, resides in the well-known capacity of olanzapine to dramatically and inappropriately favors lipids over glucose as peripheral fuel in mice, something that does not seem to be associated with aripiprazole [203]. This implies that lipids in most peripheral tissues are not only more abundantly uptaken from circulation, but also disposed at a higher rate in OLA mice. This incapability of switching to glucose from lipids as substrate of utilization perhaps explains why acute hyperglycemia arises even after a single dose of olanzapine in drug-naïve rodents [205], whereas acute administrations of aripiprazole do not seem to induce the same effect. Such olanzapine-specific dysregulations have detrimental consequences, especially because olanzapine, as above explained, does not seem to induce an adequate mobilization of lipid stores in response to higher lipid demands. However, as a result of increased food intake, ARI mice might on the long term have developed a more dyslipidemic phenotype compared to OLA mice, which are to some extent able to dispose of more lipids and thus display better metabolic profiles. This theory is concordant with the observation that, in our study, aripiprazole showed overall more adverse effects after 7 months of treatment in mice.

Further rationalizations on the more severe adverse effects induced by aripiprazole are particularly difficult as this is, to our knowledge, the only animal study conducted with aripiprazole that encompasses a period of seven months, thus it seems logical to speculate that relevant metabolic changes, which were barely detectable in previous studies in mice, would only be manifested after prolonged treatment.

However, justifying the relatively minor adverse effects that olanzapine elicits in mice, effects that in humans far exceeds the ones induced by aripiprazole, is a more complex matter and requires a level of understanding that we are currently lacking. Species-specific pharmacokinetic properties, as well as different metabolic characteristics between humans and rodents, might be the underlying

reasons why, despite very long administration lengths, olanzapine fails to promptly induce advanced metabolically altered phenotypes in rodents, whereas morbid metabolic conditions are achieved even after few weeks of treatment in humans.

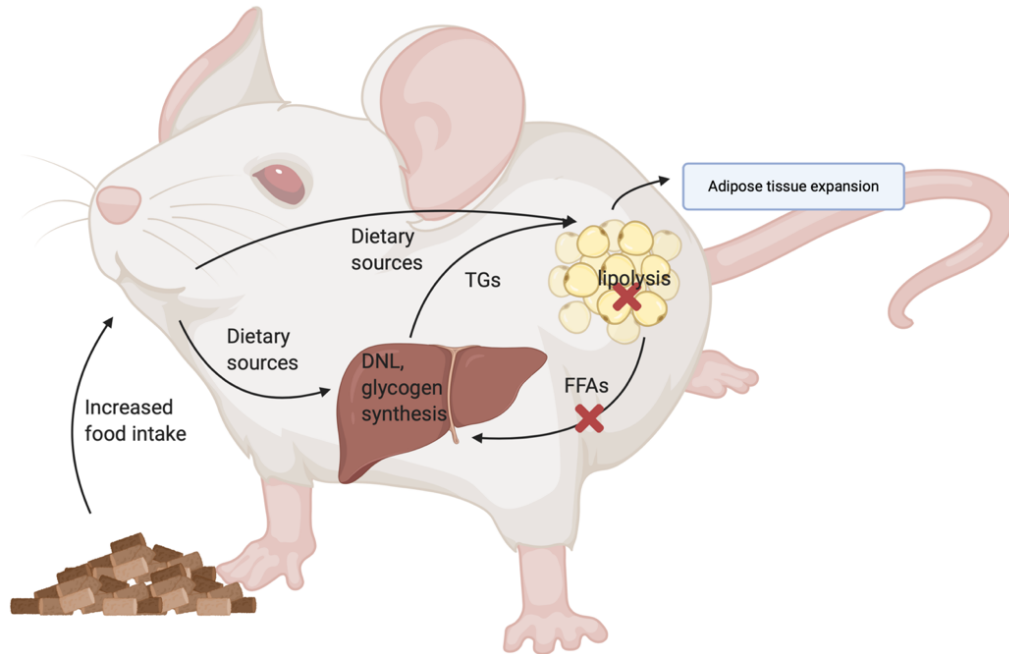


Figure 4.3 - Proposed model of adipose tissue expansion in mice treated with olanzapine. Increased food intake determines a bigger inflow of nutrients which feeds hepatic anabolic pathways such as glycogenesis and *de novo* synthesis of lipids. In the meantime, lipids of all sources reach the adipose tissue. However, the adipose tissue is incapable of guaranteeing a physiological lipid output most likely due to impaired lipolysis, hence the observed expansion of adipose stores. Of note, ARI mice might too, for some parts, adhere to this model. However further investigation is needed in order to confirm whether OLA and ARI mice have effectively suffered impairments in adipose tissue mobilization. Lipid trafficking between organs other than liver and adipose tissues have been omitted for clarity. [Figure created with BioRender.com].

Of note, if in our set-up overnutrition *per se* is the only element behind the more pronounced metabolic dysregulations observed in ARI mice, which include disrupted glucose homeostasis, it seems legit to question why we did not observe any noticeable sign of dysfunction in the liver of OLA and especially ARI mice. Overnutrition should cause a generalized state of insulin resistance that should have in rodents consequences on the liver. However, the livers of both OLA and ARI mice did not present any abnormal activity, on the other hand, glycogen deposition and hepatic lipid synthesis were fully functional.

A reasonable explanation for this is that in a generalized state of mild insulin resistance such as the one exhibited by OLA and ARI mice, impairment of hepatic glycogen deposition which, besides insulin, is also strongly regulated by high concentrations of circulating glucose, might manifest after other major events, such as impairments of glucose uptake by skeletal muscle, a process strictly governed by insulin. A similar logic also applies to DNL, whose dysregulations are evident only in advanced metabolic states. Further progression of metabolic symptoms is expected to have an impact also on liver anabolic functions. In addition to this, disrupted glucose homeostasis in OLA and ARI mice might not necessarily be only a consequence of overnutrition. The possibility that SGAs compromise, acutely or after chronic exposure, the metabolism of peripheral organs other than liver and adipose tissue, needs to be considered. As for adipose tissue, SGAs might have a specific effect on a determined aspect of an organ, an aspect that could already be in part compromised by the slightly more advanced metabolic dysfunctions of ARI mice, thus resulting in a more evident manifestation.

To sum up, we were able to propose a reasonable model for the greater adiposity observed in OLA and ARI mice; but at the moment we cannot provide one other than overnutrition that could entirely justify the observed impairments of glucose homeostasis. Hence, additional investigation aimed at elucidating these effects, is needed.

Conclusions

Although mice treated with olanzapine and aripiprazole presented a series of metabolic abnormalities, such as increase in adiposity without major concomitant increase in body weight and disrupted glucose homeostasis, we exclude hepatic insulin resistance, intended as impairment of hepatic anabolic functions, among the putative causes implicated in this phenomenon. Hepatic glycogen and lipid synthetic fluxes were not altered after chronic treatment with SGAs in mice, whereas the absolute hepatic content of these macromolecules is believed to be slightly higher. This

scenario is consistent with the increased food intake recorded during the treatment of OLA and ARI animals. Higher levels of ingested food translate into higher levels of circulating nutrients; therefore the liver, which extracts excessive circulating glucose, synthesized more glycogen, hence the modest increase in direct pathway activity in the groups treated with SGAs. At the same time, an increased amount of lipids originating from dietary sources and endogenous production, accumulates in the liver, without altering the fractional rates of lipid fluxes.

To conclude, the metabolic disturbances observed in mice treated with SGAs are most likely the result of the combined action of central and peripheral mechanisms which promote disrupted glucose homeostasis together with increased food intake and expansion of adipose stores, as observed in our study. However, liver anabolic fluxes are not involved in the primary mechanisms that elicit this response. Future studies on this matter should address other potential mechanisms and examine the role of other peripheral organs such as adipose tissue, muscle and pancreatic cells. A final important consideration concerns the animal model chose in this study. After seven months of treatment in mice, SGAs induced a series of mild metabolic dysregulations that cannot be classified as advanced and that encouraged us to investigate the role of hepatic metabolism as one of the early triggers in this process. However, SGAs-induced metabolic effects are more severe and have a much faster evolution in humans than in rodents. This needs to be taken into account during the conceptualization of future studies, especially in those that aim to investigate SGAs long-term effects, as the cost-benefits of very long animal treatments might be not worthy and overall counterproductive in terms of experimental meaningfulness.

STUDY 3

***Hepatic Metabolic Fluxes in an Animal
Model of Insulin Hypersensitivity: Protein-
Tyrosine Phosphatase 1B (PTP-1B)-
Deficient Mice***

Introduction

PTP-1B is a ubiquitously expressed tyrosine phosphatase that has gained prominent interest as a potential drug target in the treatment of diabetes. Mice with whole-body deletion of PTP-1B are lean and protected from weight gain and insulin resistance induced by high-fat diet. Moreover, PTP-1B null (PTP-1B^{-/-}) mice are born with the expected mendelian ratio 1:2:1, are healthy, grow well and are fertile, ruling out any possible toxic effect caused by PTP-1B inhibition [206], [207]. The beneficial effects resulting from PTP-1B deletion are a consequence of PTP-1B being involved in two major pathways regulating energy homeostasis: the insulin signaling pathway and the leptin signaling pathway. PTP-1B is a negative regulator of both pathways that, by dephosphorylating crucial effectors, effectively terminates the downstream signaling events. Lack of PTP-1B results in sustained insulin and leptin signaling and, as a consequence, PTP-1B^{-/-} animals are hypersensitive to both of these hormones. PTP-1B^{-/-} mice have been extensively characterized in the context of high-fat feeding and present two prominent metabolic features. First of all, when challenged with a high-fat diet, PTP-1B^{-/-} mice present increased glucose tolerance, less circulating insulin and a better lipid profile compared to their wild type counterparts. In other terms, overall insulin sensitivity is increased, and this is most likely a direct consequence of improved peripheral insulin signaling. Secondly, PTP-1B^{-/-} mice present increased energy expenditure accompanied by decreased energy intake (reduced food intake) upon high-fat feeding and exhibit diminished body weight and adiposity when compared to wild-type PTP-1B mice. This anti-obesogenic effect can be attributed to certain central mechanisms, which most likely include improved leptin signaling. These assumptions were further confirmed by tissue-specific PTP-1B knockout animal models, that showed how only brain-specific knockouts recapitulate the phenotype observed in total body knockout animals [208]. Deletion of PTP-1B in peripheral tissues such as liver and muscle does not confer weight gain protection upon high-fat feeding. Liver- and muscle-specific PTP-1B knockouts do present however, improved insulin sensitivity in the corresponding tissues [209],

[210], [211].

By administering $^2\text{H}_2\text{O}$ to PTP-1B^{-/-} mice, we examined the effects of total body PTP-1B ablation on hepatic glycogen and lipid fluxes. The reasons behind this approach are multiple. First of all, we would like to further characterize this animal model, as to date, nobody has measured hepatic fluxes in a PTP-1B^{-/-} model using a stable isotope tracer. Secondly, we can unravel new information on the role of PTP-1B. Several lines of evidence suggest that PTP-1B controls the progression of some common liver conditions, like NAFLD, acute liver injury and hepatocellular carcinoma, modulating important cellular mechanisms such as hepatocyte death, hepatic DNL, insulin resistance and ER stress response [212], thus additional characterization of the role of this phosphatase in the context of hepatic metabolism is useful also to better predict the pace of certain liver diseases. Moreover, inhibitors of PTP-1B are currently being developed for a series of metabolic conditions, including NAFLD, and the measurement of hepatic metabolic fluxes can provide a better understanding of the consequences of inhibiting PTP-1B activity from a liver-centered perspective.

The animals used in this study were not fed a high-fat diet nor induced insulin resistance states and are therefore metabolically healthy. As the primary objective of this study was to gain insight into the role of PTP-1B, we preferred a metabolically neutral background in order to avoid confounders and facilitate the interpretation of the data.

Animals and experimental set-up

Nine PTP-1B wild type mice (CTL) and seven PTP-1B knockout mice (PTP-1B^{-/-}) were used in this study. Of note, the mice hereby described as CTL are the same animals referred to as CTL in Study 2. These animals were of the same genetic background as PTP-1B^{-/-} mice, were born and sacrificed at the same time, and lived in the same environment as PTP-1B deficient mice. We therefore found acceptable and convenient to utilize the same control group for both studies.

Intervention

As the objective of this study was to investigate possible alterations in hepatic metabolic fluxes as a consequence of a specific genetic background, mice were simply maintained in the animal facility until they reached eleven months of age. Metabolic parameters were observed and recorded over a period of seven months. For the whole observational time, mice were provided with free access to water and standard chow diet.

Tracer administration:

All animals received ²H₂O at the beginning of the final evening as an intraperitoneal loading dose of 99% ²H₂O containing 0.9 mg/mL NaCl (4 mL/100 g body weight). The drinking water was enriched to 5% with ²H₂O.

Sacrifice

At the end of the dark cycle, all animals were sacrificed by decapitation. Plasma was isolated and stored at -80° C and livers were freeze-clamped and stored at -80° C until further analysis.

Results

In vivo analysis

As in the previous chapter, a series of *in vivo* metabolic tests and measurements were conducted on the animals under study at the animal facilities of the Instituto de Investigaciones Biomédicas Alberto Sols (CSIC-UAM, Madrid). As in the previous chapter, all *in vivo* data illustrated in this section were not generated by the author of this thesis and are hereby briefly described with the only purpose of offering a comprehensive description of the animal model under study.

Food intake and body composition

Body weight was monitored over a period of seven months and no difference in weight variance was reported between the two groups (data not shown). On the last night, CTL and PTP-1B^{-/-} animals had on average comparable body weights (Table 5.1). Food intake was recorded and both groups consumed equivalent amounts of food over the observational time (data not shown).

Liver and visceral depots were weighted upon collection and no differences were observed in neither liver nor epididymal fat depots weight (Table 3.1).

These data do not contradict our expectations, PTP-1B^{-/-} animals are not necessarily expected to be leaner than CTL unless challenged with a high-fat diet. Certain studies on PTP-1B^{-/-} mice reported leaner phenotypes compared to wild-type mice, even when PTP-1B^{-/-} mice were fed a standard chow diet. This most likely reflects a different nutrient composition of the standard chow diet administered to the animals, which probably contained a higher relative amount of fat [207]. This was not the case for us and PTP1B^{-/-} mice grew normally overtime and to levels comparable to those of CTLs.

Epididymal fat depots weighted on average more in PTP-1B^{-/-} animals compared to CTL. This is not in line with previous observations. However, this difference is not statistically significant, and a big variability in our measurements has been reported between mice. We can overall conclude

that no difference in body weight, body composition and food intake has been observed in PTP-1B^{-/-} mice compared to CTL mice monitored over a period of 7 months.

Table 5.1 - Body, liver and visceral depots weights in wild-type and PTP-1B deficient animals of 11 months of age. Data are expressed as mean ± SEM. CTL: n=9, PTP-1B^{-/-}: n=7.

	CTL	PTP-1B ^{-/-}
Body weight (g)	34.37 ± 1.33	34.50 ± 2.48
Liver weight (g)	1.42 ± 0.06	1.57 ± 0.13
Epididymal fat weight (g)	0.46 ± 0.04	0.71 ± 0.18

Glucose tolerance and insulin sensitivity

Fed glucose concentrations were significantly lower in PTP-1B^{-/-} mice whereas fast glucose levels were not different between the two groups (data not shown).

A GTT was carried out to assess glucose tolerance and PTP-1B^{-/-} mice exhibited an overall tendency towards improved glucose tolerance compared to CTL animals, although none of the differences observed had statistical meaning.

We did not assess circulating insulin levels in the animals under study, but previous characterizations of this animal model consistently reported less postprandial circulating levels of insulin. This information, together with the lower postprandial serum glucose concentrations, let us assume that PTP-1B^{-/-} mice were more insulin sensitive. An ITT was also performed and PTP-1B^{-/-} mice better responded to the insulin bolus and remained hypoglycemic for a longer period of time (data not shown).

GTT and ITT showed tendencies, however, none of the obtained measurements was statistically relevant. This is due to the fact that all the animals used in this study were metabolically healthy and thus barely showed any difference when challenged in tests normally used to detect metabolic

alterations. In conclusion, our observations do not contradict previous reports in which PTP-1B^{-/-} mice are generally described as insulin hypersensitive.

Hepatic glycogen metabolism

Body water, hepatic glycogen enrichment from ²H₂O, and fractional contributions of direct and indirect pathways to hepatic glycogenesis

Hepatic glycogen was extracted from each liver, digested to glucose, and then derivatized to MAG (Materials and Methods, page 107). Body water (BW) ²H-enrichments and hepatic glycogen positional ²H-enrichments were determined from plasma and MAG respectively by ²H-NMR analysis. Fractional contributions of different sources to hepatic glycogen synthesis were estimated by mathematical equations as previously explained (page 91, Table 2.1.).

Body water and glycogen positional ²H-enrichments are summarized in Table 5.2, whereas the fraction of newly synthesized glycogen and the fractional contributions of direct and indirect pathways to hepatic glycogenesis are reported in Table 5.3.

Table 5.2 - BW and liver glycogen positional ²H-enrichments (H1-H6) in wild-type and PTP-1B deficient mice. Enrichment of glycogen position 2 was adjusted by multiplication to a correction factor of 1.57 (H2_{corr}) to correct for incomplete exchange of body water and position 2 hydrogens [170]. Data are expressed as percentages (%) and shown as means (SEM). CTL: n=9, PTP-1B^{-/-}: n=7.

	BW	H1	H2	H2_{corr}	H3	H4	H5	H6R	H6S
<i>CTL</i>	4.35 (0.19)	1.49 (0.17)	2.72 (0.29)	4.27 (0.46)	1.02 (0.14)	1.44 (0.18)	1.52 (0.19)	1.12 (0.15)	1.18 (0.15)
<i>PTP-1B^{-/-}</i>	4.57 (0.05)	1.54 (0.26)	2.84 (0.43)	4.47 (0.68)	1.14 (0.22)	1.52 (0.27)	1.61 (0.28)	1.16 (0.22)	1.22 (0.23)

Table 5.3 - Fraction of newly synthesized glycogen expressed as $H2_{corr} / BW$ and fractional contributions of different glycolytic sources to overnight glycogen appearance in wild-type and PTP-1B deficient animals. Data are shown as means (SEM). CTL: n=9, PTP-1B^{-/-}: n=7.

	<i>H2_{corr} / BW</i>	<i>Direct and /or cycling (%)</i>	<i>Indirect Krebs cycle (%)</i>	<i>Indirect triose-P (%)</i>
CTL	0.99 (0.10)	65.06 (1.42)	27.18 (1.22)	7.76 (0.34)
PTP-1B^{-/-}	0.98 (0.15)	64.64 (3.03)	26.51 (2.61)	8.85 (0.79)

The ratio $H2_{corr} / BW$ is approximately equal to 1 in both groups indicating that all glycogen examined was synthesized or underwent cycling overnight, after ²H₂O administration.

Overall, PTP-1B^{-/-} mice do not manifest any alteration in the fractional contributions of different glycolytic sources to overnight glycogen appearance, whose percentages are comparable to those observed in PTP-1B wild-type animals.

Glycogen content and absolute contributions of glyco-genic sources to hepatic glycogenesis

Total hepatic glycogen content and absolute contributions of direct and indirect glyco-genic sources to glycogen deposition in CTL and PTP-1B^{-/-} mice are illustrated in Figure 5.1. Hepatic glycogen was quantified as described (Materials and Methods, page 108) and the values hereby reported were obtained by multiplication of hepatic glycogen concentrations to the respective fractional contribution.

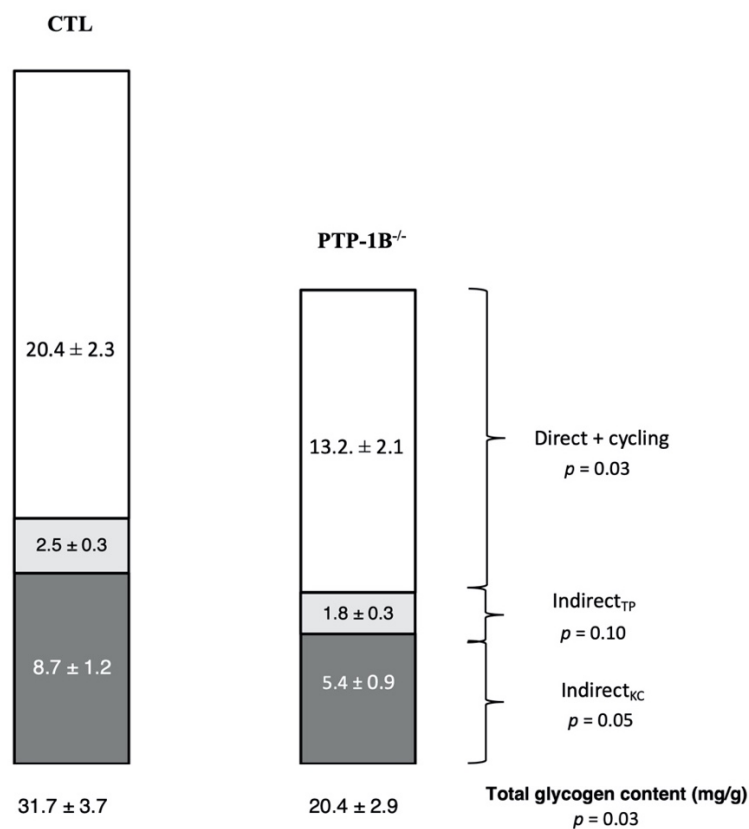


Figure 5.1 - Total glycogen content and absolute contributions of various glyco-genic sources to overnight glycogen appearance in PTP-1B wild-type and deficient mice. Results are expressed as mean ± SEM (mg/g). CTL: n=9, PTP-1B^{-/-}: n=7. Indirect_{TP}: indirect pathway via triose-P; Indirect_{KC}: indirect pathway via the Krebs cycle.

All glyco-genic sources proportionally contributed less to hepatic glycogen deposition in PTP-1B^{-/-} mice, which exhibited overall diminished glycogen content. Indirect pathway contributions present strong tendencies, but do not reach statistical significance, probably due to the relatively small sample size and high variability between subjects, however posterior experiments conducted

Study 3

on larger groups of animals confirmed with statistical relevance that glycogen deposition from all glycolytic sources is significantly reduced in PTP-1B^{-/-} mice compared to their wild-type counterparts (unpublished data). This is a counterintuitive scenario, considering that PTP-1B-deficient animals are a model of insulin hypersensitivity and hepatic glycogenesis sensibly responds to insulin regulation. Hepatic glycogen stores were therefore expected to be more abundant in PTP-1B^{-/-} mice, with the direct pathway playing a predominant role in this process. On the other hand, our data revealed reduced hepatic glycogen content. Because both direct and indirect pathways were responsible for the observed decrease in hepatic glycogen concentrations, we hypothesize that reduced glycogen content in PTP-1B^{-/-} mice is most likely not a consequence of defective glycogen synthesis but possibly results from scarce substrate availability or increased glycogenolytic rate.

Hepatic lipid metabolism

Lipidomic analysis

Hepatic TGs were extracted and purified from pulverized livers as described (Materials and Methods, pages 108). Table 5.4 illustrates the relative abundance of different hepatic lipid species obtained by ¹H-NMR analysis in CTL and PTP-1B^{-/-} mice. No significant differences have been detected in the lipidomic profile of PTP-1B^{-/-} mice compared to CTL animals.

Table 5.4 - Percentages of different lipid species in the livers of CTL and PTP-1B^{-/-} mice. Results are expressed as mean ± SEM. CTL: n=9, PTP-1B^{-/-}: n=6. **ω-3 FA**: omega-3 fatty acids; **non-ω-3 FA**: non-omega-3 fatty acids; **SFA**: saturated fatty acids; **MUFA**: monounsaturated fatty acids; **PUFA**: polyunsaturated fatty acids, **DHA**: docosahexaenoic acid.

	CTL	PTP-1B ^{-/-}
ω-3 FA (%)	1.36 ± 0.25	1.68 ± 0.29
Non-ω-3 FA (%)	98.64 ± 0.25	98.32 ± 0.29
SFA (%)	35.48 ± 1.61	33.34 ± 1.70
MUFA (%)	48.84 ± 1.12	49.81 ± 1.16
PUFA		
Linoleic acid (%)	14.65 ± 1.29	15.25 ± 1.45
DHA (%)	1.03 ± 0.19	1.14 ± 0.15

Fractional synthetic fluxes and contributions of different lipid sources to overall hepatic TG content

Fractional synthetic rates of *de novo* synthesized FAs (DNL rate), glycerol, elongated FAs and desaturated FAs were determined by NMR analysis of positional ^2H -enrichments of hepatic TG. PTP-1B^{-/-} mice present strong tendencies towards reduced values in all lipid synthetic fluxes analyzed; and glycerol synthetic rate, which reflects the rate of TG synthesis in the liver, is reduced by approximately 20% in PTP-1B^{-/-} mice (Figure 5.2).

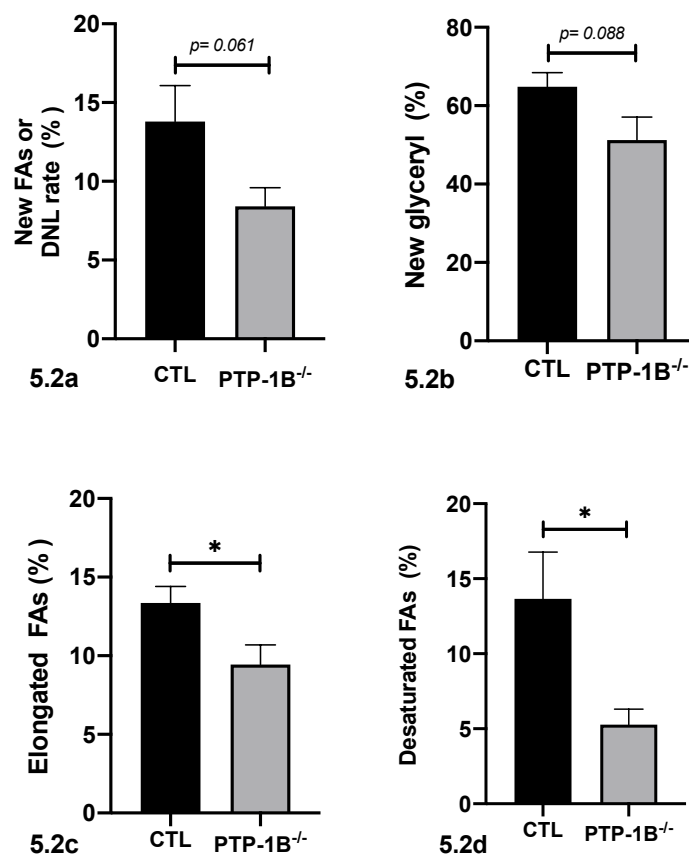


Figure 5.2 – Rates (% per overnight) of hepatic DNL (5.2a), glycerol synthesis (5.2b), elongation (5.2c) and desaturation (5.2d) in CTL and PTP-1B^{-/-} mice. Results are expressed as mean \pm SEM. CTL n=9, PTP-1B^{-/-} = 5-6.

Contributions of different sources to total hepatic TG content after one overnight feeding were calculated as explained in the previous chapter (page 153). These estimates confirmed that the reduction in new TG appearance observed in PTP-1B^{-/-} mice is primarily caused by diminished TG

synthesis via DNL. Esterification of unlabeled non-synthesized FAs is also on average decreased in PTP-1B^{-/-} mice, although not relevantly from a statistical point of view (Table 5.5).

Of note, some of the differences hereby reported do not reach the statistical relevant threshold of $p = 0.05$, but they do, however, present strong tendencies towards reduced values. As for the case of the glycogenic contributions described in the previous paragraph, we performed additional posterior experiments on hepatic lipid fluxes using larger sample sizes and confirmed our observation with statistical relevance (unpublished data).

Table 5.5 - Relative percentages of different lipid contributions to total hepatic TG content in CTL and PTP-1B^{-/-} mice after one overnight feeding, calculated as follows:

Total Hepatic TG content (100%) = Pre-existing TGs + Newly synthesized TGs = Pre-existing TGs + (TGs made from *de novo* synthesized FAs + TGs made from non-synthesized FAs);

where:

“Newly synthesized TGs” equals the rate of newly synthesized glycerol during nocturnal feeding, and “TGs made from *de novo* synthesized FAs” equals the percentage of TG synthesized overnight via DNL over total TG content. Results are expressed as mean \pm SEM. CTL n=9, PTP-1B^{-/-} n=5-6.

	<i>CTL</i>	<i>PTP-1B^{-/-}</i>	<i>p value</i>
<i>Pre-existing TGs (%)</i>	35.18 \pm 3.63	48.75 \pm 5.86	0.088
<i>Newly synthesized TGs (%)</i>	64.82 \pm 3.63	51.25 \pm 5.86	0.088
<i>TGs made from de novo synthesized FAs DNL- (%)</i>	12.05 \pm 2.40	7.22 \pm 1.00	0.063
<i>TGs made from non-synthesized FAs TG-FFA cycling and dietary sources- (%)</i>	52.77 \pm 5.42	43.70 \pm 5.14	0.252

Overall, lack of PTP-1B caused significant changes in hepatic lipid metabolism which culminated with reduced hepatic TG synthesis, mostly consequence of diminished rates of *de novo* lipid production. As in the previous chapter, we are unable to measure hepatic TG contents in the two groups of animals and convert the obtained relative measures into absolute values, however, our data firmly point towards a status of improved hepatic lipid metabolism in PTP-1B^{-/-} mice.

Discussion

As a negative regulator of insulin and leptin signaling, the phosphatase PTP-1B received a lot of attention as potential drug target in the treatment of several metabolic conditions. The majority of the animal studies conducted on this matter have focused on the role of PTP-1B and on the beneficial effects of inhibiting its activity especially in the context of metabolically morbid phenotypes, genetically provoked or induced by diet interventions. Not many studies have examined the role of PTP-1B in relation to healthy metabolism. Dissecting the primary role of a potential pharmacological target is always a good strategy that enables the rational design of more targeted pharmacological agents.

The liver plays a central role in the regulation of systemic metabolism, and alterations in hepatic glucose and lipid synthetic fluxes are a hallmark in the development and progression of many metabolic diseases. We hereby attempt to better clarify PTP-1B functions focusing on the consequences of overall PTP-1B deficiency on liver metabolism in a metabolically healthy mouse model. We specifically examined glycogen and lipid synthetic fluxes; major forms of energy store whose synthesis is for a significant extent governed by insulin.

As shown in the results section, PTP-1B^{-/-} mice exhibited reduced hepatic glycogen content. Replenishment of glycogen stores is one of the main events following food ingestion and insulin promotes this process especially via glucokinase upregulation and consequent increase in direct pathway activity. It was therefore initially surprising that a model of insulin hypersensitivity presented reduced hepatic glycogen stores. However, some considerations need to be addressed in order to better understand this animal model.

First of all, PTP-1B^{-/-} mice are total body knockout animals that lack PTP-1B^{-/-} in insulin-sensitive tissues other than the liver, among which, skeletal muscle. In skeletal muscle, insulin governs first and foremost glucose uptake by prompting the mobilization of the glucose transporter GLUT4 on the cell surface. Previous studies on total body and muscle-specific PTP-1B knockout models have

revealed increased glucose uptake in muscle cells [207], [210]. Considering that hepatic glucose uptake is controlled by insulin to a lesser extent than it is in skeletal muscle, it is reasonable to assume that skeletal muscle accounts for the disposal of more circulating glucose in PTP-1B^{-/-} mice, leaving a relatively less amount of glucose in circulation for the liver to uptake. However, the liver is the first organ to receive newly ingested nutrients through the portal vein and extracts the majority of its glucose demand before any other organ. Therefore, increased glucose uptake in skeletal muscle cells can only partially explain the reduced glycogen content in the liver and other mechanisms must be involved.

One of the most pronounced metabolic features of PTP-1B^{-/-} mice is their lower metabolic efficiency, meaning that, in these mice, a higher proportion of energy is dissipated as heat. This observation has been consistently reported in previous studies involving PTP-1B^{-/-} mice, and the mechanism behind it has not been properly elucidated, as no remarkable increase in brown adipose tissue nor UCP expression has been observed in PTP-1B^{-/-} mice and hypersensitivity to leptin seems to contribute only marginally to this phenomenon [207].

Not only the lower metabolic efficiency of PTP-1B^{-/-} mice possibly contributed to further diminish hepatic glucose inflow, but we also hypothesize that lower hepatic glycogen content might be the result of higher glycogen turnover, which is degraded faster in order to be released in circulation and be uptaken by other organs to satisfy increased energy demands. In this scenario, the process of glycogen synthesis in PTP-1B^{-/-} mice might be intact or potentiated even. Similarly, lower or unaltered glycogen content, despite enhanced glycogen synthesis, has been observed in skeletal muscle cells lacking PTP-1B [210], [213]. Our animals were sacrificed in a semi-fed condition, meaning that mice were fed *ad libitum*, and this might be the reason why improved glycogenesis is not appreciable in our set-up. However, if animals were challenged with a specific amount of food shortly prior sacrifice, we predict glycogen amounts to be similar, if not higher in PTP-1B^{-/-} mice. This theory is supported by the observation that, although glycogen concentrations are different among CTL and PTP-1B^{-/-} animals, fractional contributions of direct and indirect pathways are

equal in both groups, suggesting homogeneous glycogen breakdown in PTP-1B^{-/-} mice, rather than a defect in its synthesis.

As a general rule, a lipotoxic environment in the liver caused by lipid accumulation, is closely linked to metabolic disorders whose primary feature is insulin resistance. Insulin induces *de novo* synthesis of lipids from carbohydrate precursors and regulates this phenomenon with extreme sensitivity. Insulin-resistant conditions are normally characterized by impaired glucose handling accompanied by unaltered, if not potentiated, lipid *de novo* production. This paradox has been termed “selective insulin resistance” and has not yet found an appropriate resolution. As an animal model of hypersensitivity to insulin, PTP-1B^{-/-} mice were logically expected to exhibit higher rates of DNL in accordance with improved insulin signaling, an outcome that could partially blunt the beneficial effects of inhibiting PTP-1B in the context of many metabolic diseases. However, our results showed decreased rates of hepatic DNL, lipid elongation and desaturation, and reduced overall hepatic TG synthesis. This makes PTP-1B an ideal candidate for a therapeutic agent that aims to treat those metabolic diseases especially characterized by ectopic lipid accumulation, NAFLD being the primary example.

PTP-1B^{-/-} mice have been already described as a model of “selective” insulin hypersensitivity and the hypothesis that inhibiting PTP-1B^{-/-} could positively regulate glucose metabolism, without however worsening lipid metabolism, was already suggested [209]. By employing an isotope tracer methodology, our study drew the same conclusions, analyzing for the first time the actual lipid synthetic rates and confirming improved lipid metabolism in PTP-1B^{-/-} mice.

Improved lipid metabolism might be in part a consequence of increased leptin sensitivity. Leptin administration was previously shown to protect against hepatic steatosis downregulating hepatic DNL and increasing TG secretion mostly via central mechanism [214]. However, Delibegovic *et al.* observed overall improved lipid metabolism and reduced expression of genes involved in hepatic DNL even in a liver-specific PTP-1B knockout model and attributed this effect to an additional mechanism that most likely involves direct PTP-1B regulation over hepatic DNL [209]. The liver-

specific PTP-1B knockout animals used by Delibegovic *et al.* were fed a high-fat diet, and high-fat feeding leads to hepatic insulin and leptin resistance and elevated PTP-1B expression in the liver [212], [215]. In this particular set-up, control animals were metabolically dysfunctional and possibly presented unphysiological PTP-1B levels which might have been contributing to precipitate control mice metabolic phenotype. In our study however, where mice are total PTP-1B deficient and control animals do not present any metabolic alteration, it is reasonable to assume that the observed decrease in DNL synthetic flux is also to some extent due to improved leptin sensitivity.

Finally, reduced hepatic DNL might have in part resulted from decreased carbohydrate flux towards insulin-induced anabolic pathways in the liver. As previously explained, glycogen deposition has also possibly suffered a shortage of substrates, in light of the fact that increased overall insulin sensitivity enhances glucose clearance especially via skeletal muscle, and that increased energy expenditure possibly diminishes glucose inflow towards pathways such as DNL. However, although reduced substrate availability probably contributed to the observed phenotype, it was most likely not the only factor involved, and other mechanisms controlled by PTP-1B, such as improved leptin sensitivity, played a relevant role in this context.

An important final consideration: since our estimates of lipogenic synthetic fluxes are expressed as percentages, our interpretations are based on the important assumption that intrahepatic TG contents were approximately equal between the two groups of animals, an information that we currently do not possess. The available literature on this matter is scarce and conflictual, and at least in one previous study, lack of PTP-1B has been hypothesized to induce defects in hepatic lipid export in animals fed a high-fat diet [216]. Moreover, insulin negatively controls VLDL secretion in the liver, thus lack of PTP-1B could potentially have an impact on intrahepatic TG concentrations. Although this is a plausible scenario, we do not have any reason to believe that, in our experimental set-up, intrahepatic TGs concentrations in PTP-1B^{-/-} mice were sizable until the point of reversing our relative estimates. We nonetheless reserve to further investigate on this

matter and assess with more precision the actual extent of reduction of the examined lipogenic fluxes by integrating our analysis with intrahepatic TGs measurements.

Conclusions

Insulin is an anabolic hormone that promotes nutrient storage during “times of plenty” and in the liver, this mostly translates with the synthesis of glycogen and lipids *de novo*. From PTP-1B^{-/-} mice, a model of insulin hypersensitivity, we were expecting induction and potentiation of both of these metabolic processes. On the other hand, all insulin-regulated anabolic mechanisms appeared less prominent than expected. We were however able to rationalize our observations and helped the characterization of PTP-1B deficient mice, an animal model rarely studied in the absence of a morbid phenotype.

In mice, hepatic glucose and lipid fluxes are profoundly affected by PTP-1B deficiency. The dual role of PTP-1B in attenuating leptin and insulin signaling makes it an optimal pharmacological target for the treatment of several metabolic diseases, where the beneficial effects exerted on glucose metabolism resulting from enhanced peripheral insulin sensitivity, are complemented by improved lipid metabolism in the liver, in part consequence of potentiated leptin signaling.

GENERAL DISCUSSION

Insulin resistance is a common feature of many metabolic disorders and, in the interest of guiding the development of new much needed therapeutics tools, enormous effort has been made in order to understand the mechanistic events that provoke and sustain insulin resistance. Although new elements and connections added up to the whole picture over the course of several years of metabolic research, our understanding of the molecular basis of insulin resistance is not yet clearly defined.

As liver plays a central role in systemic glucose and lipid metabolism, hepatic insulin resistance in particular is believed to profoundly contribute to the pathogenesis of many metabolic diseases.

Stable isotope tracers are an important mean of investigation in metabolic research and their use has allowed the accurate monitoring of several metabolic pathways in physiological and pathological settings. Albeit often considered resource-intensive, stable isotope tracers studies have the potential to yield powerful insights on many metabolic questions.

In this work we have revisited some important topics frequently approached by metabolic investigators. By measuring hepatic lipid and/or glycogen fluxes in each of these particular settings, we were able to tackle these subjects from a different perspective and complement or take distance from previous research around the same matter.

Study 1 focused on hepatic glycogenesis in a mouse model in the context of chronic high-sugar feeding. By integrating $^2\text{H}_2\text{O}$ with ^{13}C -tracers of glucose and fructose, we resolved the fractional contributions of the fructose and the glucose components of the sugar provided to hepatic glycogenesis. We concluded that the fructose and glucose components of sugar contributed equally to glycogen synthesis and that chronic high-sugar feeding does not impact hepatic glycogenesis or direct pathway activity in mice.

Study 2 investigates hepatic glycogen and lipid fluxes in mice administered with second-generation antipsychotics, essential medications with deleterious metabolic side effect. Although this topic

has been and continues to be extensively investigated, the mechanistic events that cause such side effects are currently unknown. We were too not able to crack this enigma, however, by employing the use of $^2\text{H}_2\text{O}$ for the first time in this particular context, we were able to conclude that SGAs do not perturb hepatic glycogen and lipid fluxes in mice, an outcome in opposition to some of the previous research on this subject.

In Study 3, we contributed to the characterization of PTP-1B knockout mice, an animal model of insulin hypersensitivity. By administering $^2\text{H}_2\text{O}$ for the first time to this animal model, we demonstrated how the lack of PTP-1B has profound consequences on hepatic glycogen and lipid fluxes that, despite their counterintuitive nature, can be rationalized.

The fundamental element linking the three studies above described is the use of a stable isotope approach to analyze hepatic metabolic fluxes in a mouse model in three different contexts. In each one of these contexts the rates of hepatic glycogen and lipid fluxes were perturbed in different ways and, as these fluxes are to a significant extent regulated by insulin, the level of perturbation is, among other things, also a reflection of a specific insulin sensitivity status. However, insulin regulation and its pathological manifestations are systemic, and the ultimate metabolic phenotype of an organism is the result of the abnormal metabolic functioning of numerous organs, each contributing in specific ways to the overall metabolic phenotype and each controlling and affecting the metabolic well-functioning of other organs. As we focused our entire investigation on hepatic metabolic fluxes, we are aware that much more is left to do and that the metabolic assessment of other organs in these three situations is equally important and deserves as much attention as the liver; not only for the better characterization of the metabolic profile of the animals under study, but also to extract new knowledge, essential for a more comprehensive understanding of metabolism and its pathological manifestations. We therefore acknowledge the lack of a more complete metabolic profile of the animals utilized in our studies as both a limitation and a future continuation of this work.

General Discussion

Lastly, it is important to remember that our three studies present a major limitation, a limitation also shared by other studies many of which cited in this work: the use of an animal model to infer knowledge about human physiology and pathophysiology. Nonetheless, our observations are empirically valid and serve the purpose that we originally had in mind for this work: advancing our understanding of hepatic glucose and lipid metabolism by providing new perspective on some very discussed metabolic topics through the utilization of an alternative approach.

Bibliography

- [1] C.E. Geisler, C. Hepler, M.R. Higgins, B.J. Renquist. "Hepatic adaptations to maintain metabolic homeostasis in response to fasting and refeeding in mice". *Nutr Metab (Lond)*, vol. 13, p. 62, 2016.
- [2] G. Dohm, E.B. Tapscott, H.A. Barakat, G.J. Kasperek GJ. "Influence of fasting on glycogen depletion in rats during exercise". *J Appl Physiol Respir Environ Exerc Physiol*, vol. 55, no. 3, pp. 830-833, 1983.
- [3] A. Fréminet and L. Leclerc. "Effect of fasting on liver and muscle glycogen in rats and guinea pigs". *J Physiol (Paris)*, vol. 76, no. 8, pp. 877-880, 1980.
- [4] M. B. Freitas, C.B. Passos, R.B. Vasconcelos, E.C. Pinheiro. "Metabolic responses induced by fasting in the common vampire bat *Desmodus rotundus*". *J Comp Physiol B.*, vol. 173, no. 3, pp. 703-707, 2003.
- [5] L. H. Nilsson and E. Hultman. "Liver glycogen in man - the effect of total starvation or a carbohydrate-poor diet followed by carbohydrate refeeding". *Scand J Clin Lab Invest*, vol. 32, p. 325-330, 1973.
- [6] J.J. De Bruijne and P. De Koster. "De Bruijne JJ, de Koster P. Glycogenolysis in the fasting dog". *Comp Biochem Physiol B.*, vol. 75, no. 4, pp. 553-555, 1983.
- [7] F.O. Martins, J. Rito, I. Jarak, I. Viegas, M.A.Pardal, M.P. Macedo, J.G. Jones. "Disposition of [U-2H7]glucose into hepatic glycogen in rat and in seabass." *Comp Biochem Physiol A Mol Integr Physiol*, vol. 166, no. 2, pp. 316-322, 2013.

Bibliography

- [8] A. Oliveira, C.G. Candioto, D.M.S. Santos, J.G. Pereira, A.L. Sousa, C.R. Machado. "Effects of fasting and refeeding on the metabolic functions of the turtle *Kinosternon scorpioides* (Linnaeus, 1766) raised in captivity". *Pesquisa Veterinária Brasileira*, vol. 33, no. 8, pp. 1041-1044, 2013.
- [9] P. Randle, P.B. Garland, C.N. Hales, E.A. Newsholme. "The glucose fatty-acid cycle. Its role in insulin sensitivity and the metabolic disturbances of diabetes mellitus". *Lancet.*, vol. 1, no. 7285, pp. 785-789, 1963.
- [10] E. Ferrarini, O. Bjorkman, G.A. Jr Reichard, A. Pilo, M. Olsson, J. Wahren J, R.A. DeFronzo. "The disposal of an oral glucose load in healthy subjects. A quantitative study". *Diabetes*, vol. 34, pp. 580-588, 1985.
- [11] A. Olson and J. Pessin. "Structure, function, and regulation of the mammalian facilitative glucose transporter gene family". *Annu. Rev. Nutr*, vol. 16, pp. 235-256, 1996.
- [12] S. Aiston, K.Y. Trinh, A.J. Lange, C.B. Newgard, L. Agius. "Glucose-6-phosphatase overexpression lowers glucose 6-phosphate and inhibits glycogen synthesis and glycolysis in hepatocytes without affecting glucokinase translocation. Evidence against feedback inhibition of glucokinase". *JJ Biol Chem*, vol. 274, no. 35, pp. 24559-24566, 1999..
- [13] D. Nelson and M. Cox. *Lehninger Principles of Biochemistry*, 4th ed., New York: W.H. Freeman and Company, 2006.
- [14] S. Pilkis, M.R. el-Maghrabi, and T.H. Claus. "Hormonal regulation of hepatic gluconeogenesis and glycolysis". *Ann. Rev. Biochem.*, vol. 57, pp. 755-783, 1988.

- [15] L. Agius. "Glucokinase and molecular aspects of liver glycogen metabolism". *Biochem J.*, vol. 414 , no. 1, pp. 1-18, 2008.
- [16] J.D. McGarry, M. Kuwajima, C.B. Newgard, D.W. Foster, J. Katz. "From dietary glucose to liver glycogen: the full circle round". *Annu Rev Nutr*, vol. 7, pp. 51-73, 1987.
- [17] M. Bollen, S. Keppens, and W. Stalmans. "Specific features of glycogen metabolism in the liver". *Biochem J.*, vol. 336, no. 1, pp. 19-31, 1998.
- [18] R. L. Veech, "A humble hexose monophosphate pathway metabolite regulates short- and long-term control of lipogenesis". *Proc Natl Acad Sci U S A*, vol. 100, no. 10, pp. 5578-5580, 2003.
- [19] F. Rajas, A. Gautier-Stein, and G. Mithieux. "Glucose-6 Phosphate, a Central Hub for Liver Carbohydrate Metabolism". *Metabolites*, vol. 9, no. 12, p. 282, 2019.
- [20] C. Jang, S. Hui, W. Lu, A.J. Cowan , R.J. Morscher, G. Lee, W. Liu, G.J. Tesz, M.J. Birnbaum, J.D. Rabinowitz. "The Small Intestine Converts Dietary Fructose into Glucose and Organic Acids". *Cell Metab.* , vol. 27, no. 2, pp. 351-361, 2018.
- [21] M.R. Laughlin. " Normal roles for dietary fructose in carbohydrate metabolism". *Nutrients*, vol. 6, no. 8, pp. 3117-3129, 2014.
- [22] S.A. Hannou, D.E. Haslam, N.M. McKeown, M.A Herman. "Fructose metabolism and metabolic disease". *J Clin Invest*, 2018. 128(2): p. 545-5, vol. 128, no. 2, p. 545, 2018.
- [23] A. Asipu, B.E. Hayward, J. O'Reilly, D.T. Bonthron. "Properties of normal and mutant recombinant human ketohexokinases and implications for the pathogenesis of essential fructosuria". *Diabetes* , vol. 52, p. 2426–2432., 2003.

- [24] L. Tappy, K.A. Lê, C. Tran, N. Paquot. “Fructose and metabolic diseases: New findings, new questions”. *Nutrition*, vol. 26, pp. 1044-1049, 2010.
- [25] M. Alves-Bezerra and D. Cohen. “Triglyceride Metabolism in the Liver”. *Compr Physiol*, vol. 8, no. 1, pp. 1-8, 2017.
- [26] D. W. Foster. “Malonyl-CoA: the regulator of fatty acid synthesis and oxidation”. *J Clin Invest*, vol. 122, no. 6, pp. 1958-1959, 2012.
- [27] L. Reshef, Y. Olswang, H. Cassuto, B. Blum, C.M. Croniger, S.C. Kalhan, S.M. Tilghman, R.W. Hanson. “Glyceroneogenesis and the triglyceride/fatty acid cycle”. *J Biol Chem*, vol. 278, no. 33, pp. 30413-30416, 2003.
- [28] K.R. Feingold. “Introduction to Lipids and Lipoproteins”. Endotext, South Dartmouth (MA), 2018.
- [29] A. Jomard and E. Osto. “High Density Lipoproteins: Metabolism, Function, and Therapeutic Potential”. *Front Cardiovasc Med*, vol. 7, p. 39, 2020.
- [30] K.F. Petersen, D. Laurent, D.L. Rothman, G.W. Cline, G.I. Shulman. “Mechanism by which glucose and insulin inhibit net hepatic glycogenolysis in humans”. *J Clin Invest* 101: 1203–1209, vol. 101, pp. 1203-1209, 1998.
- [31] I. Lopez-soldado, R. Fuentes-Romero, J. Duran, J.J. Guinovart. “Effects of hepatic glycogen on food intake and glucose homeostasis are mediated by the vagus nerve in mice”. *Diabetologia*, vol. 60, p. 1076–1083, 2017.
- [32] A. Adina-Zada, T.N. Zeczycki, and P.V. Attwood. “Regulation of the structure and activity of pyruvate carboxylase by acetyl CoA”. *Archives of biochemistry and biophysics*, vol. 519, no. 2, pp. 118-130, 2012.

- [33] M. Dashty, "A quick look at biochemistry: Carbohydrate metabolism". *Clin Biochem*, vol. 46, no. 15, pp. 1339-1352, 2013.
- [34] C. Longuet, E.M. Sinclair, A. Maida, L.L. Baggio, M. Maziarz, M.J.. Charron, D.J. Drucker. "The glucagon receptor is required for the adaptive metabolic response to fasting". *Cell metabolism*, vol. 8, no. 5, pp. 359-371, 2008.
- [35] B. Grygiel-Górniak. "Peroxisome proliferator-activated receptors and their ligands: nutritional and clinical implications-a review". *Nutr J.* , vol. 13, p. 17, 2014.
- [36] F.W. Sanders and J.L. Griffin. "De novo lipogenesis in the liver in health and disease: more than just a shunting yard for glucose". *Biol Rev Camb Philos Soc*, vol. 91, no. 2, pp. 452-468, 2016.
- [37] P. Nguyen, "Liver lipid metabolism". *J Anim Physiol Anim Nutr*, vol. 92, no. 3, pp. 272-283, 2008 Jun;92(3):.
- [38] M. Brown and J. Goldstein, "The SREBP pathway: regulation of cholesterol metabolism by proteolysis of a membrane-bound transcription factor". *Cell*, vol. 2, no. 89, pp. 331-340, 1997.
- [39] M.M. Magaña, S.S. Lin, K.A. Dooley, T.F. Osborne. "Sterol regulation of acetyl coenzyme A carboxylase promoter requires two interdependent binding sites for sterol regulatory element binding proteins". *Journal of Lipid Research*, vol. 38, pp. 1630-1638, 1997.
- [40] M.M. Magaña and T.F. Osborne. "Two tandem binding sites for sterol regulatory element binding proteins are required for sterol regulation of fatty acid synthase promoter". *J. Biol. Chem.* 271: p. 32689-94., vol. 271, pp. 32689-32684, 1996.

Bibliography

- [41] L. Ma, N.G. Tsatsos, and H.C. Towle. “Direct role of ChREBP.Mlx in regulating hepatic glucose-responsive genes”. *J. Biol. Chem*, vol. 280, pp. 12019-12027, 2005.
- [42] S. Hubbard, L. Wei, L. Ellis, W.A. Hendrickson. “Crystal structure of the tyrosine kinase domain of the human insulin receptor”. *Nature*, 1994. 372: p. 746–54, vol. 372, pp. 746-754, 1994.
- [43] D.H. Bedinger and S.H. Adams, “Metabolic, anabolic, and mitogenic insulin responses: a tissue-specific perspective for insulin receptor activators”. *Mol Cell Endocrinol*, vol. 415, pp. 143-156, 2015.
- [44] M.C. Petersen and G.I. Shulman. “Mechanisms of Insulin Action and Insulin Resistance”. *Physiol Rev*, 2018. 98(4): p. 2133-2223., vol. 98, no. 4, pp. 2133-2223, 2018.
- [45] J.R. Gavin, J. Roth, D.M. Jr Neville, P. de Meyts, D.N. Buell. “Insulin-dependent regulation of insulin receptor cocentration: a direct demonstration in cell culture”. *Proc Natl Acad Sci USA*, vol. 71, pp. 84-88, 1974.
- [46] A. Salmeen, J.N. Andersen, M.P. Myers, N.K. Tonks, D. Barford. “Molecular basis for the dephosphorylation of the activation segment of the insulin receptor by protein tyrosine phosphatase 1B”. *Mol Cell*, vol. 6, pp. 1401-1412, 2000.
- [47] D.R. Lazar and A.R. Saltiel. “Lipid phosphatases as drug discovery targets for type 2 diabetes”. *Nat Rev Drug Discov*, vol. 5, pp. 333-342, 2006.
- [48] C.M. Taniguchi, B. Emanuelli, and C.R. Kahn. “Critical nodes in signalling pathways: insights into insulin action”. *Nat Rev Mol Cell Biol*, vol. 7, pp. 85-96, 2006.

Bibliography

- [49] L. Carabaza, C.J. Ciudad, S. Baqué, J.J. Guinovart. “Glucose has to be phosphorylated to activate glycogen synthase, but not to inactivate glycogen phosphorylase in hepatocytes”. *FEBS Lett*, vol. 296, pp. 211-214, 1992.
- [50] L. Härndahl, D. Schmoll, A.W. Herling, L. Agius. “The role of glucose 6-phosphate in mediating the effects of glucokinase overexpression on hepatic glucose metabolism”. *FEBS J.*, vol. 273, pp. 336-346, 2006.
- [51] P. Cohen. “Identification of a protein kinase cascade of major importance in insulin signal transduction”. *Phil Trans R Soc B.*, vol. 354, pp. 485-495, 1999.
- [52] J. Berg, J. Tymoczko and L. Stryer, “Glycogen Breakdown and Synthesis Are Reciprocally Regulated”. *Biochemistry, 5th edition*, New York, W H Freeman, 2002, p. Section 21.5.
- [53] X.C. Dong, K.D. Copps, S. Guo, Y. Li, R. Kollipara, R.A. DePinho, M.F. White. “Inactivation of hepatic Foxo1 by insulin signaling is required for adaptive nutrient homeostasis and endocrine growth regulation”. *Cell Metab*, vol. 8, pp. 65-67, 2008.
- [54] S.-H. Koo, L. Flechner, L. Qi, X. Zhang, R.A. Screaton, S. Jeffries, S. Hedrick, W. Xu, F. Boussouar, P. Brindle, H. Takemori, M. Montminy. “The CREB coactivator TORC2 is a key regulator of fasting glucose metabolism”. *Nature*, vol. 437, pp. 1109-1111, 2005.
- [55] Y. Liu, R. Dentin, D. Chen, S. Hedrick, K. Ravnskjaer, S. Schenk, J. Milne, D.J. Meyers, P. Cole, J 3rd Yates, J. Olefsky, L. Guarente, M.A. Montminy. “A fasting inducible switch modulates gluconeogenesis via activator/coactivator exchange”. *Nature*, vol. 456, pp. 269-273, 2008.

Bibliography

- [56] M.C. Petersen, D.F. Vatner, and G.I. Shulman. "Regulation of hepatic glucose metabolism in health and disease". *Nat Rev Endocrinol*, vol. 13, no. 10, pp. 572-587, 2017.
- [57] C. Gregori, I. Guillet-Deniau, J. Girard, J.F. Decaux, A.L. Pichard. "Insulin regulation of glucokinase gene expression: evidence against a role for sterol regulatory element binding protein 1 in primary hepatocytes". *FEBS Lett*, vol. 580, p. 410-414, 2006.
- [58] R.M. Denton and R.W. Brownsey. "The role of phosphorylation in the regulation of fatty acid synthesis by insulin and other hormones". *Philos Trans R Soc Lond B Biol Sci*, vol. 302, p. 33-45, 1983.
- [59] L. Janah, S. Kjeldsen, K.D. Galsgaard, M. Winther-Sørensen, E. Stojanovska, J. Pedersen, F.K. Knop, J.J. Holst, N.J. Wewer Albrechtsen. "Glucagon Receptor Signaling and Glucagon Resistance". *Int J Mol Sci*, vol. 20, no. 13, p. 3314, 2019.
- [60] G. Jiang and B.B. Zhang. "Glucagon and regulation of glucose metabolism". *Am J Physiol Endocrinol Metab*, vol. 284, no. 4, pp. E671-E678, 2003.
- [61] D.A. Okar and A.J. Lange. "Fructose-2,6-bisphosphate and control of carbohydrate metabolism in eukaryotes". *Biofactors*, vol. 10, pp. 1-14, 1999.
- [62] J.B. Blair, M.A. Cimbala, J.L. Foster, R.A. Morgan. "Hepatic pyruvate kinase. Regulation by glucagon, cyclic adenosine 3'-5'-monophosphate, and insulin in the perfused rat liver". *J Biol Chem*, vol. 251, no. 12, pp. 3756-3762, 1976.
- [63] C. Ramnanan, D.S. Edgerton, G. Kraft, A.D. Cherrington. "Physiologic action of glucagon on liver glucose metabolism". *Diabetes Obes Metab.*, vol. 13, no. (Suppl 1), pp. 118-125, 2011.

Bibliography

- [64] M.S Brown and J.L. Goldstein. “Selective versus total insulin resistance: a pathogenic paradox”. *Cell Metab* , vol. 7, pp. 95-96, 2008.
- [65] M. Michael, R.N. Kulkarni, C. Postic, S.F. Previs, G.I. Shulman, M.A. Magnuson, C.R. Kahn. “Loss of insulin signaling in hepatocytes leads to severe insulin resistance and progressive hepatic dysfunction”. *Mol Cell*, vol. 6, p. 87–97, 2000.
- [66] R.A. Rizza. “Pathogenesis of fasting and postprandial hyperglycemia in type 2 diabetes: implications for therapy”. *Diabetes*, vol. 59, p. 2697–2707, 2010.
- [67] I. O' Sullivan, W. Zhang, D.H. Wasserman, C.W. Liew, J. Liu, J. Paik, R.A. DePinho, D.B. Stolz, C.R. Kahn, M.W. Schwartz, T.G. Unterman. “FoxO1 integrates direct and indirect effects of insulin on hepatic glucose production and glucose utilization”. *Nat Commun*, vol. 6, p. 7079, 2015.
- [68] V. T. Samuel, S.A. Beddow, T. Iwasaki, X.M. Zhang, X. Chu, C.D. Still, G.S. Gerhard, G.I. Shulman. “Fasting hyperglycemia is not associated with increased expression of PEPCK or G6Pc in patients with Type 2 Diabetes”. *Proc Natl Acad Sci U S A.*, vol. 106, no. 29, pp. 12121-12126., 2009.
- [69] M. Krssak, A. Brehm, E. Bernroider, C. Anderwald, P. Nowotny, C. Dalla Man, C. Cobelli, G.W. Cline, G.I. Shulman, W. Waldhäusl, M. Roden. “Alterations in postprandial hepatic glycogen metabolism in type 2 diabetes”. *Diabetes*, vol. 53, no. 12, pp. 3048-3056., 2004.
- [70] R. Basu, V. Chandramouli, B. Dicke, B. Landau, Rizza R. “Obesity and type 2 diabetes impair insulin-induced suppression of glycogenolysis as well as gluconeogenesis”. *Diabetes*. 2005;54(7):, vol. 54, no. 7, pp. 1942-1948, 2005.

Bibliography

- [71] I. Magnusson, D.L. Rothman, L.D. Katz, R.G. Shulman, G.I. Shulman. “Increased rate of gluconeogenesis in type II diabetes mellitus. A ¹³C nuclear magnetic resonance study”. *J Clin Invest*, vol. 90, pp. 1323–1327., 1992.
- [72] H. Okamoto, S. Obici, D. Accili, L. Rossetti. “Restoration of liver insulin signaling in Insr knockout mice fails to normalize hepatic insulin action”. *J Clin Invest*, vol. 115, p. 1314–1322, 2005.
- [73] R.J. Perry, J.G. Camporez, R. Kursawe, P.M. Titchenell, D. Zhang, C.J. Perry, M.J. Jurczak, A. Abudukadier, M.S. Han, X.M. Zhang, H.B. Ruan ... G.I. Shulman. “Hepatic acetyl CoA links adipose tissue inflammation to hepatic insulin resistance and type 2 diabetes”. *Cell*, vol. 160, no. 4, pp. 745-758., 2015.
- [74] J. Lambert, M.A. Ramos-Roman, J.D. Browning, E.J. Parks. “Increased de novo lipogenesis is a distinct characteristic of individuals with nonalcoholic fatty liver disease”. *Gastroenterology*, vol. 146, p. 726–735., 2014.
- [75] M.K. Poulsen, B. Nellemann, H. Stødkilde-Jørgensen, S.B. Pedersen, H. Grønbaek, S. Nielsen S. “Impaired insulin suppression of VLDL-triglyceride kinetics in nonalcoholic fatty liver disease”. *J Clin Endocrinol Metab* 2016; vol. 101, p. 1637–1646., 2016.
- [76] D.F. Vatner, S.K. Majumdar, N. Kumashiro, M.C. Petersen, Y. Rahimi, A.K. Gattu, M. Bears, J.P. Camporez, G.W. Cline, M.J. Jurczak, V.T. Samuel, G.I. Shulman. “Insulin-independent regulation of hepatic triglyceride synthesis by fatty acids”. *Proc Natl Acad Sci USA*, vol. 112, p. 1143–1148, 2015.
- [77] X. Wu and K.J. Williams. “NOX4 pathway as a source of selective insulin resistance and responsiveness”. *Arterioscler Thromb Vasc Biol*, vol. 32, p. 1236–1245, 2012.

- [78] N. Kubota, E. Kajiwara, T. Iwamura, H. Kumagai, T. Watanabe, M. Inoue, I. Takamoto, T. Sasako, K. Kumagai, M. Kohjima, ... T. Kadowaki. "Differential hepatic distribution of insulin receptor substrates causes selective insulin resistance in diabetes and obesity". *Nat Commun*, vol. 7, p. 12977, 2016.
- [79] J.R. Cook, F. Langlet, Y. Kido, D. Accili. "Pathogenesis of selective insulin resistance in isolated hepatocytes". *J Biol Chem* 290: , 2015, vol. 290, p. 13972–13980, 2015.
- [80] A. Ighbariya and R. Weiss. "Insulin Resistance, Prediabetes, Metabolic Syndrome: What Should Every Pediatrician Know ?". *J Clin Res Pediatr Endocrinol*, vol. 9, no. Suppl 2, pp. 49-57, 2017.
- [81] J.T. Haas, J. Miao, D. Chanda, Y. Wang, E. Zhao, M.E. Haas, M. Hirschey, B. Vaitheesvaran, R.V. Jr Farese RV, I.J. Kurland, M. Graham ... S.B. Biddinger. "Hepatic insulin signaling is required for obesity-dependent expression of SREBP-1c mRNA but not for feeding-dependent expression". *Cell Metab.* 2012;15(6):, vol. 15, no. 6, pp. 873-884, 2012.
- [82] M. Herman and V. Samuel. "The Sweet Path to Metabolic Demise: Fructose and Lipid Synthesis". *Trends Endocrinol Metab.*, vol. 27, no. 10, pp. 719-730., 2016.
- [83] E. Fabbrini, F. Magkos, B.S. Mohammed, T. Pietka, N.A. Abumrad, B.W. Patterson, A. Okunade, S.Klein. "Intrahepatic fat, not visceral fat, is linked with metabolic complications of obesity". *Proc Natl Acad Sci USA*, vol. 106, p. 15430–15435, 2009.

- [84] K.M. Korenblat, E. Fabbrini, B.S. Mohammed, S. Klein. “Liver, muscle, and adipose tissue insulin action is directly related to intrahepatic triglyceride content in obese subjects”. *Gastroenterology*, vol. 134, p. 1369–1375, 2008.
- [85] K.W. Ter Horst, P.W. Gilijamse, R.I. Versteeg, M.T. Ackermans, A.J. Nederveen, S.E. la Fleur, J.A. Romijn, M. Nieuwdorp, D. Zhang, V.T. Samuel, D.F. Vatner ... M.J. Serlie. “Hepatic Diacylglycerol-Associated Protein Kinase C ϵ Translocation Links Hepatic Steatosis to Hepatic Insulin Resistance in Humans”. *Cell Reports*, vol. 19, pp. 1997-2004, 2017.
- [86] B.N. Finck and A.M. Hall. “Does Diacylglycerol Accumulation in Fatty Liver Disease Cause Hepatic Insulin Resistance?”. *BioMed Res Int* 2015, p. 104132, 2015.
- [87] M.C. Petersen, A.K. Madiraju, B.M. Gassaway, M. Marcel, A.R. Nasiri, G. Butrico, M.J. Marcucci, D. Zhang, A. Abulizi, X.M. Zhang, W. Philbrick. ... G.I. Shulman. “Insulin receptor Thr1160 phosphorylation mediates lipid-induced hepatic insulin resistance”. *J Clin Invest*, vol. 126, p. 4361–4371, 2016.
- [88] J.A. Chavez and S.A. Summers. “A ceramide-centric view of insulin resistance.” *Cell Metab* 15, vol. 15, p. 585–594, 2012.
- [89] M.C. Petersen and G.I. Shulman. “Roles of diacylglycerols and ceramides in hepatic insulin resistance”. *Trends Pharmacol. Sci*, vol. 38, no. 7, p. 649–665, 2017.
- [90] W.L. Holland, B.T. Bikman, L.P. Wang, G. Yuguang, K.M. Sargent, S. Bulchand, T.A. Knotts, G. Shui, D.J. Clegg, M.R. Wenk, M.J. Pagliassotti. “Lipid-induced insulin resistance mediated by the proinflammatory receptor TLR4 requires saturated fatty acid-induced ceramide biosynthesis in mice”. *J. Clin. Invest* 121, (2011), vol. 121, no. 5, p. 1858–1870, 2011.

- [91] F. Qian, A.A. Korat, V. Malik, F.B. Hu. “Metabolic effects of monounsaturated fatty acid-enriched diets compared with carbohydrate or polyunsaturated fatty acid-enriched diets in patients with type 2 diabetes: a systematic review and meta-analysis of randomized controlled trials”. *Diabetes Care*, vol. 39, no. 8, pp. 1448-1457, 2016.
- [92] F. De Vadder, P. Kovatcheva-Datchary, D. Goncalves, J. Vinera, C. Zitoun, A. Duchampt, F. Bäckhed, G. Mithieux. “Microbiota-generated metabolites promote metabolic benefits via gut-brain neural circuits”. *Cell*, vol. 156, no. 1-2, pp. 84-96, 2014.
- [93] M.F. Gregor, L. Yang, E.Fabbrini, B.S. Mohammed, J.C. Eagon, G.S. Hotamisligil, S. Klein. “Endoplasmic reticulum stress is reduced in tissues of obese subjects after weight loss”. *Diabetes* 58: , 2009., vol. 58, no. 3, p. 693–700, 2009.
- [94] U. Özcan, Q. Cao, E. Yilmaz, A.H. Lee, N.N. Iwakoshi, E. Ozdelen, G.Tuncman, C. Görgün, L.H. Glimcher, G.S. Hotamisligil. “Endoplasmic reticulum stress links obesity, insulin action, and type 2 diabetes”. *Science*, vol. 306, no. 5695, p. 457–461, 2004.
- [95] Y.H. Lee, J. Giraud, R.J. Davis, M.F. White. “c-Jun N-terminal kinase (JNK) mediates feedback inhibition of the insulin signaling cascade”. *J Biol Chem*, vol. 278, no. 5, p. 2896–2902, 2003.
- [96] A.H. Lee, E.F. Scapa, D.E. Cohen, L.H. Glimcher. “Regulation of hepatic lipogenesis by the transcription factor XBP1”. *Science*, vol. 320, no. 5882, p. 1492–1496, 2008.
- [97] M. Jurczak, A.H Lee, F.R. Jornayvaz, H.Y. Lee, A.L. Birkenfeld, B.A. Guigni, M. Kahn, V.T. Samuel, L.H. Glimcher, G.I. Shulman. “Dissociation of inositol-requiring enzyme (IRE1 α)-mediated c-Jun N-terminal kinase activation from hepatic insulin

- resistance in conditional X-box-binding protein-1 (XBP1) knock-out mice”. *J Biol Chem*, vol. 287, no. 4, p. 2558–2567, 2012.
- [98] H. Kammoun, H. Chabanon, I. Hainault, S. Luquet, C. Magnan, T. Koike, P. Ferré, F. Foufelle. “GRP78 expression inhibits insulin and ER stress-induced SREBP-1c activation and reduces hepatic steatosis in mice”. *J Clin Invest*, vol. 119, no. 5, p. 1201–1215, 2009.
- [99] S. Fu, S.M. Watkins, and G.S. Hotamisligil. “The role of endoplasmic reticulum in hepatic lipid homeostasis and stress signaling”. *Cell Metab* 15(5): , 2012, vol. 15, no. 5, p. 623–634, 2012.
- [100] J.M. Olefsky and C.K. Glass. “Macrophages, inflammation, and insulin resistance”. *Annu Rev Physiol*, vol. 72, pp. 219-246., 2010.
- [101] G. Hotamisligil, P. Arner, J.F. Caro, R.L. Atkinson, B.M. Spiegelman. “Adipose expression of tumor necrosis factor-alpha: direct role in obesity-linked insulin resistance”. *Science*, vol. 259, no. 5091, pp. 87-91, 1993.
- [102] M. Kawakami, T. Murase, H. Ogawa, S. Ishibashi, N. Mori, F. Takaku, S. Shibata. “Human recombinant TNF suppresses lipoprotein lipase activity and stimulates lipolysis in 3T3-L1 cells”. *J. Biochem*, vol. 101, p. 331–338., 1987.
- [103] D.B. Stone, J.D. Brown, and A.A Steele. “Effect of sodium salicylate on induced lipolysis in isolated fat cells of the rat”. *Metabolism*, vol. 18, p. 620–624., 1969.
- [104] M. Crino, G. Sacks, S. Vandevijvere, B. Swinburn, B. Neal. “The influence on population weight gain and obesity of the macronu- trient composition and energy density of the food supply”. *Curr Obes Rep.*, vol. 4, no. 1, pp. 1-10, 2015.

- [105] M. Ng, T. Fleming, M. Robinson, B. Thomson, N. Graetz, C. Margono, E.C. Mullany, S. Biryukov, C. Abbafati, S.F. Abera, J.P. Abraham, N.M. Abu-Rmeileh ... E.Gakidou. "Global, regional, and national prevalence of overweight and obesity in children and adults during 1980-2013: a systematic analysis for the Global Burden of Disease Study 2013". *Lancet*, vol. 384, no. 9945, pp. 766-781, 2014.
- [106] J. Weiß, M. Rau, and A. Geier. "Non-alcoholic fatty liver disease: epidemiology, clinical course, investigation, and treatment". *Dtsch Arztebl Int*, vol. 111, no. 26, pp. 447-452, 2014.
- [107] S.K. Satapathy and A.J. Sanyal. "Epidemiology and Natural History of Nonalcoholic Fatty Liver Disease". *Semin Liver Dis*, vol. 35, no. 3, pp. 221-235, 2015.
- [108] N.C. Leite, G.F. Salles, A.L. Araujo, C.A. Villela-Nogueira, C.R. Cardoso. "Prevalence and associated factors in non alcoholic fatty liver disease in patients with type 2 diabetes mellitus". *Liver Int*, vol. 29, no. 1, pp. 113-119, 2009.
- [109] S. Romeo, J. Kozlitina, C. Xing, A. Pertsemlidis, D. Cox, L.A. Pennacchio, E. Boerwinkle, J.C. Cohen, H.H. Hobbs. "Genetic variation in PNPLA3 confers susceptibility to nonalcoholic fatty liver disease". *Nat Genet.* 2008; 40(12).; vol. 40, no. 12, p. 1461-1465., 2008.
- [110] D.E. Kelley, T.M. McKolanis, R.A. Hegazi, L.H. Kuller, S.C. Kalhan. "Fatty liver in type 2 diabetes mellitus: relation to regional adiposity, fatty acids, and insulin resistance". *Am J Physiol Endocrinol Metab*, vol. 285, no. 4, pp. E906-E916., 2003.
- [111] V. Samuel and G. Shulman. "Nonalcoholic Fatty Liver Disease as a Nexus of Metabolic and Hepatic Diseases". *Cell Metab*, vol. 27, no. 1, pp. 22-41, 2018.

- [112] F. Bäckhed, H. Ding, T. Wang, L.V. Hooper, G.Y. Koh, A. Nagy, C.F. Semenkovich, J.I. Gordon. “The gut microbiota as an environmental factor that regulates fat storage”. *Proc Natl Acad Sci U S A*, vol. 101, no. 44, pp. 15718-15723, 2004.
- [113] M. Machado Verdelho and H. Cortez-Pinto. “Diet, Microbiota, Obesity, and NAFLD: A Dangerous Quartet”. *International journal of molecular sciences*, vol. 17, no. 4, p. 481, 2016.
- [114] B.A. Ramlo-Halsted and S.V. Edelman. “The natural history of type 2 diabetes. Implications for clinical practice”. *Prim Care*, vol. 26, no. 4, pp. 771-789, 1999.
- [115] J. Schofield, Y. Liu, P. Rao-Balakrishna, R.A. Malik, H. Soran. “Diabetes Dyslipidemia”. *Diabetes Ther*, vol. 7, no. 2, pp. 203-219, 2016.
- [116] Q.T. Nguyen, K.T. Thomas, K.B. Lyons, L.D. Nguyen, R.A. Plodkowski. “Current therapies and emerging drugs in the pipeline for type 2 diabetes”. *Am Health Drug Benefits*, vol. 4, no. 5, pp. 303-311, 2011.
- [117] H.A. Ferris and C.R. Kahn. “New mechanisms of glucocorticoid-induced insulin resistance: make no bones about it”. *J Clin Invest*, vol. 122, no. 11, pp. 3854-3857, 2012.
- [118] A. Rafacho, H. Ortsäter, A. Nadal, I. Quesada. “Glucocorticoid treatment and endocrine pancreas function: implications for glucose homeostasis, insulin resistance and diabetes”. *J Endocrinol*, vol. 223, no. 3, pp. R49-R62, 2014.
- [119] A.A. Verhaegen and L.F. Van Gaal. “Drugs That Affect Body Weight, Body Fat Distribution, and Metabolism”. MDText.com, Inc, Endotext. South Dartmouth (MA), 2019.

- [120] A. Provilus, M. Abdallah, and S.I. McFarlane. "Weight gain associated with antidiabetic medications". *Therapy* 8(2):, vol. 8, no. 2, pp. 113-120, 2011.
- [121] H.Y. Meltzer. "The mechanism of action of novel antipsychotic drugs". *Schizophr Bull*, vol. 17, no. 2, pp. 263-287., 1991.
- [122] S. Kapur and P. Seeman. "Does fast dissociation from the dopamine D2 receptor explain the action of atypical antipsychotics?: a new hypothesis". *American Journal of Psychiatry*, vol. 158, no. 3, p. 360–369, 2001.
- [123] R.C. Shelton and G.I. Papakostas. "Augmentation of antidepressants with atypical antipsychotics for treatment-resistant major depressive disorder". *Acta Psychiatr Scand*, vol. 117, no. 4, pp. 253-259., 2008.
- [124] C.J. McDougale, K.A. Stigler, C.A. Erickson, D.J. Posey. "Atypical antipsychotics in children and adolescents with autistic and other pervasive developmental disorders". *J. Clin. Psychiatry* , vol. 69, no. Suppl 4, pp. 15-20, 2008.
- [125] J. Pfeifer, R.A. Kowatch, and M.P. DelBello. "Pharmacotherapy of bipolar disorder in children and adolescents: recent progress". *CNS Drugs*, vol. 24, no. 7, pp. 575-593, 2010.
- [126] J.A. Lieberman, T.S. Stroup, J.P. McEvoy, M.S. Swartz, R.A. Rosenheck, D.O. Perkins, R.S. Keefe, S.M. Davis, C.E. Davis, B.D. Lebowitz, J. Severe, J.K. Hsiao. "Effectiveness of antipsychotic drugs in patients with chronic schizophrenia [published correction appears in N Engl J Med. 2010 Sep 9;]". *N Engl J Med*, vol. 353, no. 12, pp. 1209-1223, 2005.
- [127] A. Annamalai, U. Kosir, and C. Tek. "Prevalence of obesity and diabetes in patients with schizophrenia". *World J Diabetes*, vol. 8, no. 8, pp. 390-396, 2017.

Bibliography

- [128] I. Elamn, D. Borsook, and S.E. Lukas. "Food intake and reward mechanisms in patients with schizophrenia: implications for metabolic disturbances and treatment with second-generation antipsychotic agents". *Neuropsychopharmacology*, vol. 31, no. 10, pp. 2091-2120, 2006.
- [129] G. O' Malley, S. Seifert, K. Heard, F. Daly, R.C. Dart. "Olanzapine overdose mimicking opioid intoxication". *Ann Emerg Med* 34: 279–281., vol. 34, p. 279–281., 1999.
- [130] J. Sacher, N. Mossaheb, C. Spindelegger, N. Klein, T. Geiss-Granadia, R Sauer mann, E. Lackner, C. Joukhadar, M. Müller, S. Kasper. "Effects of olanzapine and ziprasidone on glucose tolerance in healthy volunteers". *Neuropsychopharmacology* , vol. 33, no. 7, p. 1633–1641, 2008.
- [131] K. Teff, M.R. Rickels, J. Grudziak, C. Fuller, H.L. Nguyen, K. Rickels. "Antipsychotic-induced insulin resistance and postprandial hormonal dysregulation independent of weight gain or psychiatric disease". *Diabetes*, vol. 62, no. 9, p. 3232–3240, 2013.
- [132] C. Deng, K. Weston-Green, and X.F. Huang. "The role of histaminergic H1 and H3 receptors in food intake: a mechanism for atypical antipsychotic-induced weight gain?". *Prog Neuropsychopharmacol Biol Psychiatry*, vol. 34, no. 1, pp. 1-4, 2009.
- [133] M. Han, K. Newell, K. Zavitsanou, C. Deng, X.F. Huang. "Effects of antipsychotic medication on muscarinic M1 receptor mRNA expression in the rat brain". *J Neurosci Res*, vol. 86, no. 2, pp. 457-464, 2008.
- [134] A.F. Chintoh, S.W. Mann, L. Lam, C. Lam, T.A. Cohn, P.J. Fletcher, J.N. Nobrega, A. Giacca, G. Remington. "Insulin resistance and decreased glucose-stimulated insulin

- secretion after acute olanzapine administration”. *J. Clin. Psychopharmacol*, vol. 28, no. 5, p. 494–499, 2008.
- [135] K. Houseknecht, A.S. Robertson, W. Zavadoski, E.M. Gibbs, D.E. Johnson, H. Rollema. “Acute effects of atypical antipsychotics on whole-body insulin resistance in rats: Implications for adverse metabolic effects”. *Neuropsychopharmacology*, vol. 32, p. 289–297., 2007.
- [136] E. Girault, A. Alkemade, E. Foppen M.T., Ackermans, E. Fliers, A. Kalsbeek. “Acute peripheral but not central administration of olanzapine induces hyperglycemia associated with hepatic and extra-hepatic insulin resistance”. *PLoS ONE*, vol. 7, p. e43244, 2012.
- [137] Y.E. Savoy, M.A. Ashton, M.W. Miller, F.N. Nedza, D.K. Spracklin, M.H. Hawthorn, H. Rollema, F.F. Matos, E. Hajos-Korcsok. “Differential effects of various typical and atypical antipsychotics on plasma glucose and insulin levels in the mouse: evidence for the involvement of sympathetic regulation”. *Schizophr Bull.* 2010;36(2):, vol. 36, no. 2, pp. 410-418, 2010.
- [138] K. Skonieczna-Żydecka, I. Łoniewski, A. Misera, E. Stachowska, D. Maciejewska, W. Marlicz, B. Gallig. “Second-generation antipsychotics and metabolism alterations: a systematic review of the role of the gut microbiome”. *Psychopharmacology (Berl)*, vol. 236, no. 5, pp. 1491-1512, 2019.
- [139] R.R. Girgis, J.A. Javitch, and J.A. Lieberman. “Antipsychotic drug mechanisms: links between therapeutic effects, metabolic side effects and the insulin signaling pathway”. *Mol Psychiatry*, vol. 13, no. 10, p. 918–929, 2008.

- [140] H.A. Nasrallah. "A typical antipsychotic-induced metabolic side effects: insights from receptor-binding profiles". *Mol. Psychiatry*, 2008, 13(1), vol. 13, no. 1, pp. 27-35, 2008.
- [141] H. Dambha-Miller, A.J. Day, J. Strelitz, G. Irving, S.J. Griffin. "Behaviour change, weight loss and remission of Type 2 diabetes: a community-based prospective cohort study". *Diabet Med*, vol. 37, no. 4, pp. 681-688, 2020.
- [142] F.L. Greenway. "Physiological adaptations to weight loss and factors favouring weight regain". *Int J Obes (Lond)*, vol. 39, no. 8, pp. 1188-1196, 2015.
- [143] P.R. Schauer, D.L. Bhatt, J.P. Kirwan, K. Wolski, A. Aminian, S.A. Brethauer, S.D. Navaneethan, R.P. Singh, C.E. Pothier, S.E. Nissen, S.R. Kashyap; STAMPEDE Investigators. "Bariatric Surgery versus Intensive Medical Therapy for Diabetes - 5-Year Outcomes". *N Engl J Med*, vol. 376, no. 7, pp. 641-651, 2017.
- [144] UK Prospective Diabetes Study (UKPDS) group. "Effect of intensive blood-glucose control with metformin on complications in overweight patients with type 2 diabetes (UKPDS 34)". *Lancet*, vol. 352, no. 9131, pp. 854-865, 1998.
- [145] L.B. Rojas and M. Brito Gomes. "Metformin: an old but still the best treatment for type 2 diabetes". *Diabetol Metab Syndr*, vol. 5, no. 1, p. 6, 2013.
- [146] R.A. DeFronzo, J.D. Tobin, and R. Andres. "Glucose clamp technique: a method for quantifying insulin secretion and resistance". *Am J Physiol*, vol. 237, no. 3, pp. E214-E223, 1979.
- [147] C.C. Hughey, D.H. Wasserman, R.S. Lee-Young, L. Lantier. "Approach to assessing determinants of glucose homeostasis in the conscious mouse". *Mamm Genome*, vol. 25, no. 9-10, pp. 522-538, 2014.

Bibliography

- [148] D. Matthews, J.P. Hosker, A.S. Rudenski, B.A. Naylor, D.F. Treacher, R.C. Turner. "Homeostasis model assessment: insulin resistance and beta-cell function from fasting plasma glucose and insulin concentrations in man". *Diabetologia*, vol. 28, no. 7, pp. 412-419, 1985.
- [149] A. Katz, S.S. Nambi, K. Mather, A.D. Baron, D.A. Follmann, G. Sullivan, M.J. Quon. "Quantitative insulin sensitivity check index: a simple, accurate method for assessing insulin sensitivity in humans". *J Clin Endocrinol Metab*, vol. 85, no. 7, pp. 2402-2410, 2000.
- [150] K. Trout, C. Homko, N.C. Tkacs. "Methods of measuring insulin sensitivity". *Biol Res Nurs*, vol. 8, no. 4, pp. 305-318, 2007.
- [151] C.B. Newgard, "Metabolomics and Metabolic Diseases: Where Do We Stand?". *Cell Metab*, vol. 25, no. 1, pp. 43-56, 2017.
- [152] C.B. Newgard, "Interplay between lipids and branched-chain amino acids in development of insulin resistance". *Cell Metab.*, vol. 15, no. 5, pp. 606-614, 2012.
- [153] D. Finegood, R.N. Bergman, and M. Vranic. "Estimation of Endogenous Glucose Production During Hyperinsulinemic-Euglycemic Glucose Clamps: Comparison of Unlabeled and Labeled Exogenous Glucose Infusates". *Diabetes*, vol. 36, no. 8, pp. 914-924, 1987.
- [154] A.M. Umpleby. "HORMONE MEASUREMENT GUIDELINES: Tracing lipid metabolism: the value of stable isotopes". *J Endocrinol. 2015;226(3)*., vol. 226, no. 3, pp. G1-G10, 2015.

Bibliography

- [155] A. Soares, F.J. Viegas, R.A. Carvalho, J.G. Jones. “Quantifying hepatic glycogen synthesis by direct and indirect pathways in rats under normal ad libitum feeding conditions”. *Magn Reson Med*, vol. 61, no. 1, pp. 1-5, 2009.
- [156] J.A.G. Duarte, F. Carvalho, M. Pearson, J.D. Horton, J.D. Browning, J.G. Jones, S.C. Burgess. “A high-fat diet suppresses de novo lipogenesis and desaturation but not elongation and triglyceride synthesis in mice”. *J Lipid Res*, vol. 55, no. 12, pp. 2541-2553, 2014.
- [157] L. Demetrius. “Of mice and men. When it comes to studying ageing and the means to slow it down, mice are not just small humans”. *EMBO Rep*, vol. 6, no. Suppl 1, pp. S39-S44, 2005.
- [158] J.E. Ayala, D.P. Bracy, O.P. McGuinness, D.H. Wasserman. “Considerations in the design of hyperinsulinemic-euglycemic clamps in the conscious mouse”. *Diabetes*, vol. 55, no. 2, p. 390–397, 2006.
- [159] S. Ghosal, A. Nunley, P. Mahbod, A.G. Lewis, E.P. Smith, J. Tong, D.A. D'Alessio, J.P. Herman. “Mouse handling limits the impact of stress on metabolic endpoints”. *Physiol Behav*, vol. 150, pp. 31-37, 2015.
- [160] J. Ghalami, H. Zardooz, F. Rostamkhani, B. Farrokhi, M. Hedayati. “Glucose-stimulated insulin secretion: Effects of high-fat diet and acute stress”. *Endocrinol Invest*, vol. 36, no. 10, p. 835–842, 2013.
- [161] S.I. Tschen, S. Dhawan, T. Gurlo, A. Bhushan. “Age-dependent decline in beta-cell proliferation restricts the capacity of beta-cell regeneration in mice”. *Diabetes*, vol. 58, no. 6, pp. 1312-1320, 2009.

- [162] F. Mauvais-Jarvis, A.P. Arnold, and K. Reue. “A Guide for the Design of Pre-clinical Studies on Sex Differences in Metabolism”. *Cell Metab*, vol. 25, no. 6, pp. 1216-1230, 2017.
- [163] B. Martin, S. Ji, Maudsley, M.P. Mattson. “ “Control” laboratory rodents are metabolically morbid: why it matters”. *Proc Natl Acad Sci U S A*, vol. 107, no. 14, p. 6127–6133, 2010.
- [164] A.M. Ingalls, M.M. Dickie, and G.D. Snell. “Obese, a new mutation in the house mouse”. *J Hered.*, vol. 41, no. 12, pp. 317-318, 1950.
- [165] J.R. Speakman, “Use of high-fat diets to study rodent obesity as a model of human obesity”. *Int J Obes (Lond)*, vol. 43, no. 8, pp. 1491-1492., 2019.
- [166] R. Buettner, J. Schölmerich, and L.C. Bollheimer. “High-fat diets: modeling the metabolic disorders of human obesity in rodents”. *Obesity*, vol. 15, no. 4, p. 798–780, 2007.
- [167] E.W. Kraegen, P.W. Clark, A.B. Jenkins, E.A. Daley, D.J. Chisholm, L.H. Storlien. “Development of muscle insulin resistance after liver insulin resistance in high-fat-fed rats”. *Diabetes*, vol. 40, no. 11, pp. 1397-1403, 1991.
- [168] A. Chicco, M.E. D'Alessandro, L. Karabatas, C. Pastorale, J.C. Basabe, Y.B. Lombardo. “Muscle lipid metabolism and insulin secretion are altered in insulin-resistant rats fed a high sucrose diet”. *J Nutr*, vol. 133, no. 1, pp. 127-133, 2003.
- [169] M. Sumiyoshi, M. Sakanaka, and Y. Kimura. “Chronic intake of high-fat and high-sucrose diets differentially affects glucose intolerance in mice”. *J Nutr*, vol. 136, no. 3, pp. 582-587, 2006.

- [170] I. Jarak, C. Barosa, F.O. Martins, J.C.P. Silva, C. Santos, G.D. Belew J. Rito, I. Viegas, J. Teixeira, P.J. Oliveira, J.G. Jones. "Sources of hepatic glycogen synthesis in mice fed with glucose or fructose as the sole dietary carbohydrate". *Magn Reson Med*, vol. 81, no. 1, pp. 639-644, 2019.
- [171] T.C. Delgado, F.O. Martins, F. Carvalho, A. Gonçalves, D.K. Scott, R. O'Doherty, M.P. Macedo, J.G. Jones. "²H enrichment distribution of hepatic glycogen from ²H₂O reveals the contribution of dietary fructose to glycogen synthesis". *Am J Physiol Endocrinol Metab.*, vol. 304, no. 4, pp. E384-391, 2013 .
- [172] J.G. Jones, R. Perdigoto, T.B. Rodrigues, C.F. Geraldes. "Quantitation of absolute ²H enrichment of plasma glucose by ²H NMR analysis of its monoacetone derivative". *Magnetic Resonance in Medicine*, vol. 48, no. 3, pp. 535-539, 2002.
- [173] J.G. Jones, M.A. Solomon S.M. Cole, A.D. Sherry, C.R. Malloy. "An integrated ²H and ¹³C NMR study of gluconeogenesis and TCA cycle flux in humans". *Am J Physiol Endocrinol Metab*, vol. 281, no. 4, pp. E848-856., 2001.
- [174] T. C. Delgado, C. Barosa, P.M. Nunes, S. Cerdán, C.F. Geraldes, J.G. Jones. "Resolving the Sources of Plasma Glucose Excursions following a Glucose Tolerance Test in the Rat with Deuterated Water and [U-¹³C]Glucose". *PLoS ONE*, vol. 7, no. 3, p. e34042, 2012.
- [175] J. Rito, I. Viegas, M.A. Pardal, I. Metón, I.V. Baanante, J.G. Jones. "Disposition of a glucose load into hepatic glycogen by direct and indirect pathways in juvenile seabass and seabream". *Scientific Reports*, vol. 8, no. 1, p. 464, 2018.
- [176] G. DiNunzio, G.D. Belew, A.N. Torres, J.G. Silva, L.P. Silva, C. Barosa, L. Tavares, J.G. Jones. "Determining the contribution of a high-fructose corn syrup formulation to

- hepatic glycogen synthesis during ad-libitum feeding in mice”. *Sci Rep*, vol. 10, no. 1, p. 12852, 2020.
- [177] J. Silva, C. Marques, F.O. Martins, I. Viegas, L. Tavares, M.P. Macedo, J.G. Jones. “Determining contributions of exogenous glucose and fructose to de novo fatty acid and glycerol synthesis in liver and adipose tissue”. *Metab Eng*, vol. 56, pp. 69-76, 2019.
- [178] J.G. Jones, M. Merritt, C. Malloy. “Quantifying tracer levels of $^2\text{H}_2\text{O}$ enrichment from microliter amounts of plasma and urine by ^2H NMR”. *Magn Reson Med.*, vol. 45, no. 1, pp. 156-158, 2001.
- [179] J.G. Jones, C. Barosa, F. Gomes, A.C. Mendes, T.C. Delgado, L.Diogo, P. Garcia, M. Bastos, L. Barros, A. Fagulha, C. Baptista, M. Carvalheiro M.M. Caldeira. “Derivatives for Quantification of ^2H and ^{13}C -Enrichment of Human Glucuronide from Metabolic Tracers”. *Journal of Carbohydrate Chemistry*, vol. 25, no. 2-3, pp. 203-217, 2006.
- [180] S.J. Burke, H.M. Batdorf, T.M. Martin, D.H. Burk, R.C. Noland, C.R. Cooley, M.D. Karlstad, W.D. Johnson, J.J. Collier. “Liquid Sucrose Consumption Promotes Obesity and Impairs Glucose Tolerance Without Altering Circulating Insulin Levels”. *Obesity*, vol. 26, no. 7, pp. 1188-1196, 2018.
- [181] E. Sakamoto, Y. Seino, A. Fukami, N. Mizutani, S. Tsunekawa, K. Ishikawa, H. Ogata, E. Uenishi, H. Kamiya, Y. Hamada, H. Sato, N. Harada ... N. Ozaki. “Ingestion of a moderate high-sucrose diet results in glucose intolerance with reduced liver glucokinase activity and impaired glucagon-like peptide-1 secretion”. *J Diabetes Investig*, vol. 3, no. 5, pp. 432-440, 2012.

- [182] K. Mock, S. Lateef, V.A. Benedito, J.C. Tou. “High-fructose corn syrup-55 consumption alters hepatic lipid metabolism and promotes triglyceride accumulation”. *J Nutr Biochem*, vol. 39, pp. 32-39, 2017.
- [183] M.R. Taskinen, S. Söderlund, L.H. Bogl, A. Hakkarainen, N. Matikainen, K.H. Pietiläinen, S. Räsänen, N. Lundbom, E. Björnson, B. Eliasson, R.M. Mancina. “Adverse effects of fructose on cardiometabolic risk factors and hepatic lipid metabolism in subjects with abdominal obesity”. *J Intern Med*. 2017 Aug, vol. 282, no. 2, pp. 187-201, 2017.
- [184] S. Softic, M.K. Gupta, G.X. Wang, S. Fujisaka, B.T. O'Neill, T.N. Rao, J. Willoughby, C. Harbison, K. Fitzgerald, O. Ilkayeva, C.B. Newgard ... C.R. Kahn. “Divergent effects of glucose and fructose on hepatic lipogenesis and insulin signaling”. *J Clin Invest*, vol. 127, no. 11, pp. 4059-4074, 2017.
- [185] S. Zhao, C. Jang, J. Liu, K. Uehara, M. Gilbert, L. Izzo, X. Zeng, S. Trefely, S. Fernandez, A. Carrer, K.D. Miller ... K.E. Wellen. “Dietary fructose feeds hepatic lipogenesis via microbiota-derived acetate”. *Nature*. 2020, vol. 579, no. 7800, pp. 586-591, 2020.
- [186] M.A. Herman and V.T. Samuel. “The Sweet Path to Metabolic Demise: Fructose and Lipid Synthesis”. *Trends Endocrinol Metab.*, vol. 27, no. 10, pp. 719-730, 2016.
- [187] A. Soares, R.A. Carvalho, F.J. Veiga, M.G. Alves, F.O. Martins, I. Viegas, J.D. González, I. Metón, I.V. Baanante, J.G. Jones. “Restoration of direct pathway glycogen synthesis flux in the STZ-diabetes rat model by insulin administration”. *Am J Physiol Endocrinol Metab.*, vol. 303, no. 7, pp. E875-E885, 2012.

- [188] K.F. Petersen, D. Laurent, C. Yu, G.W. Cline, G.I. Shulman. “Stimulating effects of low-dose fructose on insulin-stimulated hepatic glycogen synthesis in humans”. *Diabetes*, vol. 50, no. 6, pp. 1263-1268, 2001.
- [189] G.D. Belew, G. Di Nunzio, L. Tavares, J.G. Silva, A.N. Torres, J.G. Jones. “Estimating pentose phosphate pathway activity from the analysis of hepatic glycogen ¹³C-isotopomers derived from [U-¹³C]fructose and [U-¹³C]glucose”. *Magn Reson Med*, vol. 84, no. 5, pp. 2765-2771, 2020.
- [190] R. Doi, K. Oishi, N. Ishida. “CLOCK regulates circadian rhythms of hepatic glycogen synthesis through transcriptional activation of Gys2”. *J Biol Chem*, vol. 285, no. 29, pp. 22114-22121, 2010.
- [191] M. Sullivan, S.T. Aroney, S. Li, F.J. Warren, J.S. Joo, K.S. Mak, D.I. Stapleton, K.S. Bell-Anderson, R.G. Gilbert. “Changes in glycogen structure over feeding cycle sheds new light on blood-glucose control”. *Biomacromolecules*, vol. 15, no. 2, pp. 660-665, 2014.
- [192] M. Shiota, P. Galassetti, M. Monohan, D.W. Neal, A.D. Cherrington. “Small amounts of fructose markedly augment net hepatic glucose uptake in the conscious dog”. *Diabetes*, vol. 47, no. 6, pp. 867-873, 1998.
- [193] M. Watford. “Small amounts of dietary fructose dramatically increase hepatic glucose uptake through a novel mechanism of glucokinase activation”. *Nutrition Reviews*, vol. 60, no. 8, pp. 253-257, 2002.
- [194] H.N. Boyda, L. Tse, R.M. Procyshyn, D. Wong, T.K. Wu, C.C. Pang, A.M. Barr. “A parametric study of the acute effects of antipsychotic drugs on glucose sensitivity in

- an animal model". *Prog Neuropsychopharmacol Biol Psychiatry*, vol. 34, no. 6, pp. 945-954, 2010.
- [195] M. Hahn, T.M. Wolever, T. Arenovich, C. Teo, A. Giacca, V. Powell, L. Clarke, P. Fletcher, T. Cohn, R.S. McIntyre, S. Gomes ... G.J. Remington. "Acute effects of single-dose olanzapine on metabolic, endocrine, and inflammatory markers in healthy controls". *Journal of Clinical Psychopharmacology*, vol. 33, no. 6, pp. 740-746, 2013.
- [196] C. Kowalchuk, L.N. Castellani, A. Chintoh, G.J. Remington, A. Giacca, M.K. Hahn. "Antipsychotics and glucose metabolism: how brain and body collide". *Am J Physiol Endocrinol Metab*, vol. 316, no. 1, pp. E1-E15, 2019.
- [197] R.H. Schmidt, J.D. Jokinen, V.L. Massey, K.C. Falkner, X. Shi, X. Yin, X. Zhang, J.I. Beier, G.E. Arteel. "Olanzapine activates hepatic mammalian target of rapamycin: new mechanistic insight into metabolic dysregulation with atypical antipsychotic drugs". *J Pharmacol Exp Ther*, vol. 347, no. 1, pp. 126-135, 2013.
- [198] P.J. Martins, M. Haas, and S. Obici. "Central nervous system delivery of the antipsychotic olanzapine induces hepatic insulin resistance". *Diabetes*, vol. 59, no. 10, pp. 2418-2425, 2010.
- [199] L. Ren, X. Zhou, X. Huang, C. Wang, Y. Li Y. "The IRS/PI3K/Akt signaling pathway mediates olanzapine-induced hepatic insulin resistance in male rats". *Life Sciences*, vol. 217, p. 229-236, 2019.
- [200] R. Musil, M. Obermeier, P. Russ, M. Hamerle. "Weight gain and antipsychotics: a drug safety review". *Expert Opin Drug Saf*, vol. 14, no. 1, pp. 73-96, 2015.

Bibliography

- [201] R. Kaddurah-Daouk, J. McEvoy, R.A. Baillie, D. Lee, J.K. Yao, P.M. Doraiswamy, K.R. Krishnan. "Metabolomic mapping of atypical antipsychotic effects in schizophrenia". *Mol Psychiatry*, vol. 12, no. 10, pp. 934-945, 2007.
- [202] S. Vidarsdottir, J.E. de Leeuw van Weenen, M. Frölich, F. Roelfsema, J.A. Romijn, H. Pijl. "Effects of olanzapine and haloperidol on the metabolic status of healthy men". *J Clin Endocrinol Metab*, vol. 95, no. 1, pp. 118-125, 2010.
- [203] V.L. Albaugh, T.C. Vary, O. Ilkayeva, B.R. Wenner, K.P. Maresca, J.L. Joyal, S. Breazeale, T.D. Elich, C.H. Lang, C.J. Lynch. "Atypical antipsychotics rapidly and inappropriately switch peripheral fuel utilization to lipids, impairing metabolic flexibility in rodents". *Schizophr Bull*, vol. 38, no. 1, pp. 153-166, 2012.
- [204] V.L. Albaugh, J.G. Judson, P. She, C.H. Lang, K.P. Maresca, J.L. Joyal, C.J. Lynch. "Olanzapine promotes fat accumulation in male rats by decreasing physical activity, repartitioning energy and increasing adipose tissue lipogenesis while impairing lipolysis". *Mol Psychiatry*, vol. 16, no. 5, pp. 569-581, 2011.
- [205] M. Nagata, M. Nakajima, Y. Ishiwata, Y. Takahashi, H. Takahashi, K. Negishi M. Yasuhara. "Mechanism Underlying Induction of Hyperglycemia in Rats by Single Administration of Olanzapine". *Biol Pharm Bull*, vol. 39, no. 5, pp. 754-761, 2016.
- [206] M. Elchebly, P. Payette, E. Michaliszyn, W. Cromlish, S. Collins, A.L. Loy, D. Normandin, A. Cheng, J. Himms-Hagen, C.C. Chan, C. Ramachandran ... B.P. Kennedy. "Increased insulin sensitivity and obesity resistance in mice lacking the protein tyrosine phosphatase-1B gene". *Science*, vol. 283, no. 5407, pp. 1544-1548, 1999.

- [207] L.D. Klaman, O. Boss, O.D. Peroni, J.K. Kim, J.L. Martino, J.M. Zabolotny, N. Moghal, M. Lubkin, Y.B. Kim, A.H. Sharpe, A. Stricker-Krongrad ... B.B. Kahn. "Increased energy expenditure, decreased adiposity, and tissue-specific insulin sensitivity in protein-tyrosine phosphatase 1B-deficient mice". *Mol Cell Biol*, vol. 20, no. 15, pp. 5479-5489, 2000.
- [208] K.K. Bence, M. Delibegovic, B. Xue, C.Z. Gorgun, G.S. Hotamisligil, B.G. Neel, B.B. Kahn. "Neuronal PTP1B regulates body weight, adiposity and leptin action". *Nat Med*, vol. 12, no. 8, pp. 917-924, 2006.
- [209] Delibegovic M, D. Zimmer, C. Kauffman, K. Rak, E.G. Hong, Y.R. Cho, J.K. Kim, B.B. Kahn, B.G. Neel, K.K. Bence. "Liver-specific deletion of protein-tyrosine phosphatase 1B (PTP1B) improves metabolic syndrome and attenuates diet-induced endoplasmic reticulum stress". *Diabetes*, vol. 58, no. 3, pp. 590-599, 2009.
- [210] M. Delibegovic, K.K. Bence, N. Mody, E.G. Hong, H.J. Ko, J.K. Kim, B.B. Kahn, B.G. Neel. "Improved glucose homeostasis in mice with muscle-specific deletion of protein-tyrosine phosphatase 1B". *Mol Cell Biol*, vol. 27, no. 21, pp. 7727-7734, 2007.
- [211] C. Owen, E.K. Lees, L. Grant, D.J. Zimmer, N. Mody, K.K. Bence, M. Delibegović. "Inducible liver-specific knockdown of protein tyrosine phosphatase 1B improves glucose and lipid homeostasis in adult mice". *Diabetologia*, vol. 56, no. 10, pp. 2286-2296, 2013.
- [212] P. Chen, S.P. Cai, C. Huang X.M. Meng, J. Li. "Protein tyrosine phosphatase 1B (PTP1B): A key regulator and therapeutic target in liver diseases". *Toxicology*, vol. 337, pp. 10-20, 2015.

- [213] M. Alonso-Chamorro, I. Nieto-Vazquez, M. Montori-Grau, A.M. Gomez-Foix, S. Fernandez-Veledo, M. Lorenzo. “New emerging role of protein-tyrosine phosphatase 1B in the regulation of glycogen metabolism in basal and TNF- α -induced insulin-resistant conditions in an immortalised muscle cell line isolated from mice”. *Diabetologia*, vol. 54, no. 5, pp. 1157-1168, 2011.
- [214] M.T. Hackl, C. Fürnsinn, C.M. Schuh, M. Krssak, F. Carli, S. Guerra, A. Freudenthaler, S. Baumgartner-Parzer, T.H. Helbich, A. Luger, M. Zeyda M, A. Gastaldelli, C. Buettner, T. Scherer. “Brain leptin reduces liver lipids by increasing hepatic triglyceride secretion and lowering lipogenesis”. *Nat Commun*, vol. 10, no. 1, p. 2717, 2019.
- [215] S. Shimizu, S. Ugi, H. Maegawa, K. Egawa, Y. Nishio, T. Yoshizaki, K. Shi, Y. Nagai, K. Morino, K. Nemoto, T. Nakamura, A. Kashiwagi. “Protein-tyrosine phosphatase 1B as new activator for hepatic lipogenesis via sterol regulatory element-binding protein-1 gene expression”. *J Biol Chem*, vol. 278, no. 44, pp. 43095-43101, 2003.
- [216] E.R. Miraldi, H. Sharfi, R.H. Friedline, H. Johnson, T. Zhang, K.S. Lau, H.J. Ko, T.G. Curran, K.M. Haigis, M.B. Yaffe, R. Bonneau. “Molecular network analysis of phosphotyrosine and lipid metabolism in hepatic PTP1b deletion mice”. *Integr Biol (Camb)*, vol. 5, no. 7, pp. 940-963, 2013.

